Inaugural dissertation for

obtaining the doctoral degree

of the

Combined Faculty of Mathematics, Engineering and Natural Sciences

of the

Ruprecht - Karls - University

Heidelberg

Presented by

Jona Rada

born in Prizren, Kosovo

Oral examination: 25. September 2024

THE LINK BETWEEN GLYCOLYSIS AND SIGNALING DURING MOUSE EMBRYO SEGMENTATION

Referees

Prof. Dr. Rüdiger Hell (University of Heidelberg)

Dr. Aissam Ikmi (EMBL)

Acknowledgments

My project has been the result of many good people's support and collaborative effort. It is important for me to present this work as a collective effort, which is the only way I can imagine doing science.

I want to start by acknowledging my supervisor, Alexander Aulehla. Thank you for sharing your knowledge and your passion for science with me and accepting me into your lab, where I had a chance to grow scientifically as well as personally.

It has been my big joy and privilege to do my whole work in very close collaboration with Hidenobu Miyazawa. Thank you, Hide, for confirming my belief that science is a fundamentally collaborative space, and thanks for making our work on a topic of mutual interest not only possible but also engaging, stimulating, and an absolute pleasure!

Paul Gerald Layague Sanchez taught me a lot about entrainment and microfluidics, so thank you, Paul, for sharing your knowledge and supporting me in the very beginnings of this project!

Apart from Alexander, Hide, and Paul, I had the incredible luck of being surrounded by other amazing labmates during my PhD years. Thank you, Ana, Jan, Luc, Sapna, Simon, Ali, Michael, Silvija, Simona, Sarkis, Emilia, Takehito, Carina, Philipp, Christine, Mussa, and Nobuko (in no particular order), for your empathy, friendship, support, and scientific mentorship. You have been a very important part of my PhD experience, and I cannot find the right way to thank you enough for all the fundamental building blocks you laid down for me, regardless of how big or small.

Thank you to Christian and Paul for our discussions and your help on the theoretical part of my project! Thank you to all my friends inside and outside EMBL! Thank you to all the people working at EMBL, whose support is crucial for all our work: the animal facility, the

imaging facility, the cleaning staff, the cafeteria and canteen staff, the library, IT services, human resources, and administration.

Thank you, Nora, for being such a safe space for me during this whole journey! Thank you, Dhurata, for absolutely everything! Thank you, Soraya, for your pure love and support! And thank you, Finfin, for the best company!

Për Jonën dhjetë vjeçare. Ky ishte testi i fundit: tash shko luaj!

Contributions

This thesis had to be written in the first-person singular; I conceptualized the project, conducted the experiments, performed data analysis, visualized the data, and wrote the thesis. However, writing it in first-person singular does not resonate with me because, as with any scientific work, the work was conducted as a collective effort. This chapter recognizes the crucial contributions of the main people involved in this scientific work.

Alexander Aulehla: supervision and guidance regarding conceptualization, investigation, methodology, and writing.

Hidenobu Miyazawa: guidance regarding conceptualization, investigation, and methodology. The combinatorial entrainment experiments (Results: Part I) were conducted in collaboration with Hidenobu Miyazawa. His other contributions are noted in the text.

Paul G.L. Sanchez: teaching about the microfluidic setup, preparation of microfluidic mold and writing of the script for entrainment data analysis and visualization.

Christine Ho and Emilia Esposito: teaching about the RAFL setup.

Takehito Tomita: writing of the script for posterior analysis of entrainment data.

Christian Mauffette Denis and Paul François: guidance and teaching about dynamical systems theory.

Gregor Moenke: development of the pyBOAT wavelet analysis toolkit.

Ina Sonnen: development of the microfluidics entrainment setup.

Nobuko Tsuchida-Straeten and Ana Mestre: preparation of medium used for dissection and culturing of mouse tail explants.

Animal facility EMBL: providing care for the animal models used in this project.

Imaging facility EMBL: providing microscopy setups for the experiments conducted in this project.

Cleaning staff EMBL: cleaning and preparation of all lab dishes used in this work.

TABLE OF CONTENTS

List of tables

Summary

New phenotypes can arise in organisms as a response to changing environments. Changes in environmental conditions, such as temperature fluctuations, pressure changes, or nutrient availability, are translated into cellular processes, thus giving rise to new phenotypes without affecting the genotype. Metabolism can be a translator of such environmental changes. It is being recognized more and more how metabolism can not only have a bioenergetic role but also affect signaling, gene expression, epigenetics, post-translational modifications, etc.

I have conducted this work in mouse embryos, where Hidenobu Miyazawa has observed a phenotype in developmental timing as a result of changes in glycolytic flux. Previous data shows that increasing glycolytic flux in the presomitic mesoderm (PSM) slows down the tempo of the segmentation clock (a molecular clock that controls the patterning of the PSM). Because of these previous findings, I was interested in investigating the link between glycolysis and signaling in the PSM.

I addressed the questions in the first part of this work by applying a microfluidics-based entrainment approach. Entrainment is a fundamental property of oscillating systems, which occurs when an oscillator adjusts its phase and its period to an external periodic perturbation, thus getting entrained to it. It has been shown before that glucose can entrain the segmentation clock, so first, I expanded the approach of glycolytic entrainment and tested which glycolytic metabolites can entrain the segmentation clock. The segmentation clock consists of an intricate network of different signaling pathways, such as Notch, Wnt, and FGF. I attempted entrainment of Notch oscillations (which are the core oscillatory component of the segmentation clock) with fructose-6-phosphate (F6P), fructose-1,6-bisphosphate (FBP), and pyruvate. I quantified the efficiency of entrainment by F6P, FBP and pyruvate by using the entrainment phase and in-phase synchrony as readouts. I identified FBP as a Zeitgeber (an external cue that synchronizes an organism's intrinsic clock), which entrained

both Notch and Wnt oscillations based on the predefined criteria. I showed that FBP pulses change the phase of entrainment when pulses are applied at different periods (detunings). I saw a difference in timing to entrainment between Wnt and Notch during entrainment with FBP pulses, hinting at a differential relationship between FBP and these two signaling pathways. The segmentation clock did not get entrained by pulses of pyruvate. Therefore, I suggest that the part of glycolysis that is linked to signaling might be confined between FBP and pyruvate (excluding pyruvate).

Furthermore, I investigated whether glycolysis has a signaling role in the segmentation clock and how glycolysis is functionally linked to signaling during mouse embryo segmentation. I tried to disentangle the functional link of FBP to signaling by entraining with combination pulses of FBP and signaling perturbations of Wnt and Notch. By using predictions from theory of dynamical systems, I showed that FBP functions as a signal in entraining the segmentation clock, hinting at a role of FBP in the PSM that goes beyond its bioenergetic function. I made some predictions about the functional link between FBP and signaling based on the resulting phases of entrainment after applying combined pulses of FBP and signaling perturbations.

In the second part of this work, I explored the presence of glycolytic oscillations in the PSM by using Ca^{2+} oscillations as indirect evidence. I discovered that there are Ca^{2+} oscillations present in the PSM, which are induced by glucose and F6P supplementation in the medium, whereas they are depleted by FBP and pyruvate supplementation. Thus, I gathered some first evidence, which suggests that it might be worth it to develop FBP sensors in mice in order to consolidate the presence of glycolytic rhythms in the PSM.

Zusammenfassung

Neue Phänotypen können in Organismen als Reaktion auf eine sich verändernde Umwelt auftreten. Fluktuationen der unmittelbaren Umweltbedingungen, wie beispielsweise variierende Temperaturen, Druckverhältnisse oder Nährstoffverfügbarkeit, können in zelluläre Prozesse übersetzt werden und so bei konstantem Genotyp zu neuen Phänotypen führen. Der Stoffwechsel, oder Metabolismus, ist einer der möglichen Prozesse, durch welche solche Umweltveränderungen übersetzt werden können. Neue Erkenntnisse zeigen mehr und mehr auf, dass der Stoffwechsel nicht nur eine bioenergetische Rolle allein spielt, sondern auch zelluläre Signalübertragung, Genexpression, Epigenetische Veränderungen oder posttranslationale Modifikationen modulieren kann.

Durch experimentelle Arbeit mit Mausembryonen berichtet Hidenobu Miyazawa von der Beobachtung eines Phänotyps in der temporalen Progression, oder dem Timing, der Embryonalentwicklung als Konsequenz von Änderungen in der Glukose Supplementierung im Medium. Vorangegangene Daten zeigen auf, dass eine Erhöhung des glykolytischen Flusses im PSM das Tempo der Segmentationssuhr (einer molekularen Uhr, die die räumlich-zeitliche Musterbildung innerhalb des PSM steuert) verlangsamt. Diese früheren Ergebnisse dienten als Motivation für eine genauere Untersuchung der Verbindung zwischen Glykolyse und Signalübertragung im PSM zu untersuchen.

Im ersten Teil dieser Arbeit adressierte ich diese Fragestellung mit Hilfe eines auf Mikrofluidik basierendem Entrainment-Ansatzes. Entrainment ist eine grundlegende Eigenschaft oszillierender Systeme, die auftritt, wenn ein Oszillator seine Phase und seine Periode an den eines anderen Oszillators, beispielsweise in Form einer äußeren periodischen Perturbation, anpasst und sich somit in diesem Sinne koppelt ("entraint"). Es wurde bereits gezeigt, dass Glukose die Segmentationsuhr koppeln kann. Auf diesem Ergebnis aufbauend erweiterte ich zunächst den Ansatz des glykolytischen Entrainments und testete,

welche glykolytischen Stoffwechselmetabolite die Segmentationsuhr koppeln können. Die Segmentationsuhr besteht aus einem komplexen Netzwerk verschiedener zellulärer Signalgebungswege, unter anderem Notch, Wnt und FGF. Ich berichte von Versuchen, die Notch-Oszillationen (die die zentrale oszillatorische Komponente der Segmentationsuhr bilden) mit Fruktose-6-Phosphat (F6P), Fruktose-1,6-Bisphosphat (FBP) und Pyruvat zu beeinflussen. Ich quantifizierte die Effizienz des Entrainments durch F6P, FBP und Pyruvat, indem ich die Entrainment-Phase und die phasengleiche Synchronität als Messwerte verwendete. Ich identifizierte FBP als einen Zeitgeber, der nach unseren Kriterien sowohl Notch- als auch Wnt-Oszillations-Entrainment erreichte. Des Weiteren zeigte ich, dass pulsatile FBP-Supplementierung die charakteristische Phase des Entrainments verändert, wenn die Impulse in unterschiedlicher zeitlicher Differenz (Detuning) angewendet werden. Ich sah einen Unterschied im Timing des Entrainments zwischen Wnt und Notch während des Entrainments mit FBP-Pulsen, was auf differenzielle Effekte von FBP auf diese beiden Signalwege hindeutet. Die Segmentationsuhr hat sich an Pyruvat-Pulsen nicht gekoppelt. Aufgrund dieser Ergebnisse mit Pyruvat postulierte ich, dass der Abschnitt der Glykolyse, der mit zellulärer Signalübertragung verbunden ist, auf den Abschnitt zwischen FBP und Pyruvat (ausschließlich Pyruvats selbst) beschränkt sein könnte. Darüber hinaus untersuchte ich, ob die Glykolyse eine Signalfunktion innerhalb der Segmentationsuhr hat und wie die Glykolyse funktionell mit der Signalgebung während der embryonalen Segmentierung des Mausembryos verbunden ist. Ich versuchte, die funktionelle Verknüpfung von FBP mit der Signalübertragung zu entschlüsseln, indem ich FBP-Pulse mit pharmakologischen Signalwegsperturbationen von Wnt und Notch kombinierte. Mit Hilfe von Erwartungen aus der Theorie dynamischer Systeme zeigte ich, dass FBP als Signal bei dem Entrainment der Segmentationsuhr fungiert, was auf eine Rolle von FBP im PSM hinweist, die über seine bioenergetische Funktion hinausgeht. Ich postulierte Eigenschaften der funktionellen Verbindung zwischen FBP und Signalgebung, basierend auf den resultierenden Phasen des Entrainments nach der Anwendung kombinierter Pulse von FBP und Signalwegsperturbationen. Im zweiten Teil unserer Arbeit untersuchte ich das Vorhandensein von glykolytischen Oszillationen im PSM anhand von $[Ca^{2+}]$-Oszillationen. Ich entdeckte, dass es im PSM Ca^{2+}-Oszillationen vorhanden sind, die durch Glukose- und F6P-Zusatz im Medium induziert werden, während sie durch FBP-

und Pyruvat-Zusatz verarmt werden. So sammelte ich erste Beweise, die darauf hindeuten, dass es sich lohnen könnte, FBP-Sensoren in Mäusen zu entwickeln, um das Vorhandensein glykolytischer Rhythmen im PSM zu konsolidieren.

1.

Introduction

1.1 Nature vs Nurture: How environment defines phenotype.

Over the past few decades, the role of the genotype in determining the phenotype of the organism has been extensively studied, while the role of the organism's environment on its phenotype was overlooked. The overarching belief was that all the information was compressed and contained in the genetic information in the nucleus (Weismann (1893); Hertwig (1896)). Interesting history lies behind the gene-centric perspective in developmental biology and evolution. In the late 19th century, embryology was being moved more and more from its ecological environment into the lab. One group of scientists was interested in determining whether the nucleus or the cytoplasm controls developmental outcomes, along with another group, who were focused on studying the morphological mechanisms that lead to such outcomes: both groups competing in this way to explain development (Gilbert (2016)). In the early 20th century, phenotypic variability resulting from environmental factors was considered noise, and genetic determinism of phenotypic outcomes was the focus, especially during World War II when the argument that chromosomes contain all information that makes us who we are fueled eugenics in the US and Europe. This idea that life and personality are defined already at the union of sperm and egg and cannot be instructed later during development is, to this day, erroneously propagated by the anti-abortion movement. All throughout the 20th century, it was thought that all the information that constitutes life and predicts organisms' behavioral and phenotypic outcomes lies within the information encoded in the nucleus, making only the DNA responsible for controlling the program of a developing embryo (Gilbert (2016, 2017)).

Before the century of the gene began, scientists such as Johannsen and Hertwig were proposing that the interactions of embryonic cells with their environment have detrimental outcomes on the embryo's phenotype (Hertwig (1896); Johannsen (1909)). Although they agreed that development is genetically controlled, they argued that the environment could make changes to development, especially in later stages (Roll-Hansen (2009, 2014)). Around this time, the hypothesis of "Reaktionsnorm" was introduced: the norm of reaction (Johannsen (1909)). Reaktionsnorm represents the genetically encoded *potential range* of phenotypes, which can be expressed by the environment's influence. Although the genotype encodes the potential of the organism to manifest different phenotypes, it is the environment that decides which part of that potential will be realized by the organism. Because of this reaction norm, the organism can *titrate* its phenotype based on the strength of the environmental cues (Relyea (2004)). This challenges the idea that the environment is only permissive for the phenotype, while all the instruction lies in the nucleus. There are cases when the environment instructs the organism to build a specific structure, whereas the genome is permissive by encoding the information for building the required structure (Gilbert (2001, 2017)). This ability of the genome to be responsive to the environment is inherited. Over a longer adaptive period of time, the changes caused to the phenotype by the environment can also be fixed in the genome (genetic accommodation) (Nijhout et al. (2021)).

1.1.1 Examples of phenotypic plasticity.

Phenotypic plasticity is defined as the organism's ability to change its phenotypic traits in response to changes in its environment without changing its genotype (Nijhout (2003); Gilbert (2017)). When observed in embryological or larval stages, this ability of the organism is known as developmental plasticity. Examples of developmental plasticity showcase a variety of phenotypes as responses to a wide range of environmental conditions, such as nutrient availability (Kamakura (2011), temperature (Kari and Huey (2000)), pressure (Kirschner et al. (1980)), presence of predators (Relyea (2003)) and so on. I want to introduce some examples where nutrient availability in the embryo's environment defines the later phenotype of the organism, independent of genetic changes. A well-studied example here is the dung beetle (*Onthophagus taurus*). Based on the quality of the larval nutrition, dung beetle males

can develop into large males with a full set of horns or become small males with no horns, exhibiting differences in behavior, morphology, and physiology between them (Emlen and Nijhout (1999); Moczek and Emlen (2000); Moczek (2006)). Similarly, in honey bees, there are strong dimorphisms in queen bees and worker bees that also depend on larval nutrition (Figure 1.1). Queen bees, which are fed with royal jelly during their larval stage, develop a bigger body and more ovaries compared to worker bees (Rachinsky and Hartfelder (1990); Kamakura (2011)). In the work in our lab, we have also observed cases where the mouse embryo's nutritional environment affects its developmental response. Nicole Prior titrated concentrations of glucose ranging from 0.5 to 75 mM and monitored the development of mouse embryo tail explants (Figure 1.2), specifically the formation of somites (precursors of vertebrae) and tail elongation. She observed that with increasing concentrations of glucose, the tails got shorter, and their somite patterning got impaired, indicating that glycolytic alterations are affecting developmental processes in this tissue (Prior (2014)).

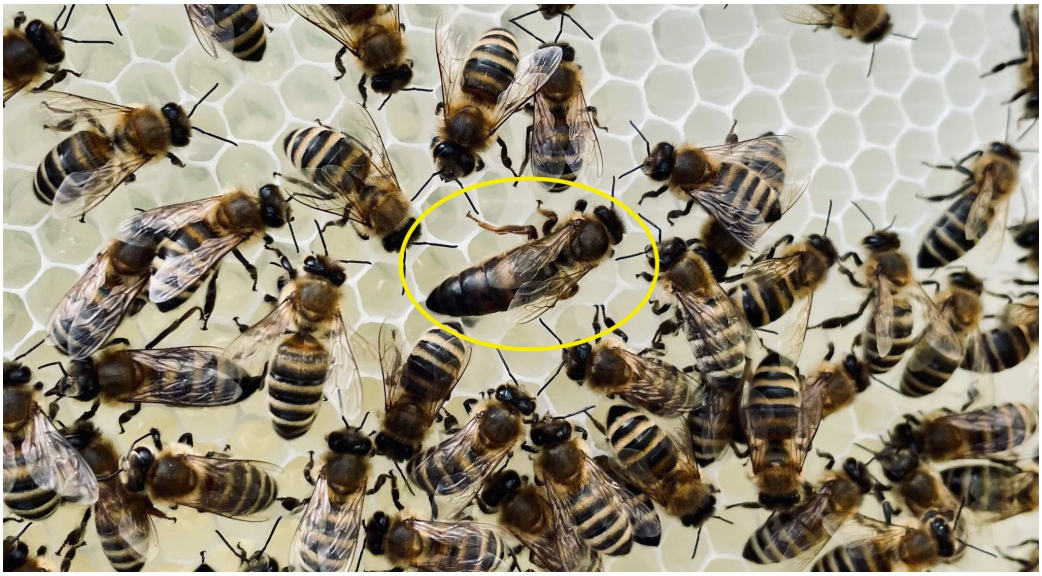

Figure 1.1: Nutritional polyphenism in worker bees and queen bee (middle). Courtesy of the EMBL Bee Club.

1.1.2 The segmentation clock and its response to glucose.

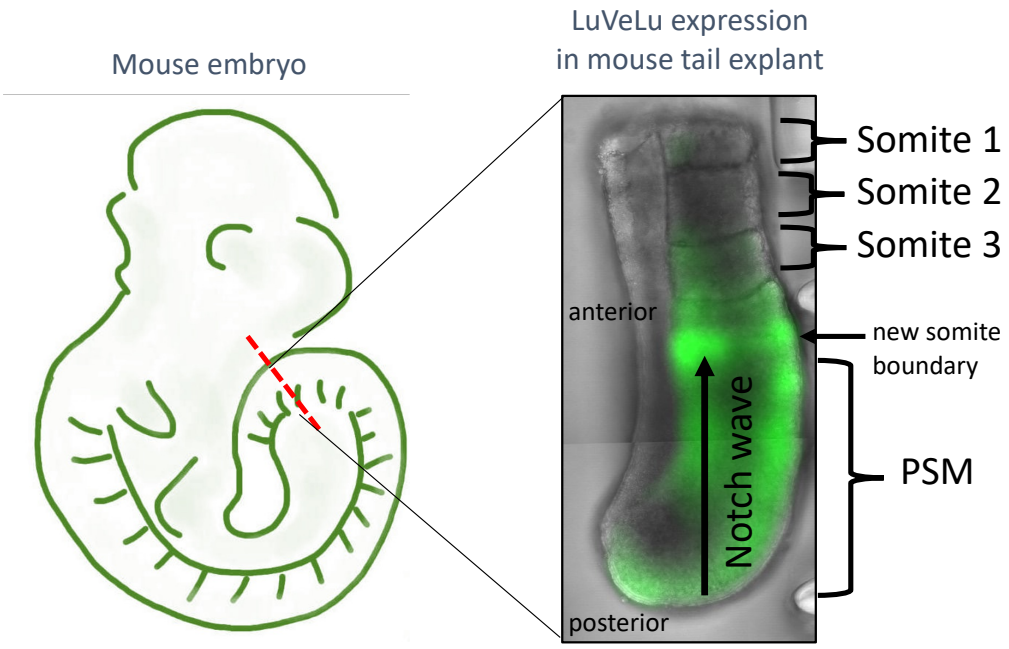

Figure 1.2: Somitogenesis.

Schematic representation of a mouse embryo at stage E10.5 of development. A light microscopy image of the dissected mouse tail explant is shown on the right. The LuVeLu expression can be seen in green.

Apart from drastically affecting the mouse tail phenotype, glycolysis can also fine-tune the process of somite formation. Somites are generated in a periodic fashion in the presomitic mesoderm (PSM) (Figure 1.2). The process of somite formation (i.e., somitogenesis) is controlled by a molecular oscillator called the segmentation clock. The segmentation clock consists of different signaling pathways, such as Notch, Wnt, and FGF (Figure 1.3). The oscillatory activity of Notch, together with signaling information from fibroblast growth factor (FGF), Wnt, and other signaling gradients, is spatially translated into somites. Somites in the mouse embryo are generated every 140 minutes as a periodic Notch signaling wave sweeps the PSM from posterior to anterior, defining the boundary of the new somite at the position where the wave stops (Gibb et al. (2010); Hubaud and Pourquié (2014); Sanaki-Matsumiya

et al. (2022)). In this context, Hidenobu Miyazawa has shown that different levels of glucose in the environment of mouse tail explants can modulate the tempo of the segmentation clock. An increase in glucose concentration can slow down the tempo of the clock. Genetically increasing glycolytic flux in mouse embryos slowed down the tempo of the segmentation clock even further, increasing the period of Notch oscillations to 170 minutes (Miyazawa and Rada (2024)). This was achieved in a transgenic mouse model, in which over-expression of the enzyme cytoPfkfb3 leads to allosteric activation of phosphofructokinase (Pfk), which results in high glycolytic flux (Miyazawa et al. (2022)). These observations raise the question of whether glycolysis works as a messenger between the environment and the segmentation clock by exerting cellular functions that link it to signaling. The next section will introduce how metabolism can translate the environment into cellular processes.

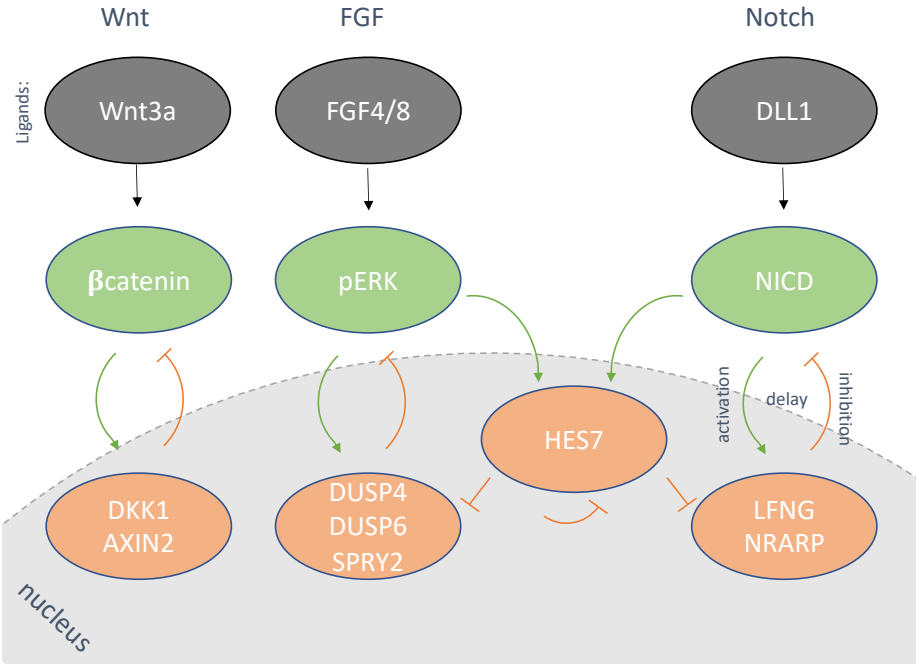

Figure 1.3: Signaling pathways involved in the segmentation clock.

In mouse embryos, the Wnt, FGF, and Notch signaling pathways, which make up the segmentation clock, are shown to be oscillating. The segmentation clock's oscillatory behavior is believed to be generated by negative feedback loops involving time delays. The diagrams show the main ligands of the pathways (grey), which activate downstream players (green) after binding to their respective receptors. The activation of the pathways eventually leads to the rhythmic expression of each pathway's transcriptional effectors (orange). Scheme adapted and modified from Hubaud and Pourquié, 2014.

1.2 The connection of metabolism to cellular programs.

To revisit the role of metabolism, specifically glycolysis, as a translator of the environment, we need to recognize the function of glycolysis beyond its bioenergetic role during development. It is known that there is a gradient of glycolytic activity along the anteroposterior axis of PSM (Bulusu et al. (2017); Oginuma et al. (2017)). This gradient is not connected to cell proliferation in the PSM, which contests its bioenergetic role and makes us wonder about the potential signaling functions of glycolysis in the PSM. It was speculated in the 1940s that metabolism's high spatiotemporal regulation might be relevant for developmental patterning (Child (2011, 1943)). Nowadays, it is becoming increasingly clear how metabolism can go beyond its bioenergetic functions and connect to cell signaling and gene expression through epigenetic and post-translational modifications (Zhang et al. (2021); Xu et al. (2021)).

1.2.1 Organization of glycolysis in time and space.

Glycolysis can be organized spatially in different ways. Glycolytic enzymes and metabolites can have moonlighting functions that are other than their canonical, bio-energetic ones (Chang et al. (2013); Feng et al. (2014)). As a result of this, they can translocate into the nucleus and change transcription and gene expression (Zheng et al. (2003); Waterland and Jirtle (2003)) or bind other proteins, thus exerting signaling functions that affect cell proliferation, survival, hypoxic responses, and so on (Zhang et al. (2017); Peeters et al. (2017); Lee et al. (2015); Bond and Hanover (2015); Hardivillé and Hart (2014); Heidenreich et al. (2020)). This also means that the spatial (nuclear or cytoplasmic) compartmentalization of glycolytic enzymes can indicate whether they exert signaling functions.

Glycolysis is regulated not only in space but also in time; e.g., during the cell cycle, oscillations in energy metabolism oscillate with cell cycle stages (Tu et al. (2005); Tu and McKnight (2006)). The fundamental principle of how glycolytic oscillations occur has already been described in the 60s in yeast cells (Ghosh and Chance (1964); Richard (2003)). The oscillatory activity of Pfk facilitates glycolytic oscillations in yeast. Pfk is positively regulated by its product, FBP, and inhibited by ATP (Figure 1.4). Both FBP and ATP engage in feedback loops with Pfk, thus establishing the enzyme's oscillatory activity (Madsen et al.

(2005). Later on, glycolytic oscillations were discovered in other contexts too, such as in pancreatic β-cells or in muscle cells (Merrins et al. (2016); Tornheim et al. (1991)), where these oscillations are physiologically relevant.

The temporal organization of metabolism allows organisms to match their physiology to environmental changes. Environmental cues, such as nutrients, can work as Zeitgebers (external cues that can synchronize organisms' biological rhythms) and signal circadian time in tissues, such as the liver (Hirao et al. (2009)). Furthermore, metabolic pathways themselves are known to oscillate (e.g. uracil salvage pathway) in a circadian, clock-dependent manner (Eckel-Mahan et al. (2012); Qian and Scheer (2016)). All this demonstrates the complexity of cellular metabolic changes and their effect on cellular processes.

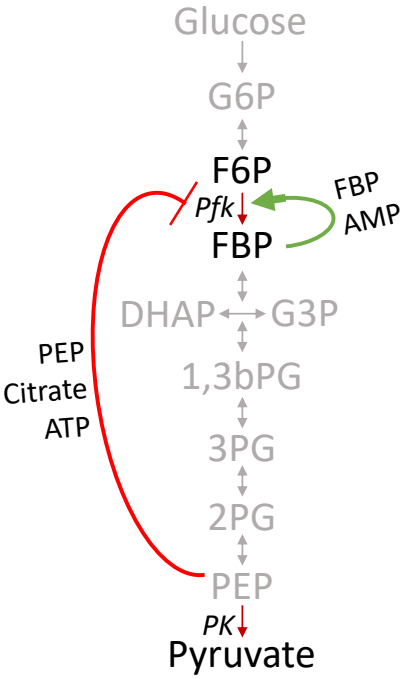

Figure 1.4: Pfk as an oscillophore.

Pfk is allosterically activated by its product, FBP. This increases the glycolytic flux, which leads to more ATP production. ATP and PEP accumulate and feedback into Pfk, negatively regulating Pfk activity and decreasing glycolytic flux. Eventually, this leads to a decrease in ATP and PEP levels, which lifts the inhibition of Pfk, thus upregulating its activity again. The interplay of these negative and positive feedback loops leads to the oscillatory activity of Pfk, making it an oscillophore.

1.2.2 The role of metabolism in the segmentation clock.

In our lab, we have noticed that the presence of the glycolytic metabolite fructose-1,6-bisphosphate (FBP) in the medium of segmenting mouse tail explants affects the segmentation clock more strongly than all other glycolytic metabolites (Prior (2014); Snaebjornsson (2014)). In these experiments, a baseline of 0.5 mM glucose maintains a functional oscillating segmentation clock (Bulusu et al. (2017)). Upon the addition of FBP, the dynamic signaling activity of Notch stops, while the addition of other glycolytic metabolites does not disrupt the clock. Further research revealed FBP to be a sentinel metabolite that mirrors glycolytic flux and potentially affects PSM patterning by changing the subcellular localization of glycolytic enzymes (Miyazawa et al. (2022)). Apart from the role of FBP, other parts of metabolism have been shown to affect PSM development. E.g., changes in central carbon metabolism impact Wnt signaling and the period of the segmentation clock (Gibb et al. (2009)). We have been exploring the instructive role of glycolysis in controlling developmental timing in the PSM (Miyazawa and Rada (2024)).

We can monitor and quantify glycolysis' impact on signaling during the study of somitogenesis. As mentioned before, the segmentation clock instructs somitogenesis and consists of an intricate network of signaling pathways. We can dynamically perturb these pathways and monitor them through quantitative live imaging. That is why I decided to use microfluidics and take an entrainment approach to investigate the link between glycolysis and signaling in the PSM, an approach that I will explain in the next section.

1.3 Entrainment: a property of the segmentation clock.

Entrainment is a universal principle in synchronization that occurs when an autonomous oscillator matches its phase and frequency to that of one other external oscillator. An entrainment-based dynamical systems approach utilizes an oscillator's ability to cycle in synchrony with another external oscillator (Pikovsky et al. (2002); Balanov et al. (2008)). Two or more oscillatory systems synchronize their rhythms when they establish a stable phase relationship. The entrainment approach has been used before to control the segmentation clock by perturbing Notch and Wnt signaling pathways and also to study the interactions of

signaling oscillations during somitogenesis (Sanchez (2021); Sonnen et al. (2018)). Through these previous studies, which were done in spreadouts (an ex vivo PSM culture assay), it was uncovered that Wnt and Notch oscillations are functionally coupled in the PSM, and decoupling them impairs somite formation (Sonnen et al. (2018)).

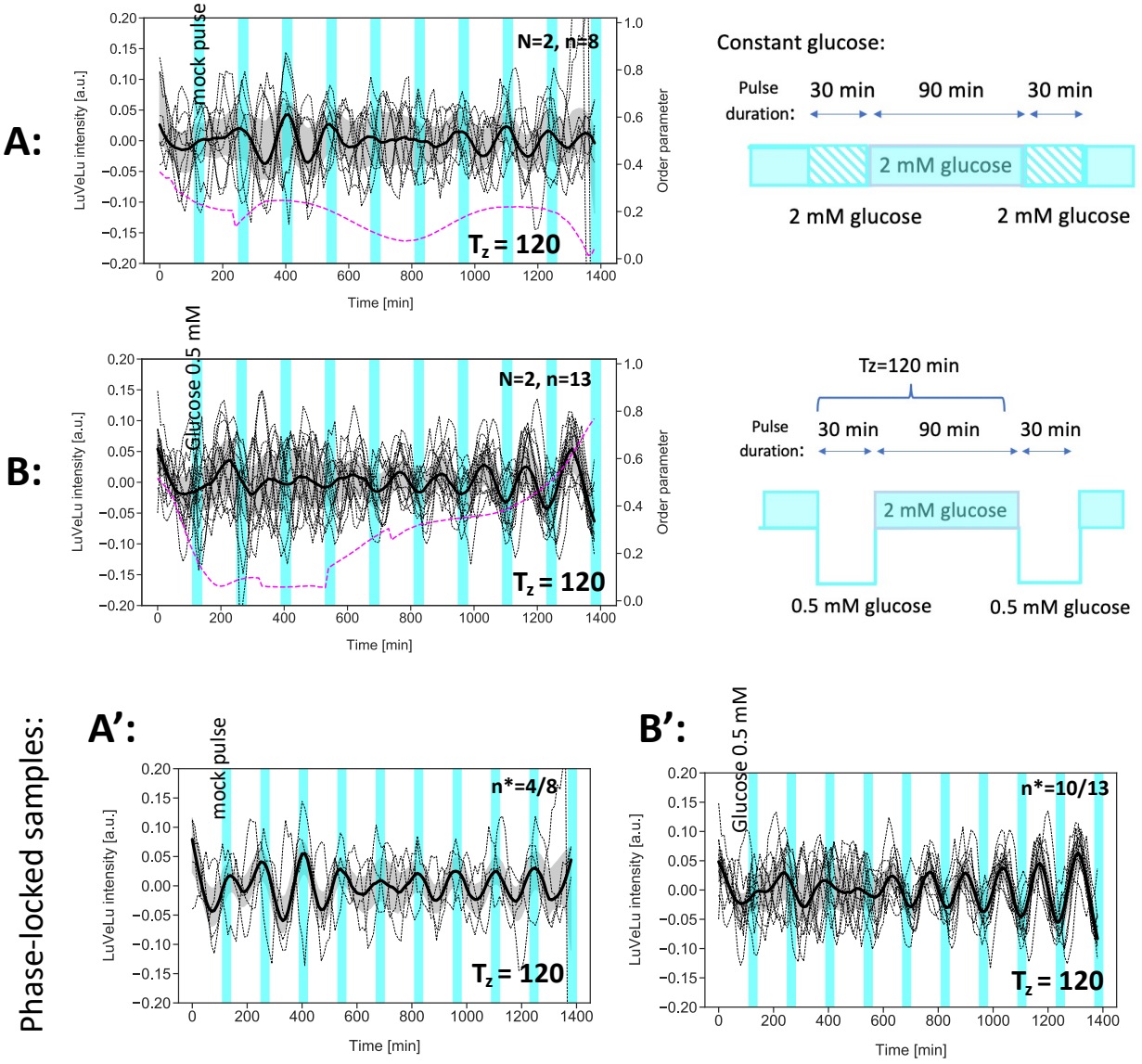

Figure 1.5: Metabolic entrainment of segmentation clock with glucose pulses.

(A,B:) Detrended time-series of LuVeLu oscillations in PSM explants. The detrending was done using a sinc-filter with a cut-off period of 240 minutes. Dashed black lines show single-sample oscillations, the median value of all oscillations is shown by the thick black line and the gray shading shows the first to third quartile range. The magenta line shows the Kuramoto order parameter. The y-axis on the right indicates the Kuramoto values, a value of

one representing complete synchrony of oscillations. All samples were kept in a medium with a constant glucose concentration of 2.0 mM throughout the experiment. Periodic pulses of 0.5 mM glucose **(B)** were applied with a period of 120 minutes and a pulse length of 30-min (cyan). Non-metabolizable glucose (3-OMG) was added to the medium when glucose was absent, to keep the molarity constant. In the control **(A)**, a mock pulse of medium (containing 2 mM glucose) was applied instead of the 0.5 mM glucose pulse. A schematic representation of the experimental setup is depicted on the right side of the time series graphs. (**A', B':**) Detrended time-series of only phase-locked LuVeLu oscillations in PSM explants. n: total number of samples, N: number of experiments, n*: number of phase-locked samples within the total n. See supplementary figure 6.1 for entrainment phase readout. Data and timeseries graphs by Hidenobu Miyazawa.

Previous work by Hidenobu Miyazawa aimed to understand how glycolytic flux is connected to the signaling oscillations in the segmentation clock by using a microfluidic-based entrainment setup. In this setup, mouse embryo tails are dissected and mounted on a microfluidic chip, in which they are exposed to periodic pulses of any chosen compound (Sonnen et al. (2018). Hidenobu Miyazawa tested how periodic changes in glucose concentration affect Notch signaling oscillations in PSM explants. He used the LuVeLu mouse reporter line to visualize Notch signaling oscillations. This line expresses a destabilzed Venus reporter, which is driven from the lunatic fringe (Lfng) promoter, a nuclear target of Notch (Aulehla et al. (2008)). Indeed, changing glycolytic flux with a rhythm of 120 minutes synchronized the segmentation clock of 10 out of 13 PSM samples (Figure 1.5).

The entrainment approach offers a quantitative readout through which one can discriminate the number of samples that get entrained. I determined entrainment efficiency based on the following criteria: **evidence of phase-locking**, which was quantified and visualized on stroboscopic maps, **circular standard deviation (circSD)**, as a quantification of in-phase synchrony and **first Kuramoto order parameter**, which depicts temporal evolution of entrainment between samples.

1.3.1 Characteristics of entrainment.

An entrained oscillation creates a stable phase relationship with the external pulse by adjusting its intrinsic phase to the phase of the external pulse. This is known as phase-locking. An oscillator is phase-locked, i.e. reaches entrainment phase (ϕ_{ent}), when it adjusts its phase to fit the phase of the Zeitgeber and then keeps it constant with the pulse of the Zeitgeber. Characteristics of entrainment (i.e., phase and period of entrainment) can be

affected by parameters, such as detuning (the mismatch between the intrinsic period of the oscillator and the period of the external pulse) and Zeitgeber strength (i.e., the strength of external pulse). A change in detuning increases or decreases the difference between the periods of the endogenous and external oscillator, thus affecting the speed and efficiency of entrainment. In a similar fashion, increasing or decreasing the strength of the Zeitgeber allows the endogenous oscillation to reach entrainment to the external pulse faster or slower, respectively. It is important to remember that an oscillator's entrainment is possible as long as detuning and Zeitgeber strength are modulated within the oscillator's range of entrainment (see discussion: Arnold tongues). Modulating these two parameters too drastically or not strongly enough can result in the system not being able to reach entrainment in the first place.

1.3.2 Criteria for scoring entrainment.

- The first Kuramoto order parameter:

One parameter that captures the temporal evolution of in-phase synchrony between multiple phase oscillators is the first Kuramoto order parameter (KOP) (Figure 1.6). The order parameter achieves its maximum value of 1 when all phases of the oscillators are aligned identically. The lowest value this parameter can reach is 0, which indicates that none of the oscillators have the same phase as another oscillator, and no in-phase synchrony is achieved. By following the temporal change of the Kuramoto order parameter (average value between all samples), one can see the temporal evolution of all samples towards phase-locking. The value of the first Kuramoto order parameter between the last two pulses is a complementary or indirect readout for entrainment in that it indicates how in-phase the samples are by the end of the experiment.

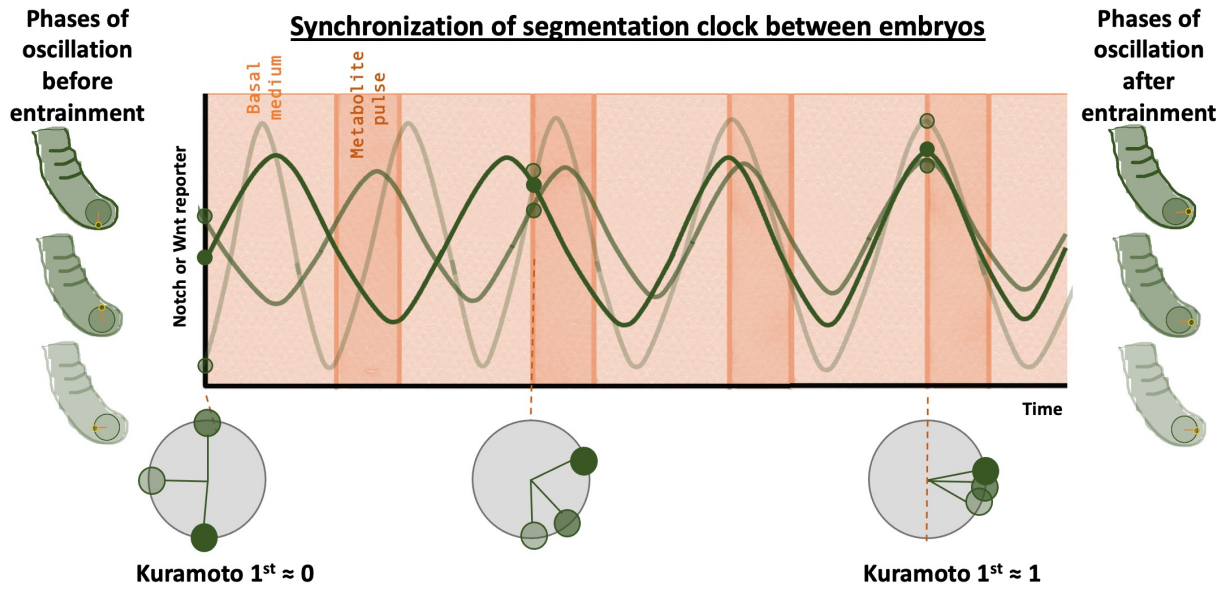

Figure 1.6: Kuramoto first order parameter captures synchrony between two or more oscillators.

- Circular standard deviation and phase-locking:

Another parameter that captures the degree of in-phase synchrony between samples by the end of entrainment is the circular standard deviation (circSD). circSD is used as a measure to report the spread of sample phases at the end of experiment. circSD is visualized with a magenta cross on the stroboscopic map. Stroboscopic maps depict changes that happen to the phase of oscillation in time while the oscillation is being exposed to an external perturbation (Figure 3.3). A dot on the stroboscopic map plots the value of the phase at the moment the oscillation encounters the external pulse (old phase, ϕ_{n}) over the value of the phase at the time the oscillation encounters the next external pulse that will follow (new phase, $\phi_{\mathrm{n+1}}$). If the oscillation gets entrained to the external pulse, the difference between the phase of oscillation and the phase of the external pulse will gradually become zero. This is reflected as a gradual conversion of the dots toward the diagonal, where the old phase equals the new phase. The fixed region on the diagonal around which the dots converge indicates the entrainment phase (ϕ_{ent}). It is worth noting here that the spread of the dots

around ϕ_{ent} represents in-phase synchrony and is quantified by circSD. Our phase criterion for phase-locking is defined as the number of samples with a phase difference of less than $\pi/8$ at the last two pulses. If a sample fulfills this criterium, it is considered phase-locked (i.e. entrained) (Figure 1.7).

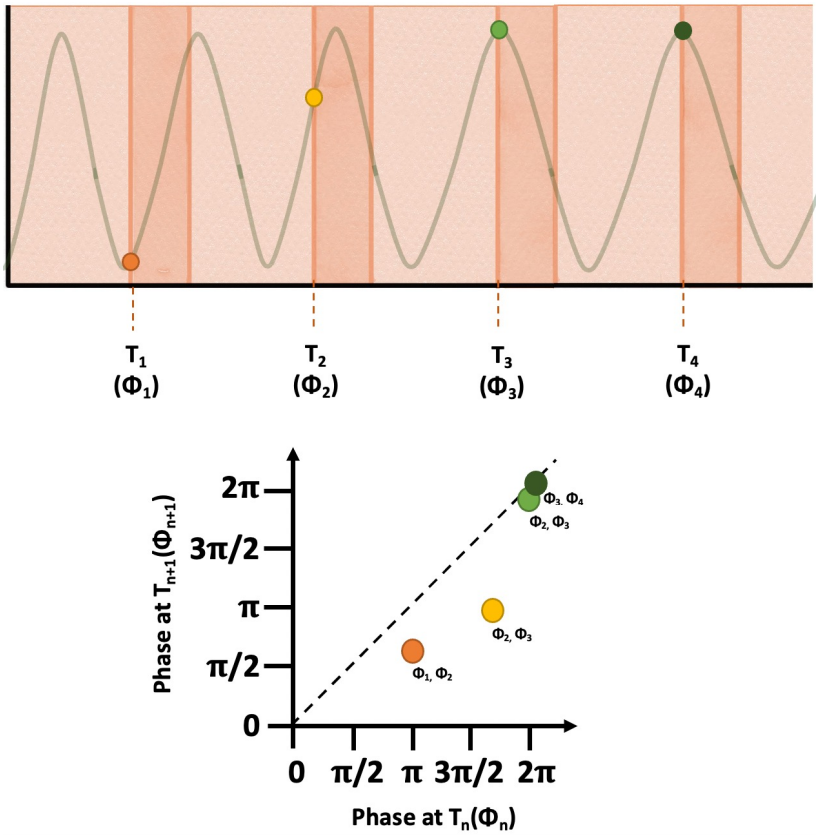

Figure 1.7: Stroboscopic maps visualize progressive changes of phase at each pulse. Figure adapted and modified from Sanchez et al. 2022.

In summary, I have introduced the idea that new phenotypes can arise in organisms as a response to changing environments, and metabolism can be a translator of such environmental changes. This work is conducted in mouse embryos, where we have observed a phenotype in developmental timing as a result of changes in glucose supplementation in the medium (Miyazawa and Rada (2024)). Previous data shows that increasing glycolytic flux in the PSM slows down the tempo of the segmentation clock(Miyazawa and Rada (2024)). This thesis uses the above-mentioned criteria to score metabolic entrainment in order to investigate whether glycolysis has a signaling role in the PSM and shed light on the functional link

between signaling in the segmentation clock and glycolysis. The specific aims of the thesis are presented next.

2.

Aims of this study

The motivation behind this project was to explore how metabolism affects the plasticity of a phenotype, which, in this case, is developmental timing. To this end, I used the PSM as a model to monitor developmental timing by following the oscillations of the segmentation clock. I have evidence that changing glycolytic flux in the PSM affects the tempo of the segmentation clock (Miyazawa and Rada (2024)). The main goal of this project was to investigate whether glycolysis itself has a signaling role in the segmentation clock and to better understand this link between glycolysis and signaling in the PSM. While there are many ways in which such a link can be explored, I aimed to:

1) identify **which glycolytic metabolites are linked to signaling** in the PSM (**Part I**),

2) investigate **whether glycolysis has a non-canonical signaling role** (**Part I**)

3) explore if **glycolytic oscillations** are present in the PSM (**Part II**).

In **Part I**, I used microfluidics-based entrainment, which is a top-down approach to studying dynamical systems. Entrainment allows us to use transient, non-genetic perturbations to address these questions. Oscillating systems (i.e., the segmentation clock) follow universal entrainment principles, the properties of which (period, phase, synchrony, etc) I can quantify.

To identify which glycolytic metabolites are linked to signaling in the PSM (**Aim 1**), I tested several glycolytic metabolites and checked which ones can entrain the segmentation clock by scoring the phase of entrainment and in-phase synchrony.

To investigate whether glycolysis has a signaling function (**Aim 2**), I dynamically perturbed the segmentation clock with combinations of both glycolytic and signaling perturbations. The goal was to use dynamical systems theory predictions on the phase of entrainment

to explain the outcomes. Furthermore, I aimed to refer to these predictions to understand how glycolysis is functionally linked to signaling in the segmentation clock.

In **Part II**, I move away from the microfluidics-based entrainment approach and instead use Ca^{2+} oscillations as a gateway to explore the possible existence of metabolic rhythms in the PSM, specifically glycolytic oscillations (**Aim 3**).

3.

Results: Part I

3.1 Metabolic entrainment: which dynamic glycolytic perturbations can synchronize the segmentation clock?

3.1.1 Providing the segmentation clock with F6P pulses at a period of 120 minutes.

While periodic glucose pulses can entrain the segmentation clock, little is known about the potential of other glycolytic metabolites to dynamically perturb signaling during PSM development. In this chapter I aimed to identify which glycolytic metabolites downstream of glucose can entrain the segmentation clock. My goal was to quantify the entrainment efficiency of different glycolytic metabolites to identify candidate metabolites or parts of glycolysis that link glycolysis to signaling. I focused on F6P and FBP, the substrate and product of the Pfk reaction: an irreversible reaction in glycolysis, thus a major regulatory point. I also tested pyruvate, the last metabolite in glycolysis, the product of pyruvate kinase (PK), another enzymatic control point (Figure 3.1).

I started by testing the entrainment efficiency of F6P. I monitored oscillations of the dynamic Notch signaling reporter LuVeLu in mouse tail explants during periodic perturbations with F6P pulses. The endogenous segmentation clock period in mouse embryos is 140 minutes. With the aim of speeding up the tempo of the segmentation clock to 120 minutes, I provided a glycolytic pulse of 4mM F6P, in addition to the basal levels of 2 mM glucose in the medium.

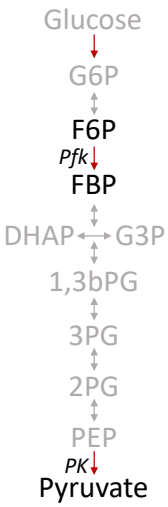

Figure 3.1: Tested glycolytic metabolites for entrainment of segmentation clock.

I quantified how efficiently I could entrain the segmentation clock with glycolytic metabolites, starting with 4mM F6P pulses. I found evidence that 7 out of 13 tail explants locked the phase of their Notch oscillations to the phase of F6P pulses (Figure 3.2). The stroboscopic maps show 7 tail samples that converge towards the diagonal.

To analyze the distribution of phase-locking across samples, I calculated the circular standard deviation, which indicates the in-phase synchrony of the samples that have converged towards the diagonal of the stroboscopic map. Both the phase of entrainment and circSD were taken into consideration when quantifying the number of entrained samples. Although 7 out of 13 samples got phase-locked to the phase of 4 mM F6P pulses, the in-phase synchrony between all samples was as high as that of the controls (Figure 3.2).

Next, to test whether higher concentrations of F6P would lead to more efficient entrainment, I provided Notch oscillations with pulses of 20 mM F6P, keeping the Zeitgeber period (T_z) at 120 minutes. As shown in figure 3.2, the number of phase-locked samples decreased in these parameters: 2 out of 16 samples locked their oscillation phase to 20 mM F6P. Combined, these results show that at a period of 120 minutes, 7 out of 13 samples show phase-locking with 4 mM pulses of F6P; however, the in-phase synchrony of these samples was comparable to the control condition. Higher concentrations of F6P did not make entrainment more efficient. In fact, the 20 mM F6P condition even lowered efficiency by showing phase-locking for 2 out of 16 samples.

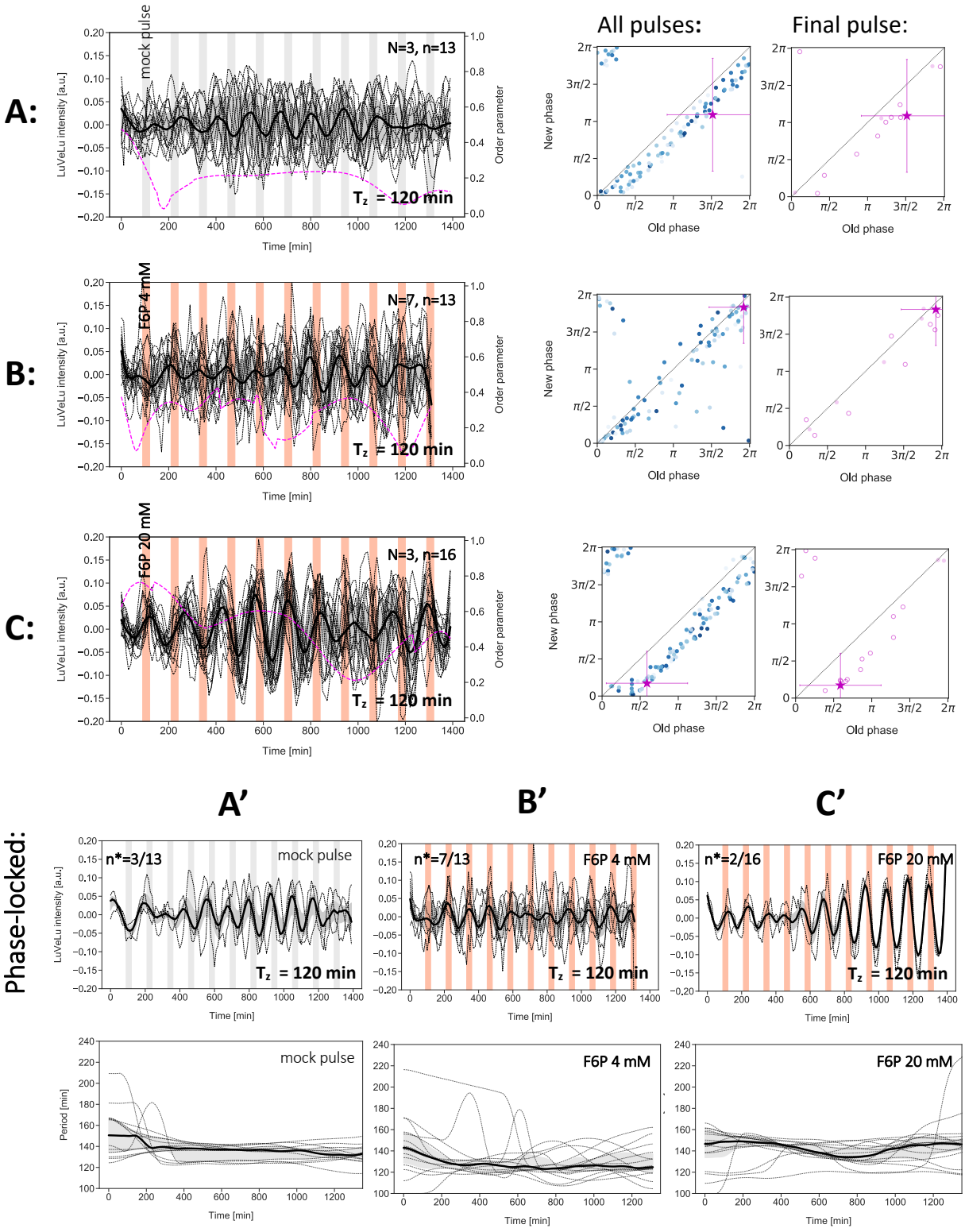

Figure 3.2: Perturbations of LuVeLu oscillations with periodic pulses of F6P, at a period of 120 minutes.

(A-C:) Detrended time-series of LuVeLu oscillations in PSM explants. The detrending was done using a sinc-filter with a cut-off period of 240 minutes. Dashed black lines show single-sample oscillations, the median value of all oscillations is shown by the thick black line and the gray shading shows the first to third quartile range. The magenta line shows the Kuramoto order parameter. The y-axis on the right indicates the Kuramoto values, a value of one representing complete synchrony of oscillations. Samples were kept in a medium with a constant glucose concentration of 2.0 mM throughout the experiment. Periodic pulses of 4 mM F6P (A) or 20 mM F6P (B) were applied with a period of 120 minutes and a pulse length of 30-min (orange). Non-metabolizable glucose (3-OMG) was added to the medium when F6P was absent, to keep the molarity constant. In the control, a mock pulse (light grey) of medium was applied instead of the glycolytic pulse. n: total number of samples, N: number of experiments, n*: number of phase-locked samples within the total n. Corresponding stroboscopic maps that depict a step-wise progression of the phase of LuVeLu oscillations during the experiment are shown on the right side of each time-series graph. Each dot represents a snapshot of the phase of the oscillation at the beginning of the F6P pulse (old phase) plotted against the phase of the oscillations at the beginning of the *next* F6P pulse (new phase). The phase of entrainment can be read out from the region around the diagonal, to which the dots have converged (marked here with a magenta star). The spread of the dots represents in-phase synchrony and is quantified by circSD (magenta cross). The blue shading of the dots depicts the step-wise phase progression of every sample (n) in time. Darker dots represent later time points. The magenta dots represent the phase dynamics of every sample (n) at the last external pulse. The filled magenta dots represent phase-locked LuVeLu oscillations (n*). The unfilled magenta circles represent non-phase-locked LuVeLu oscillations. (**A', C':**) Detrended time-series of only phase-locked LuVeLu oscillations in PSM explants. Below each graph, the time progression of the periods of all samples is shown for the corresponding condition.

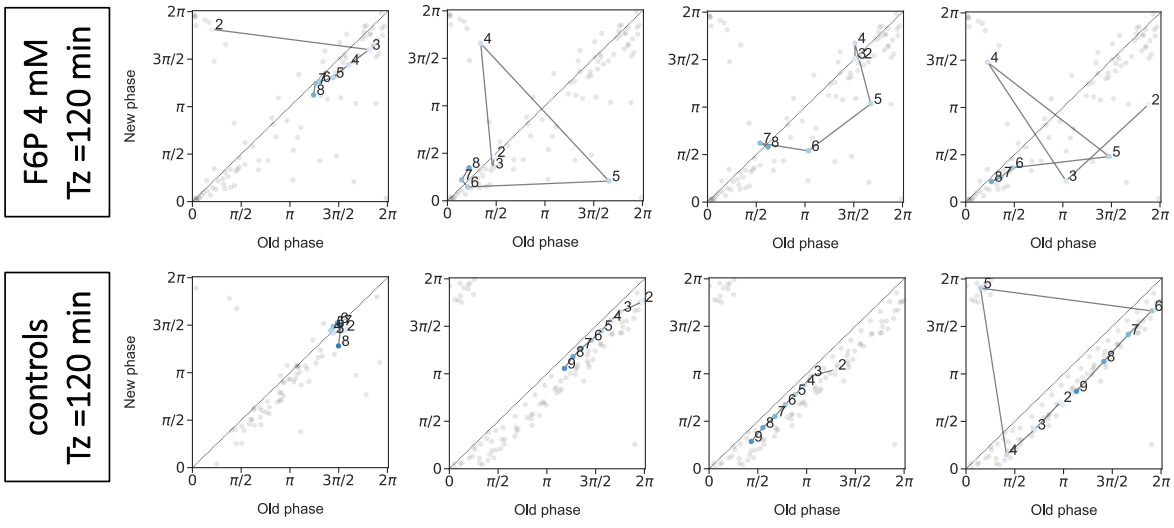

Figure 3.3: Representative stroboscopic maps of entrained samples and controls.

(A, B:) Stroboscopic maps that depict a step-wise progression of the phase of LuVeLu oscillations during the experiment. Eight maps depicting the phase progression of single representative samples are shown. Each dot represents a snapshot of the phase of the oscillation at

the beginning of the F6P pulse (old phase) plotted against the phase of the oscillations at the beginning of the *next* F6P pulse (new phase). The phase of entrainment can be read out from the region around the diagonal, to which the dots have converged. The blue shading of the dots depicts the progression of the phase of one single oscillation in time., with darker dots being the later time points. Grey dots in the background show an overview of all the samples in the experiment. The numbers on the dots represent the numbers of the external pulses: (A) 4 mM F6P and (B) mock pulse (control).

3.1.2 FBP pulses entrain the segmentation clock at a period of 140 minutes.

For the next metabolite, I tested the entrainment efficiency of FBP pulses on Notch oscillations. Previous findings in the lab (see introduction) have shown that a constant application of 20 mM FBP on mouse tail explants completely stops dynamic Notch oscillations. Therefore, I was curious to see the effect of a pulsatile application of FBP in clock dynamics. I initially applied pulses of 4 mM FBP at a period of 120 mins (Figure 3.4). 4 out of 11 tail samples showed evidence for phase-locking to the phase of FBP pulses at these conditions. circSD showed a high value, indicating low in-phase synchrony between these 4 samples. I decided to increase the concentration to 20 mM FBP to see if the entrainment efficiency of FBP increases accordingly. Similarly, with pulses of 20 mM FBP, 4 out of 12 tail samples showed phase-locking to a $\phi_{\text{ent}}=3\pi/2$.

Finally, I decided to change the Zeitgeber period and see how that affected the efficiency of entrainment with FBP. I applied periodic pulses of 20 mM FBP at a Zeitgeber period of 140 min, which matches the natural period of the segmentation clock. When applied at a concentration of 20 mM and a period of 140 mins, FBP entrained 13 out of 20 tail samples, which show evidence for phase-locking at the peak of oscillations ($\phi_{\text{ent}}=0$) (Figure 3.4). The oscillations were highly synchronous, with a small circSD value, compared to the other conditions and controls (see Supplement). In summary, these results show that the entrainment efficiency of 20 mM FBP pulses increases significantly at a Zeitgeber period of 140 minutes, leading to 13 out of 20 samples getting entrained with high in-phase synchrony.

A:

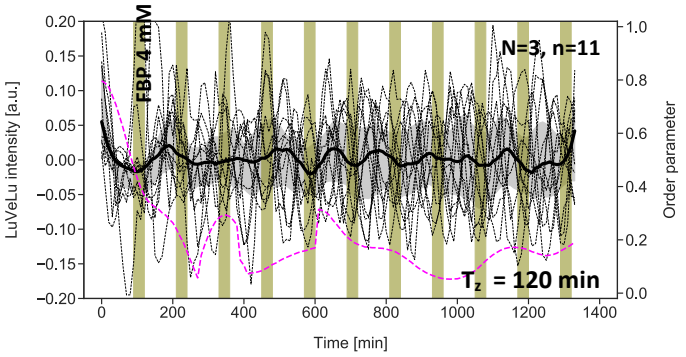

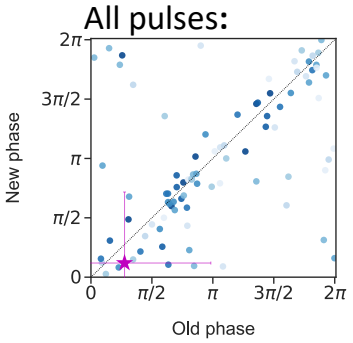

A': Phase-locked:

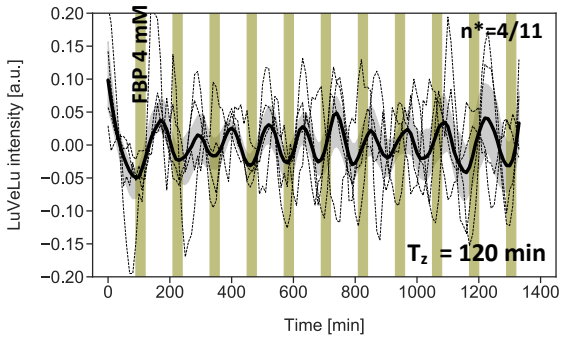

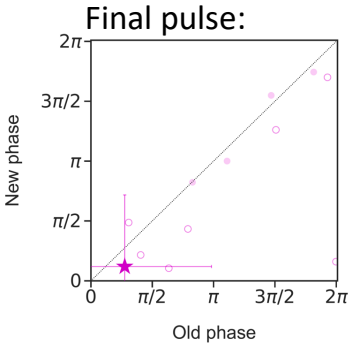

B:

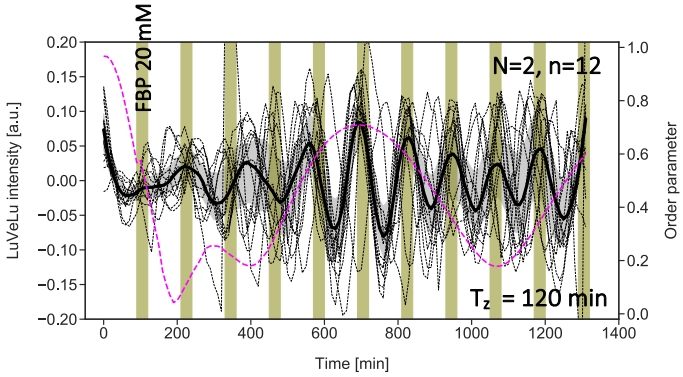

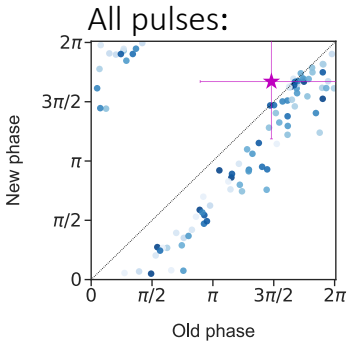

B': Phase-locked:

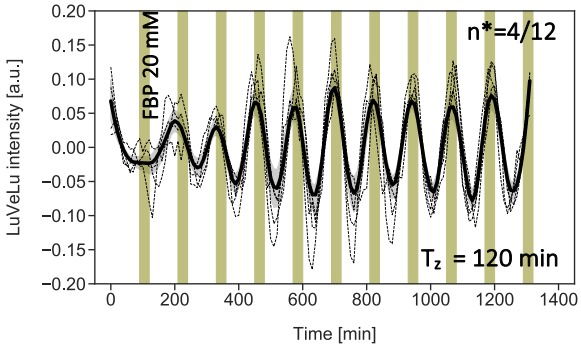

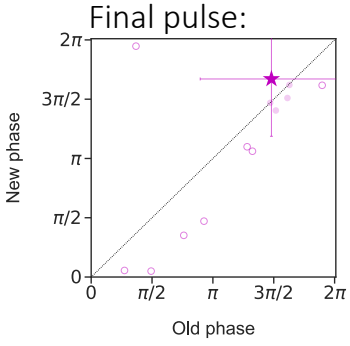

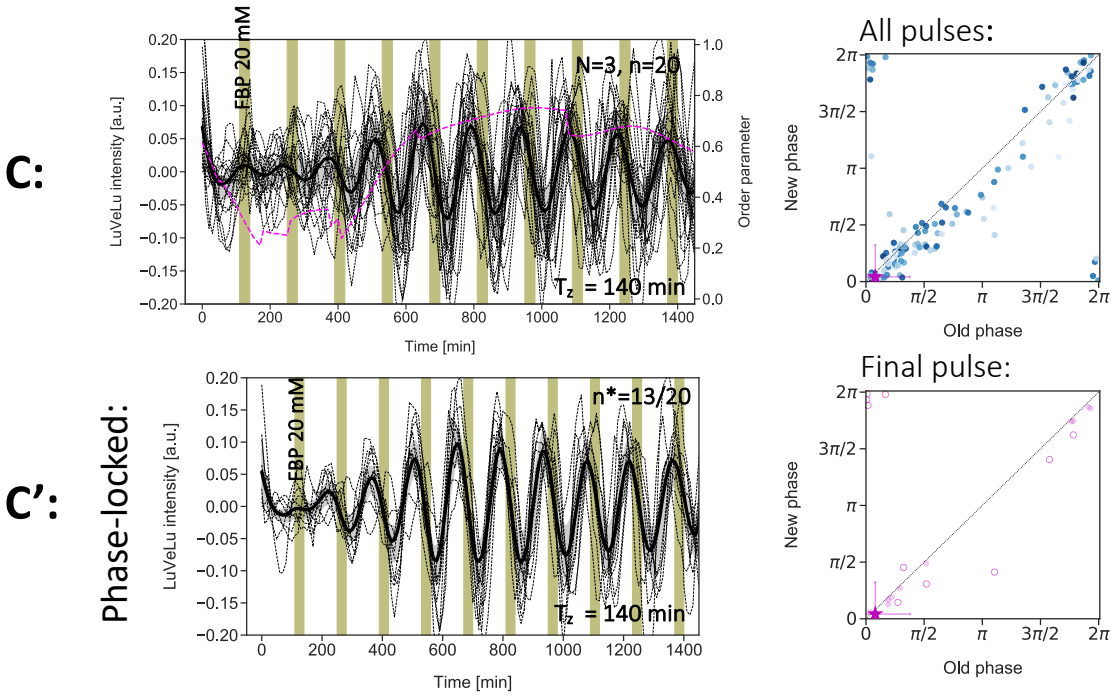

Figure 3.4: Perturbations of LuVeLu oscillations with periodic pulses of FBP.

(A,B:) Detrended time-series of LuVeLu oscillations in PSM explants. The detrending was done using a sinc-filter with a cut-off period of 240 minutes. Dashed black lines show single-sample oscillations, the median value of all oscillations is shown by the thick black line and the gray shading shows the first to third quartile range. The magenta line shows the Kuramoto order parameter. The y-axis on the right indicates the Kuramoto values, a value of one representing complete synchrony of oscillations. Samples were incubated in a constant glucose concentration of 2.0 mM throughout the experiment. Periodic pulses of (**A, A'**) 4 mM FBP or (**B, B'**) 20 mM FBP were applied with a period of 120-min and a pulse length of 30-min (green). Periodic pulses of 20 mM FBP were applied with a period of (**C, C'**) 140-min and a pulse length of 30-min (green). Non-metabolizable glucose (3-OMG) was added to the medium when FBP was not present to keep the molarity constant. n: total number of samples, N: number of experiments, n*: number of phase-locked samples within the total n. Corresponding stroboscopic maps that depict a step-wise progression of the phase of LuVeLu oscillations during the experiment are shown on the right side of each time-series graph. Each dot represents a snapshot of the phase of the oscillation at the beginning of the FBP pulse (old phase) plotted against the phase of the oscillations at the beginning of the *next* FBP pulse (new phase). The phase of entrainment can be read out from the region around the diagonal, to which the dots have converged (marked here with a magenta star). The spread of the dots represents in-phase synchrony and is quantified by circSD (magenta cross). The blue shading of the dots depicts the step-wise phase progression of every sample (n) in time. Darker dots represent later time points. **(A', B,' C':)** Detrended time-series of only phase-locked LuVeLu oscillations in PSM explants. Corresponding stroboscopic maps of phase-locked samples are shown on the right. The magenta dots represent the phase dynamics of every sample (n) at the last external pulse. The filled magenta dots represent phase-locked LuVeLu oscillations (n*). The unfilled magenta circles represent non-phase-locked LuVeLu oscillations.

3.1.3 20 mM pyruvate pulses are not sufficient to entrain the segmentation clock to a period of 120 or 140 minutes.

As a next step, I tested entrainment of the segmentation clock with pyruvate, the last metabolite in the glycolytic pathway.

The initial concentration I chose for pyruvate pulses was 8 mM, which stoichiometrically corresponds to 4 mM F6P or FBP. As depicted in figure 3.5, pulses of pyruvate at this concentration did not entrain the segmentation clock to 120 minutes. 1 out of 5 samples locked its phase to the phase of 4mM pyruvate pulses. Increasing the concentration of pyruvate to 20 mM and changing the entrainment period to 140 minutes also did not improve the entrainment efficiency by pyruvate: 3 out of 17 samples showed evidence for phase-locking. Compared to 20 mM F6P and 20 mM FBP, pyruvate pulses showed the lowest efficiency in entraining the segmentation clock at a period of 140 minutes.

In summary, I tested several entrainment parameters to gauge which glycolytic metabolites can entrain the segmentation clock. I focused on F6P, FBP, and pyruvate, all of which are involved in irreversible regulatory reactions in glycolysis. Based on the entrainment criteria defined before, 20 mM FBP with pulses of 140 minutes entrained the most samples (n* = 13/20), and the samples reached high in-phase synchrony, based on circSD readout (Figure 3.4). The number of samples entrained by 20 mM F6P (n* = 2/16) and 20 mM pyruvate (n* =3/17) was considerably smaller and comparable to the controls (Figures 3.2, 3.5). I conclude that I have the strongest evidence of entrainment by FBP and the least evidence of entrainment by pyruvate. Since previous data suggests that glucose entrains the segmentation clock and I have some evidence of entrainment by F6P, this data suggests that the link between glycolysis and signaling is confined in the part of glycolysis between FBP and pyruvate, excluding pyruvate. Therefore, I focused on FBP to further explore the functional link between glycolysis and the segmentation clock through microfluidic entrainment.

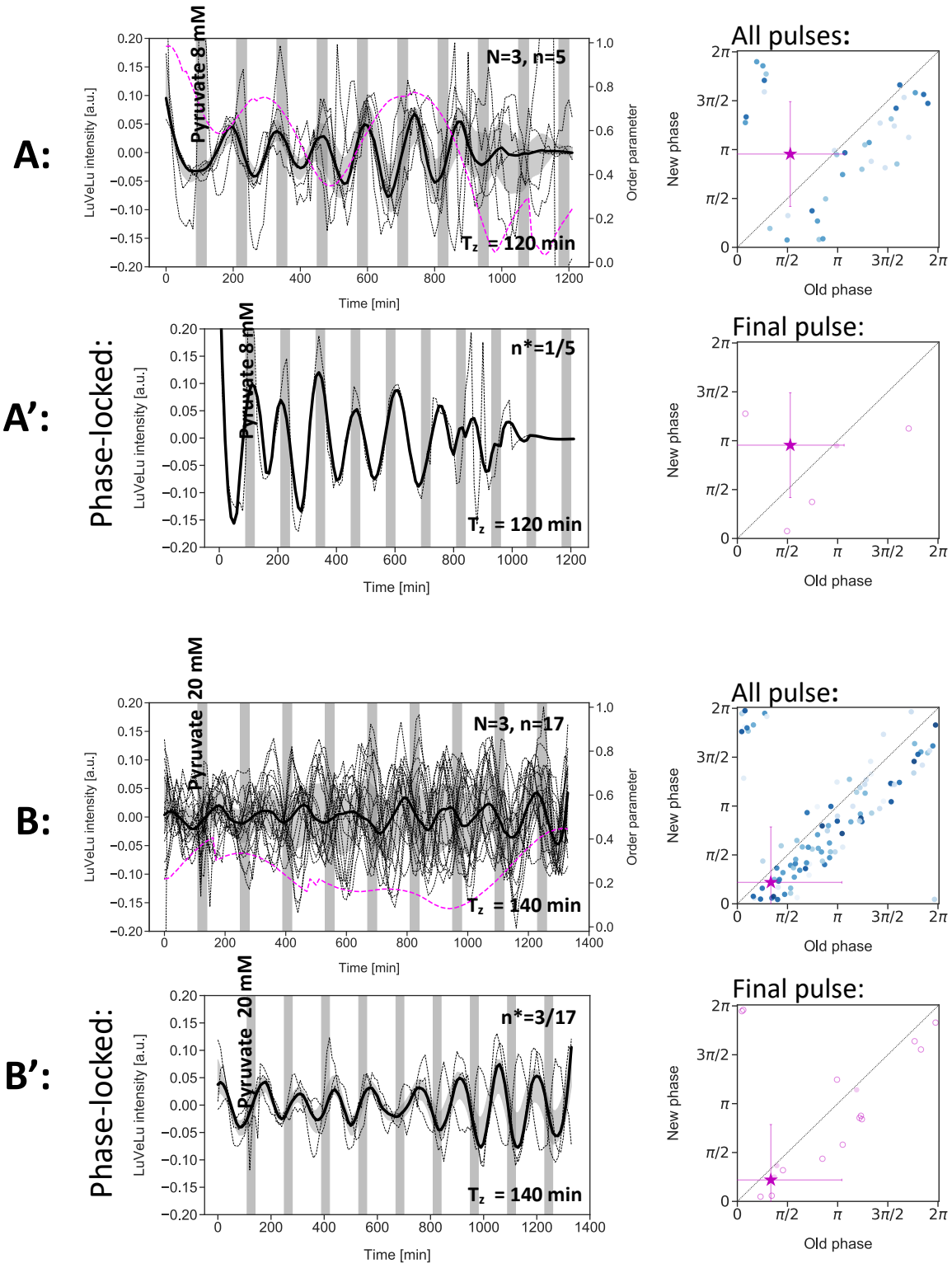

Figure 3.5: Perturbations of LuVeLu oscillations with periodic pulses of pyruvate.

(A,B:) Detrended time-series of LuVeLu oscillations in PSM explants. The detrending was done using a sinc-filter with a cut-off period of 240 minutes. Dashed black lines show single-sample oscillations, the median value of all oscillations is shown by the thick black line and the gray shading shows the first to third quartile range. The magenta line shows the Kuramoto order parameter. The y-axis on the right indicates the Kuramoto values, a value of one representing complete synchrony of oscillations. Samples were incubated in a constant glucose concentration of 2.0 mM throughout the experiment. Periodic pulses of 8 mM pyruvate (**A, A'**) or 20 mM pyruvate (**B, B'**) were applied with a period of 120 minutes and 140 minutes, respectively. The pulse length is 30-min (gray). Non-metabolizable glucose (3-OMG) was added to the medium when pyruvate was not present to keep the molarity constant. n: total number of samples, N: number of experiments, n*: number of phase-locked samples within the total n. Corresponding stroboscopic maps that depict a step-wise progression of the phase of LuVeLu oscillations during the experiment are shown on the right side of each time-series graph. Each dot represents a snapshot of the phase of the oscillation at the beginning of the pyruvate pulse (old phase) plotted against the phase of the oscillations at the beginning of the *next* pyruvate pulse (new phase). The phase of entrainment can be read out from the region around the diagonal, to which the dots have converged (marked here with a magenta star). The spread of the dots represents in-phase synchrony and is quantified by circSD (magenta cross). The blue shading of the dots depicts the step-wise phase progression of every sample (n) in time. Darker dots represent later time points. **(A', B':)** Detrended time-series of only phase-locked LuVeLu oscillations in PSM explants. Corresponding stroboscopic maps of phase-locked samples are shown on the right. The magenta dots represent the phase dynamics of every sample (n) at the last external pulse. The filled magenta dots represent phase-locked LuVeLu oscillations (n*). The unfilled magenta circles represent non-phase-locked LuVeLu oscillations.

3.1.4 20 mM FBP pulses with a period of 140 minutes entrain Wnt oscillations.

The previous results put the focus on FBP as a glycolytic metabolite, which can entrain Notch oscillations with the highest efficiency. To further characterize the effect of FBP entrainment on the segmentation clock, I looked at another component of the clock; I tested the effect of FBP pulses on Wnt signaling oscillations.

To visualize Wnt oscillations, I imaged the Axin2-Achilles line. I used the same entrainment parameters that I had used when perturbing Notch oscillations: a concentration of 20 mM FBP and pulses at a period of 140 minutes. 4 out of 4 samples showed phase-locking to FBP pulses. I observed a synchronization of Wnt oscillations to FBP pulses already at the second pulse (Figure 3.6, KOP=0.9) and a phase-locking at $\phi_{\text{ent}}=\pi$, at the trough of the oscillations. Although I did not have many replicates for this experiment, I observed that FBP entrained every sample (n* = 4/4).

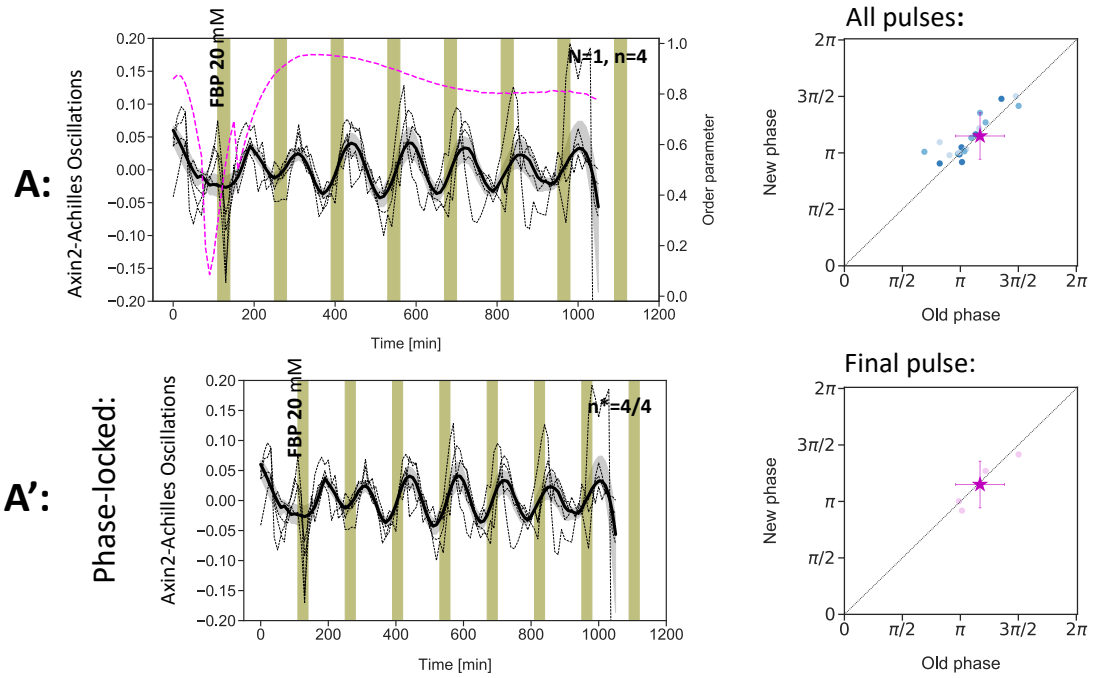

Figure 3.6: Perturbations of Axin2-Achilles oscillations with periodic pulses of FBP, at a period of 140 minutes.

(A:) Detrended time-series of Axin2-Achilles oscillations in PSM explants. The detrending was done using a sinc-filter with a cut-off period of 240 minutes. Dashed black lines show single-sample oscillations, the thick black line shows the median value of all oscillations, and the gray shading shows the first to third quartile range. The magenta line shows the Kuramoto order parameter. The y-axis on the right indicates the Kuramoto values, a value of one representing complete synchrony of oscillations. Samples were incubated in a constant glucose concentration of 2.0 mM throughout the experiment. Periodic pulses of 20 mM FBP were applied with a period of 140 minutes and a pulse length of 30 minutes (green). Non-metabolizable glucose (3-OMG) was added to the medium when FBP was absent to keep the molarity constant. n: total number of samples, N: number of experiments, n*: number of phase-locked samples within the total n. Corresponding stroboscopic maps that depict a step-wise progression of the phase of LuVeLu oscillations during the experiment are shown on the right side of each time-series graph. Each dot represents a snapshot of the phase of the oscillation at the beginning of the FBP pulse (old phase) plotted against the phase of the oscillations at the beginning of the *next* FBP pulse (new phase). The phase of entrainment can be read out from the region around the diagonal, to which the dots have converged (marked here with a magenta star). The spread of the dots represents in-phase synchrony and is quantified by circSD (magenta cross). The blue shading of the dots depicts the step-wise phase progression of every sample (n) in time. Darker dots represent later time points. **(A':)** Detrended time-series of only phase-locked Axin2-Achilles oscillations in PSM explants. Corresponding stroboscopic maps of phase-locked samples are shown on the right. The magenta dots represent the phase dynamics of every sample (n) at the last external pulse. The filled magenta dots represent phase-locked Axin2-Achilles oscillations (n*). The unfilled magenta circles represent non-phase-locked Axin2-Achilles oscillations.

3.1.5 Wnt oscillations respond first to entrainment by FBP, while Notch oscillations follow with a time delay.

Having seen that FBP efficiently entrains both Notch and Wnt oscillations in the mouse PSM, I analyzed the time to entrainment using the quantification for the evolution of in-phase synchrony between samples during entrainment. Based on the first Kuramoto order parameter, I noticed that Wnt and Notch oscillations lock their phase to pulses of FBP at significantly different times. As seen in figure 3.7, KOP reaches a value of high synchrony, already at the second FBP pulse during Wnt entrainment. Notch oscillations lock their phase to FBP pulses at the fifth FBP pulse. This indicated that there might be a different functional link between FBP and Wnt signaling versus FBP and Notch signaling.

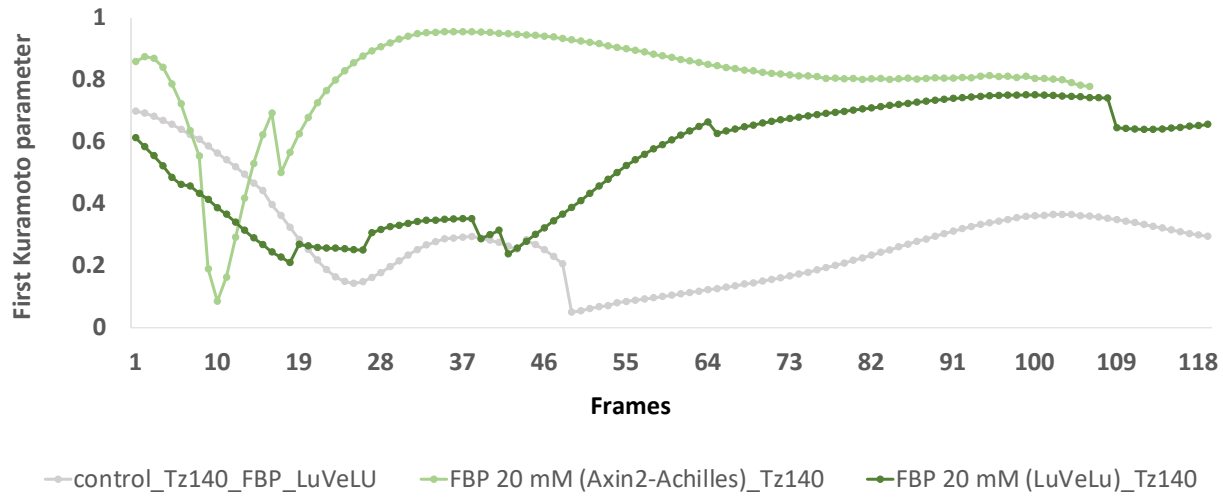

Figure 3.7: Temporal evolution of first Kuramoto order parameters during entrainment of Notch and Wnt oscillations with periodic pulses of FBP at a period of 140 minutes.

To expand on the previous finding about the time to entrainment with FBP pulses, I aimed to compare the temporal evolution of entrainment of Notch oscillations exposed to glycolytic modulators (e.g., glycolytic metabolites) vs. signaling modulators (e.g., activators/inhibitors of Notch/Wnt). Therefore, I provided Notch oscillations in mouse PSM explants with two drugs that perturb specifically Notch and Wnt pathways: DAPT (an inhibitor of γ-secretase, which inhibits Notch signaling) and Chiron (an inhibitor of GSK3-β, which activates Wnt signaling). I aimed to quantify the entrainment phase and time to entrainment of Notch

oscillations after entrainment with Chiron and DAPT and compare these parameters to the ones I quantified during entrainment with FBP.

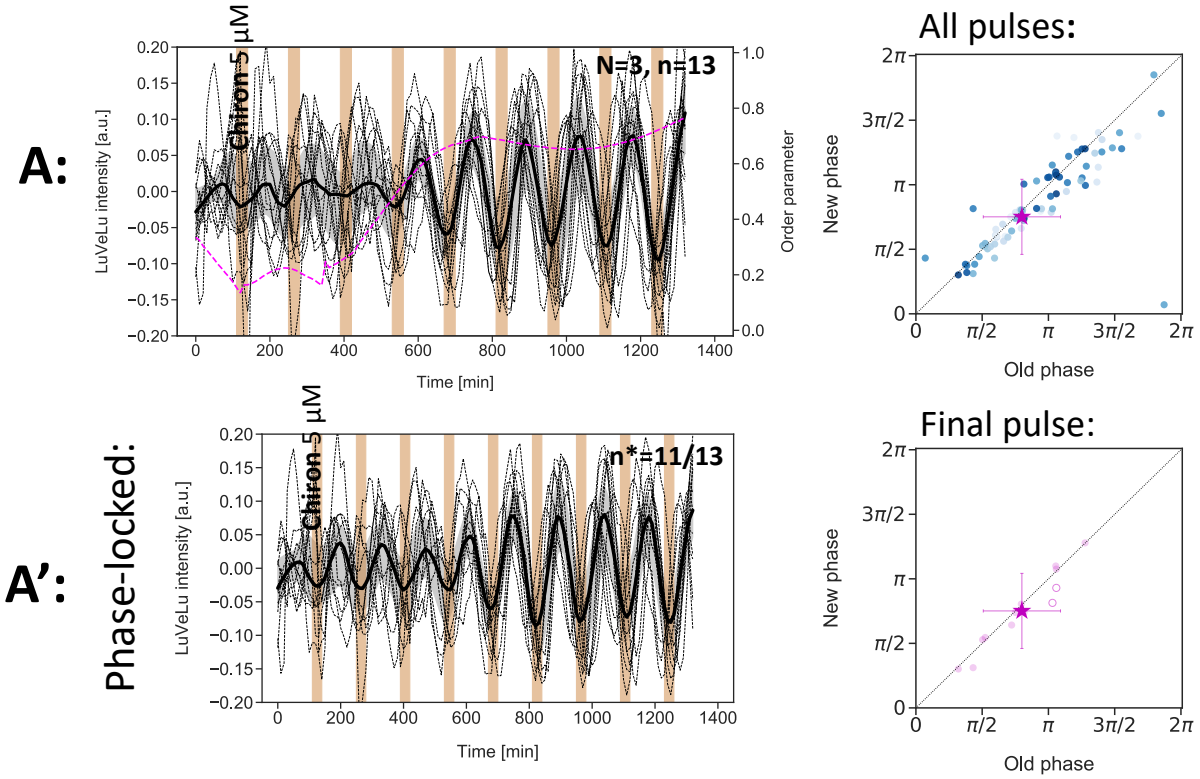

Figure 3.8: Perturbations of LuVeLu oscillations with periodic pulses of Chiron, at a period of 140 minutes.

(A-D:) Detrended time-series of LuVeLu oscillations in PSM explants. The detrending was done using a sinc-filter with a cut-off period of 240 minutes. Dashed black lines show single-sample oscillations, the median value of all oscillations is shown by the thick black line and the gray shading shows the first to third quartile range. The magenta line shows the Kuramoto order parameter. The y-axis on the right indicates the Kuramoto values, a value of one representing complete synchrony of oscillations. Samples were incubated in a constant a glucose concentration of 2.0 mM throughout the experiment. Periodic pulses of 5 μM Chiron were applied with a period of 140-min and a pulse length of 30-min (brown). n: total number of samples, N: number of experiments, n*: number of phase-locked samples within the total n. Corresponding stroboscopic maps that depict a step-wise progression of the phase of LuVeLu oscillations during the experiment are shown on the right side of each time-series graph. Each dot represents a snapshot of the phase of the oscillation at the beginning of the Chiron pulse (old phase) plotted against the phase of the oscillations at the beginning of the *next* Chiron pulse (new phase). The phase of entrainment can be read out from the region around the diagonal, to which the dots have converged (marked here with a magenta star). The spread of the dots represents in-phase synchrony and is quantified by circSD (magenta cross). The blue shading of the dots depicts the step-wise phase progression of every sample (n) in time. Darker dots represent later time points. **(A':)** Detrended time-series of only phase-locked LuVeLu oscillations in PSM explants. Corresponding stroboscopic maps of phase-locked samples are

shown on the right. The magenta dots represent the phase dynamics of every sample (n) at the last external pulse. The filled magenta dots represent phase-locked LuVeLu oscillations (n*). The unfilled magenta circles represent non-phase-locked LuVeLu oscillations.

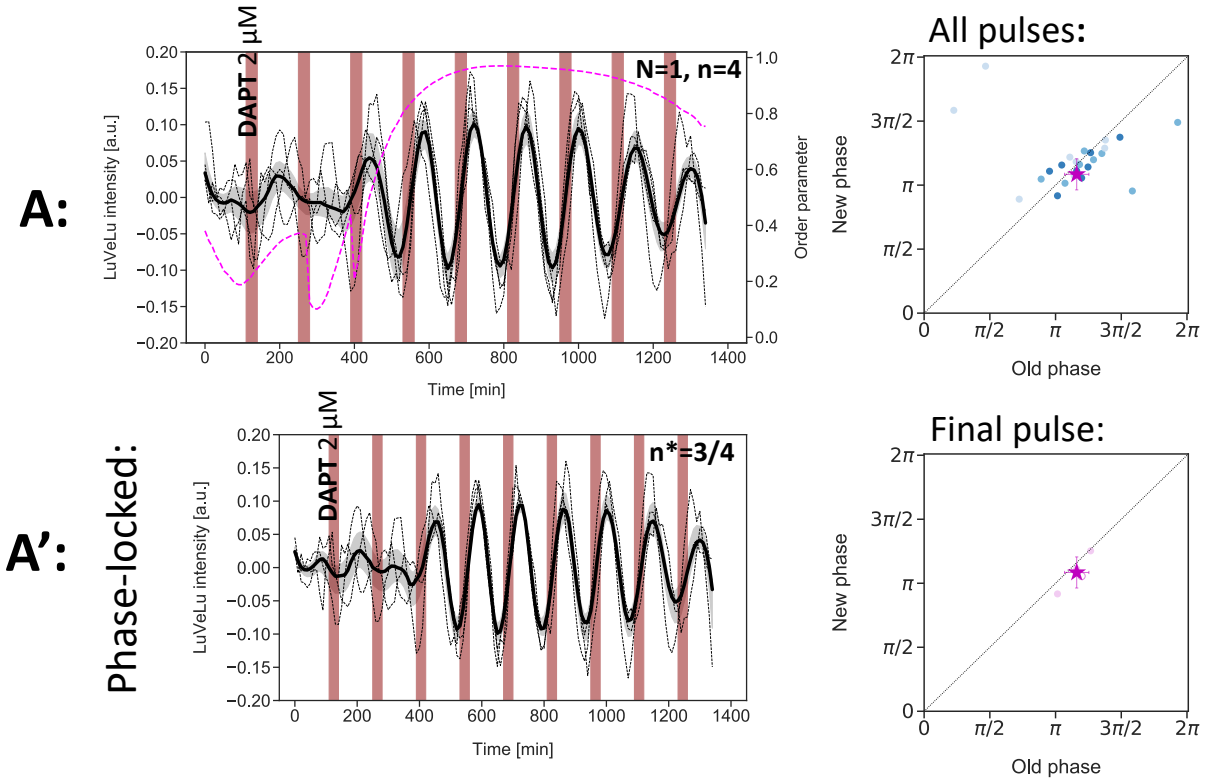

Figure 3.9: Perturbations of LuVeLu oscillations with periodic pulses of DAPT, at a period of 140 minutes.

(A:) Detrended time-series of LuVeLU oscillations in PSM explants. The detrending was done using a sinc-filter with a cut-off period of 240 minutes. Dashed black lines show single-sample oscillations, the thick black line shows the median value of all oscillations, and the gray shading shows the first to third quartile range. The magenta line shows the Kuramoto order parameter. The y-axis on the right indicates the Kuramoto values, a value of one representing complete synchrony of oscillations. Samples were incubated in a constant glucose concentration of 2.0 mM throughout the experiment. Periodic pulses of 2 μM DAPT were applied with a period of 140-min and a pulse length of 30-min (red). n: total number of samples, N: number of experiments, n*: number of phase-locked samples within the total n. Corresponding stroboscopic maps that depict a step-wise progression of the phase of LuVeLu oscillations during the experiment are shown on the right side of each time-series graph. Each dot represents a snapshot of the phase of the oscillation at the beginning of the DAPT pulse (old phase) plotted against the phase of the oscillations at the beginning of the *next* DAPT pulse (new phase). The phase of entrainment can be read out from the region around the diagonal, to which the dots have

converged (marked here with a magenta star). The spread of the dots represents in-phase synchrony and is quantified by circSD (magenta cross). The blue shading of the dots depicts the step-wise phase progression of every sample (n) in time. Darker dots represent later time points. **(A':)** Detrended time-series of only phase-locked LuVeLu oscillations in PSM explants. Corresponding stroboscopic maps of phase-locked samples are shown on the right. The magenta dots represent the phase dynamics of every sample (n) at the last external pulse. The filled magenta dots represent phase-locked LuVeLu oscillations (n*). The unfilled magenta circles represent non-phase-locked LuVeLu oscillations.

Both DAPT (2 μM pulses) and Chiron (5 μM pulses) effectively entrained LuVeLu oscillations at a period of 140 minutes (with 3 out of 4 samples phase-locked by DAPT and 11 out of 13 samples phase-locked by Chiron) (Figure 3.8 and Figure 3.9). The progression to in-phase synchrony is visible in the evolution of KOP for both perturbations. I noticed that an additional pulse of Chiron (compared to DAPT) was needed for the Notch oscillations to achieve high in-phase synchrony, defined as the plateau reached by the KOP value (n(Chiron)=5 pulses, n(DAPT)=4 pulses). Although I did not have many samples for the DAPT entrainment (n=4), I was confident in the results based on the quick evolution into in-phase synchrony and the small circSD. The phase of entrainment during entrainment with both Chiron and DAPT was around π. Combined, this data indicates that DAPT and Chiron entrain Notch oscillations with the same (ϕ_{ent})=π, albeit with different timing until in-phase synchrony.

In conclusion, I compared the temporal evolution of the first Kuramoto order parameters during entrainment with the metabolites and signaling drugs tested so far to get an overview of the time until entrainment (Figure 3.10). To summarize, I saw that the KOP value for DAPT entrainment reaches a plateau after 4 pulses, indicating that DAPT is the perturbation that locks Notch oscillations into in-phase synchrony first compared to the other perturbations. Samples provided with either FBP or Chiron pulses reach a plateau in their KOP values after 5 pulses, showing the same temporal evolution for in-phase synchrony of Notch oscillations for FBP and Chiron perturbations. In comparison, 7 glucose pulses were needed to increase the KOP value above the value of the control.

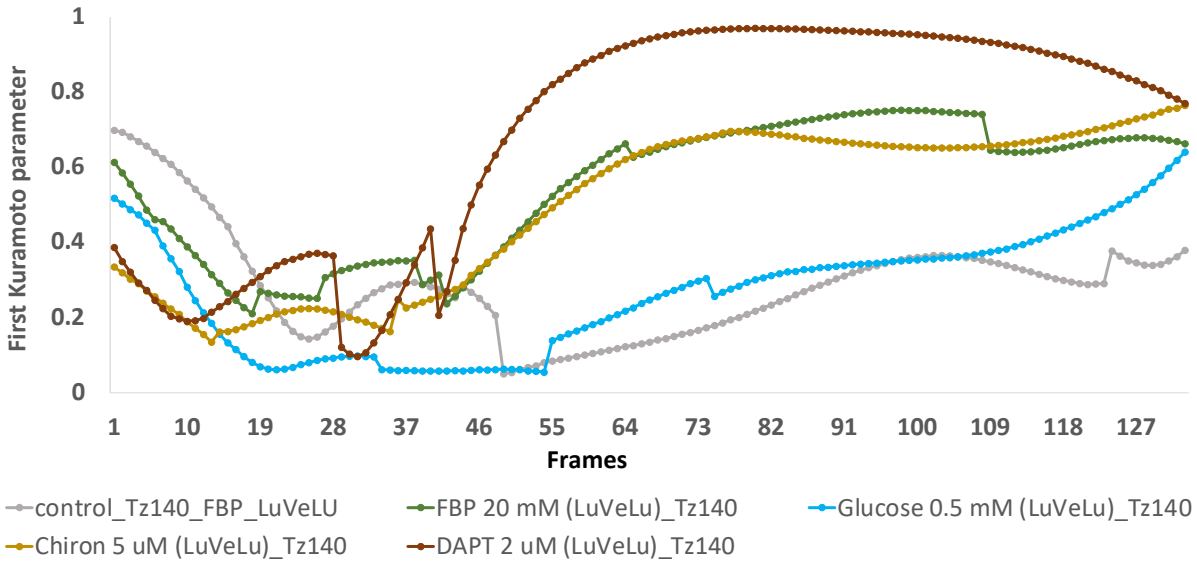

Figure 3.10: Temporal evolution of first Kuramoto order parameters during entrainment of Notch oscillations with periodic pulses of 140 minutes. Colors label perturbations with different metabolic and signaling modulators.

3.2 Metabolic entrainment: investigating the functional link between glycolysis and signaling in the developing PSM.

3.2.1 Perturbing the dynamics of the clock with alternating and combined pulses of FBP and Chiron.

The second aim was to investigate whether FBP has a non-canonical signaling role. A canonical metabolic role of glycolysis would be a global modulator of biochemical reactions, such as protein transcription, translation, etc. Through entrainment, I aimed to distinguish such a canonical role of glycolysis from a potential signaling role. I sought to tackle this aim by combining FBP pulses with either Chiron or DAPT and observing how the entrainment phase of Notch oscillations changes. If FBP still changes the phase of the oscillations when combined with a signaling modulator, this could indicate that FBP might have a signaling role. So far, I have observed that FBP pulses entrain Notch signaling oscillations and lock the oscillations to a specific phase of entrainment. Dynamical systems theory predicts a set of outcomes in the entrainment phase when signaling perturbations are combined into a single pulse. For example, if the phase of entrainment during entrainment with a combined

FBP-Chiron pulse preferentially adjusts itself to the entrainment phase that is locked by independent pulses of FBP, that would indicate that FBP is overriding the entrainment result of Chiron (Figure 3.11, B). The other predictions were that a new entrainment phase might result from a combination of perturbations or that a combined pulse might cancel entrainment. The outcomes of the addition of several phases of entrainment are based on the vectorial addition of the perturbations and are explained further in the discussion of this chapter.

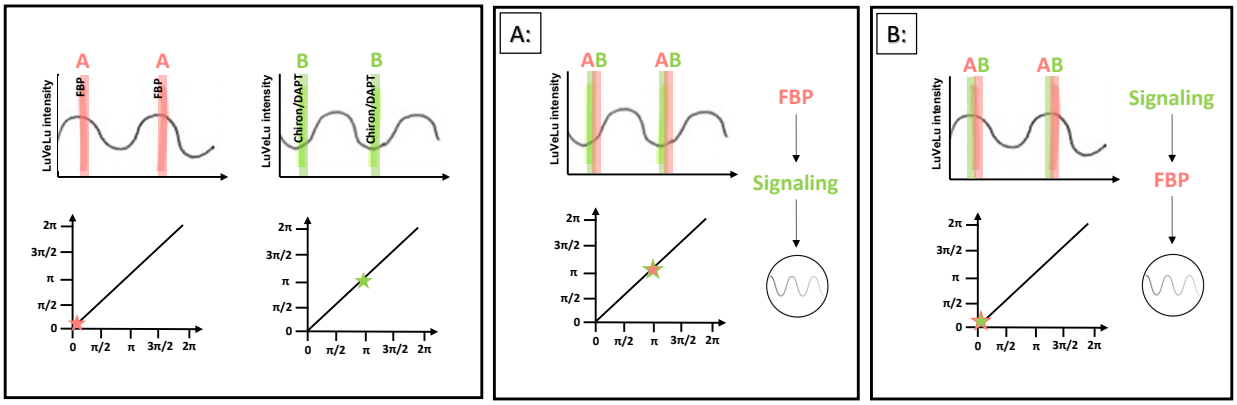

Figure 3.11: Disentangling the functional dependencies between glycolysis and signaling.

Schematic representation of hypothesis. Left: two different perturbations (A (FBP) and B (Chiron or DAPT)), which entrain the segmentation clock to different phases of entrainment. Right: possible outcomes in the phase of entrainment when both A and B are combined into a single pulse. **(A:)** Pulse B is masking the effect of pulse A, therefore the pathway perturbed by pulse B is hypothesized to be directly upstream of the segmentation clock. **(B:)** Pulse A is masking the effect of pulse B, therefore the pathway perturbed by pulse A is hypothesized to be directly upstream of the segmentation clock.

Furthermore, combining signaling modulators with FBP in one pulse could give insight into how glycolysis is functionally linked to signaling in the segmentation clock. If the phase of entrainment during entrainment with a combined FBP-Chiron pulse preferentially adjusts itself to the entrainment phase that is locked by independent pulses of Chiron, this could hint that Wnt is directly upstream of the segmentation clock, and FBP is entraining via

Wnt (Figure 3.11, A). The outcome of a new entrainment phase might suggest a synergistic effect between FBP and the signaling modulator. Canceling of entrainment might suggest a combination of a signaling activator and a deactivator.

To address these hypotheses, I first referred back to the single-perturbation entrainment data with FBP, DAPT, and Chiron (Figures 3.4, 3.8, 3.9). Based on those LuVeLu entrainment results at T_z=140 min, I know that the entrainment phase defined by signaling modulators is different from the entrainment phase defined by FBP: pulses of 20 mM FBP show evidence for phase-locking of Notch oscillations at ϕ_{ent}=0 while 5 μM Chiron and 2 μM DAPT both show phase-locking of Notch oscillations at ϕ_{ent}=π. Therefore, the phase relationship between FBP-entrained Notch oscillations and DAPT/Chiron-entrained Notch oscillations has a difference of π. I used this information to choose a control condition that does not challenge this phase relationship created by FBP and the signaling perturbations. For the control, I applied phase-shifted pulses of 20 mM FBP and 5 μM Chiron with a period of 140 minutes. I observed how the phase of LuVeLu responded to FBP pulses and Chiron pulses, respectively (Figure 3.12, A, A'). During this control perturbation, samples show evidence of phase-locking to the entrainment phase of 0 when exposed to FBP pulses, while they show phase-locking to the entrainment phase of π when exposed to Chiron pulses. These are the same phase values as those of the phases of entrainment locked by FBP and Chiron as separate, independent pulses (Figures 3.4, 3.8). However, combining the pulses into one single perturbation of 20 mM FBP and 5 μM Chiron and applying it on the clock with a period of 140 minutes showed evidence of phase-locking from 9 out of 11 LuVeLu samples at $\pi/2$, which seems to be the in-between value of the entrainment phases locked by alternating pulses of FBP and Chiron (Figure 3.12, B, B').

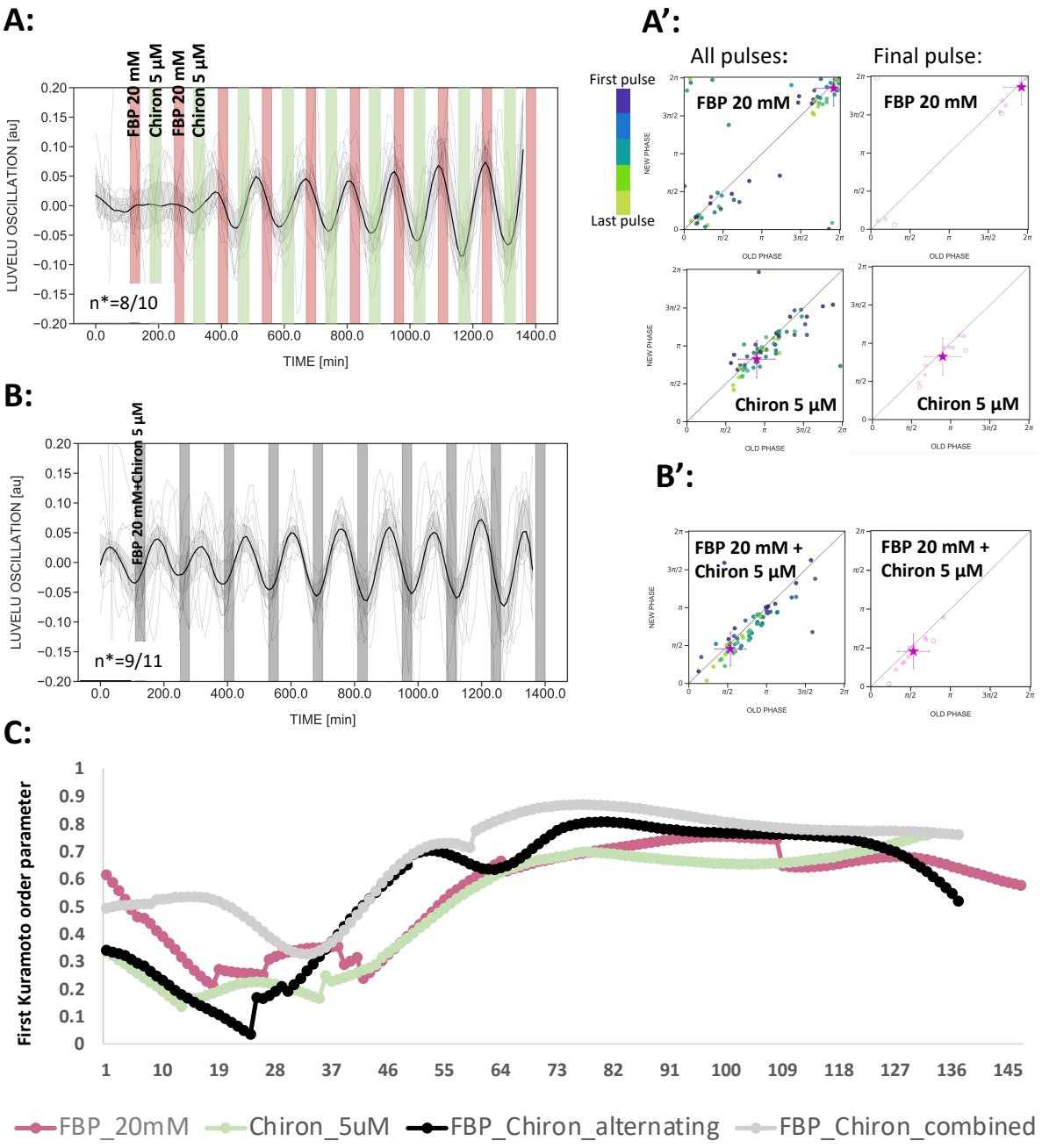

Figure 3.12: Perturbing the dynamics of the clock with alternating and combined pulses of FBP and Chiron.

(A,B:) Detrended time-series of LuVeLu oscillations in PSM explants. The detrending was done using a sinc-filter with a cut-off period of 240 minutes. Dashed black lines show single-sample oscillations, the thick black line shows the median value of all oscillations, and the gray shading shows the first to third quartile range. Samples were kept in a medium with a constant glucose concentration of 2.0 mM throughout the experiment. Periodic pulses of 20 mM FBP (red) and 5 μM Chiron (green) were applied (**A**) alternatingly (control), every 140 minutes or **(B)** combined in one pulse, every 140 minutes. The pulse length is 30 minutes in all conditions.

Non-metabolizable glucose (3-OMG) was added to the medium when FBP was absent to keep the molarity constant. n*: number of phase-locked samples within the total n. **(A', B':)** Corresponding stroboscopic maps that depict a step-wise progression of the phase of LuVeLu oscillations during the experiment are shown on the right side of each time-series graph. Each dot represents a snapshot of the phase of the oscillation at the beginning of the pulse (old phase) plotted against the phase of the oscillations at the beginning of the *next* pulse (new phase). The phase of entrainment can be read out from the region around the diagonal, to which the dots have converged (marked here with a magenta star). The spread of the dots represents in-phase synchrony and is quantified by circSD (magenta cross). The colorful shading of the dots depicts the step-wise phase progression of every sample (n) in time. Yellow dots represent last time points. The magenta dots represent the phase dynamics of every sample (n) at the last external pulse. The filled magenta dots represent phase-locked LuVeLu oscillations (n*). The unfilled magenta circles represent non-phase-locked LuVeLu oscillations. (**C:**) Temporal evolution of first Kuramoto order parameters during entrainment of Notch oscillations with single, alternating, and combined pulses of 20 mM FBP and 5 μM Chiron.

3.2.2 Perturbing the dynamics of the clock with alternating and combined pulses of FBP and DAPT.

As a next step in tackling the functional link of FBP to signaling, I aimed to combine FBP pulses with DAPT and observe how the entrainment phase of Notch oscillations changes. Samples exposed to alternating pulses of FBP (20 mM) and DAPT (2 μM) at a period of 140 minutes showed evidence for phase-locking to the phase of entrainment of 0 and π, respectively. It is worth noting here again that these phases of entrainment correspond to the phases that are locked by independent pulses of FBP and DAPT (Figures 3.4, 3.9). A combined pulse of FBP and DAPT however, did not entrain the clock when applied at a period of 140 minutes. Only 1 sample out of 10 showed as phase-locked (Figure 3.13).

In conclusion, I did not observe a masking effect of the phase of entrainment of one perturbation by the phase of the other perturbation. The controls of alternating pulses of FBP and signaling perturbation (DAPT/Chiron) entrained Notch oscillations to the same entrainment phase to which single pulses of these perturbations entrain the oscillations. Alternating FBP-DAPT pulses as well as FBP-Chiron pulses locked LuVeLu oscillations at a π-shifted relationship; peak and trough, respectively (Figures 3.12, 3.13, A, A'). Combined FBP-DAPT pulses abolished the entrainment I saw in the FBP-DAPT control, whereas combined FBP-Chiron pulses locked the oscillations to a new phase of entrainment ($\phi_{\text{ent}}=\pi/2$), which lies between the respective ϕ_{ent} of FBP entrainment and ϕ_{ent} of Chiron entrainment.

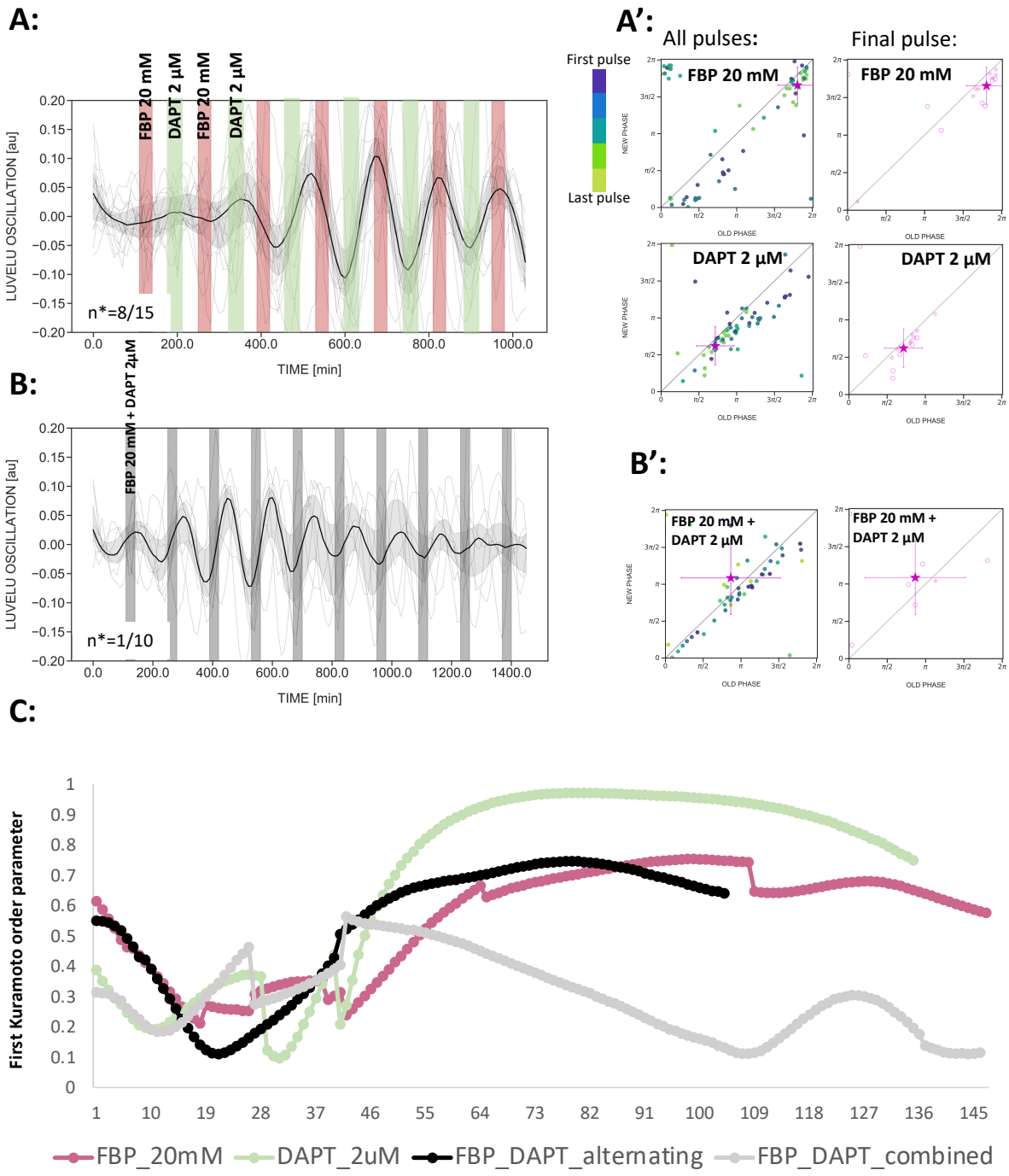

Figure 3.13: Perturbing the dynamics of the clock with alternating and combined pulses of FBP and DAPT.

(A,B:) Detrended time-series of LuVeLu oscillations in PSM explants. The detrending was done using a sinc-filter with a cut-off period of 240 minutes. Dashed black lines show single-sample oscillations, the thick black line shows the median value of all oscillations, and the gray shading shows the first to third quartile range. Samples were kept in a medium with a constant glucose concentration of 2.0 mM throughout the experiment. Periodic pulses of 20 mM FBP

(red) and 2 μM DAPT (green) were applied (**A**) alternatingly (control), every 70 minutes or (B) combined in one pulse, every 140 minutes. The pulse length is 30 minutes in all conditions. Non-metabolizable glucose (3-OMG) was added to the medium when FBP was absent to keep the molarity constant. n*: number of phase-locked samples within the total n. **(A', B':)** Corresponding stroboscopic maps that depict a step-wise progression of the phase of LuVeLu oscillations during the experiment are shown on the right side of each time-series graph. Each dot represents a snapshot of the phase of the oscillation at the beginning of the pulse (old phase) plotted against the phase of the oscillations at the beginning of the *next* pulse (new phase). The phase of entrainment can be read out from the region around the diagonal, to which the dots have converged (marked here with a magenta star). The spread of the dots represents in-phase synchrony and is quantified by circSD (magenta cross). The colorful shading of the dots depicts the step-wise phase progression of every sample (n) in time. Yellow dots represent last time points. The magenta dots represent the phase dynamics of every sample (n) at the last external pulse. The filled magenta dots represent phase-locked LuVeLu oscillations (n*). The unfilled magenta circles represent non-phase-locked LuVeLu oscillations. (**C:**) Temporal evolution of first Kuramoto order parameters during entrainment of Notch oscillations with single, alternating, and combined pulses of 20 mM FBP and 2 μM DAPT.

3.3 Discussion

3.3.1 Understanding which part of glycolysis is linked to signaling.

In this chapter, I investigated which part of glycolysis is linked to signaling by testing which glycolytic metabolites can entrain the segmentation clock. Previous work in the lab has unveiled that glycolysis plays an important role in controlling the tempo of the segmentation clock (Miyazawa and Rada (2024)). Furthermore, Hidenobu Miyazawa successfully entrained the tempo of the segmentation clock with pulses of glucose (Figure 1.5). All this implies that glucose is involved in signaling during PSM development, prompting the question whether a specific glycolytic metabolite is involved in this link between glycolysis and signaling. I focused on testing how F6P, FBP, and pyruvate pulses would affect the synchronization of the segmentation clock. Pyruvate and FBP are catalyzed by the enzymes Pfk1 and PK, respectively, both of which are committed steps in glycolysis. The advantage of testing products of committed steps in glycolysis is that it narrows down the link between glycolysis and signaling to the metabolites that come after FBP or after pyruvate since these committed steps are irreversible. F6P, on the other hand, is the direct precursor of FBP.

I quantified entrainment efficiency by scoring phase-locking, circSD, and the first Kuramoto order parameter as a readout. I observed that for the entrainment parameters that I chose, FBP is the metabolite that entrained the highest number of tail explants with the

highest in-phase synchrony. I applied metabolite pulses at different periods, both at 120 minutes (detuning = 20 minutes), trying to speed up the clock, and at 140 minutes (detuning = 0 minutes), which matches the natural period of the segmentation clock. When I did not change the detuning (Tz=140 min), I observed that 20 mM FBP could entrain 13 out of 20 tail explants to the same phase. In contrast, for 20 mM pyruvate pulses, only 3 out of 17 samples showed evidence of phase-locking. As dynamical systems theory predicts, entrainment strength is also important for entrainment efficiency. I think that I modified entrainment strength by changing the concentration of the metabolites. FBP seems to be the most efficient entrainer at a concentration of 20 mM, compared to 20 mM F6P and 20 mM pyruvate. Interestingly, F6P was more efficient at the lower concentration of 4 mM, entraining 7 out of 13 samples, while 4 mM FBP pulses entrained 4 out of 11 samples, and 8 mM pyruvate pulses entrained 1 out of 5. However, at a F6P concentration of 4 mM, the in-phase synchrony was very low, as seen in the values of circSD and first the Kuramoto order parameter at the last pulses.

Dynamical systems theory defines the entrainment phase (ϕ_{ent}) as an attractor (a stable fixed point). The attractor is represented as a fixed point on the diagonal of the stroboscopic map. Upon entrainment, samples converge towards this fixed point, reflecting phase-locking. It is a characteristic of entrained oscillators to vary their (ϕ_{ent}) as a function of detuning. This means that with different detunings, the entrained oscillations lock at different phases of entrainment. I observe this variation in the phase of entrainment with pulses of 20 mM FBP. In this case, I tested two different detuning periods for 20 mM FBP pulses: a 20-minute and a 0-minute period difference between the pulse's period and the segmentation clock's natural period (Figure 3.14). The entrainment phase of the phase-locked samples on the diagonal of the stroboscopic map changed based on the detuning of the Zeitgeber period. These phase dynamics reflect the fundamental properties of a dynamical system that is responding to an external perturbation. This allows to use FBP to directly take control of Notch and Wnt oscillations and learn more about the characteristics of the segmentation clock in relation to glycolysis. Entrainment has been achieved before with direct perturbators of the Notch and Wnt pathways, and it is remarkable that I can achieve entrainment in the same way with a glycolytic metabolite.

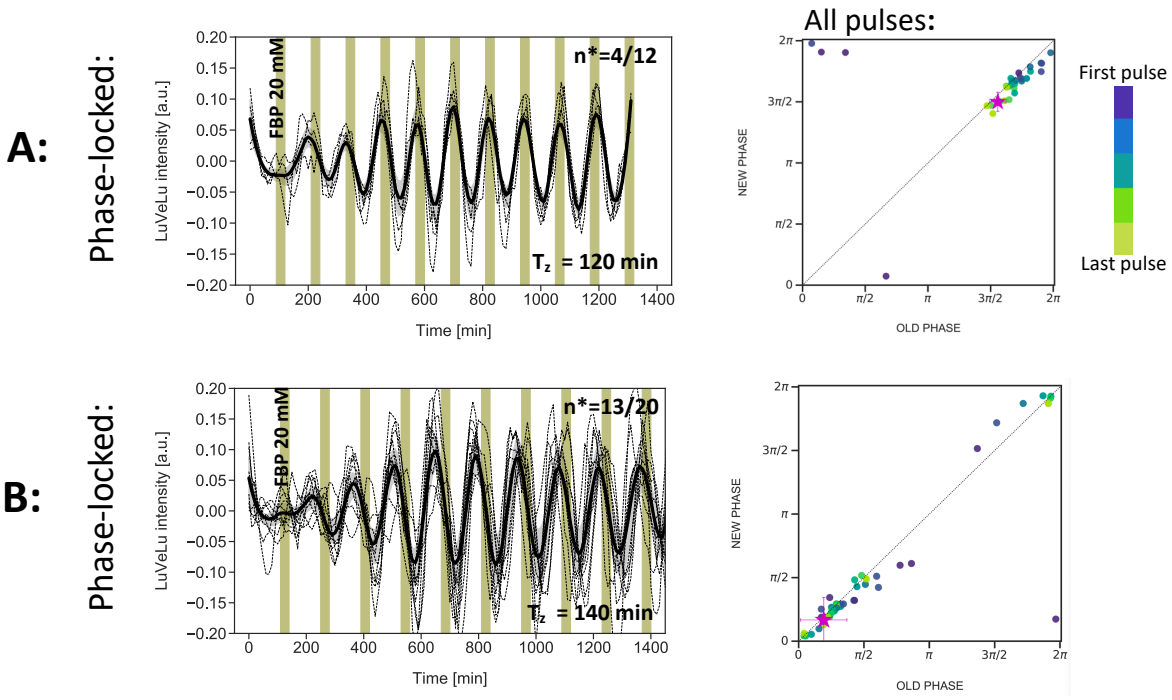

Figure 3.14: Entrainment phase of LuVeLu oscillations entrained by 20 mM FBP pulses with different detunings.

(A, B:) Detrended time-series of only phase-locked LuVeLu oscillations in PSM explants. The detrending was done using a sinc-filter with a cut-off period of 240 minutes. Samples were incubated in a constant glucose concentration of 2.0 mM throughout the experiment. Periodic pulses of 20 mM FBP were applied with a period of **A:** 120 min and a period of **B:** 140 min, as well as a pulse length of 30 min (green). Corresponding stroboscopic maps of phase-locked samples are shown on the right. The colorful shading of the dots depicts the step-wise phase progression of every sample (n) in time. Yellow dots represent last time points.

Nevertheless, the entrainment data with 20 mM FBP at a period of 120 min is preliminary and still needs validation. Ideally, I would like to build a fuller picture of how FBP entrains the segmentation clock by testing different detunings and thus defining the range of entrainment for FBP. Ultimately, the goal would be to sample across entrainment phases of the segmentation clock and define the limits of the entrainment range with FBP. Such a plot of Zeitgeber strength versus detuning is known as an Arnold tongue and visually represents an oscillator's entrainment range. An Arnold tongue would allow to understand and predict the range of control that FBP has over the segmentation clock. Paul L. G. Sanchez has used the entrainment approach with DAPT, the Notch signaling modulator, to define the Arnold

tongue of the segmentation clock (Sanchez (2021)). It is exciting that I can use the same approach to define the Arnold tongue of the clock for a metabolic modulator.

On the other hand, entrainment with pyruvate allowed to check the involvement of pathways below glycolysis in entraining the segmentation clock. At 8 mM and 20 mM concentrations, pyruvate pulses showed evidence of phase-locking 1 out of 5, and 3 out of 17 samples, respectively. Combined with the low value of circSD, I did not have any evidence for entrainment of the segmentation clock by pyruvate at these parameters. In this case, I could argue against the involvement of the Krebs cycle or oxidative phosphorylation in the link between glycolysis and the segmentation clock. It seems that there might be signaling specificity along glycolysis, which, according to these results, is confined between FBP and pyruvate and the glycolytic metabolites in between. The Pfk reaction that produces FBP and the PK reaction that produces pyruvate are irreversible reactions, and all the enzymatic steps between them are reversible (Park et al. (2019)). Since I have not seen any convincing entrainment with pyruvate pulses yet, this leaves FBP and the glycolytic metabolites until pyruvate (excluding pyruvate), as molecular candidates for the link between glycolysis and signaling. It is not excluded that pathways that branch out of glycolysis, such as the hexosamine pathway or pentose phosphate pathway (PPP), are also somehow involved in linking glycolysis to the segmentation clock. A way to investigate the involvement of other pathways would be to block them and see if I can still entrain the clock with the same metabolites I have tested.

FBP has been previously identified as a sentinel metabolite in the mouse PSM (Miyazawa et al. (2022). Sentinel metabolites are known to impact downstream biochemical reactions or protein modifications when their levels change (Cai et al. (2011)). Since FBP mirrors changes in glycolytic flux through changes in its own levels, it raises the question whether it is glycolytic flux or the FBP molecule itself acting as a signal toward the segmentation clock. To address this question, it should be possible to block glycolytic flux below FBP and then check if adding FBP would still cause the same clock phenotype, either by slowing down the tempo of the segmentation clock upon increased FBP levels or by entraining the clock. This would indicate that the FBP molecule itself is involved in signaling. Another possibility is that enzymes that metabolize FBP, such as Pfk or aldolase, might have moonlighting

functions related to signaling. It is already known that these two enzymes translocate out of the nucleus upon FBP supplementation (Miyazawa et al. (2022)).

3.3.2 The functional link between glycolysis and signaling

Entrainment can be used as a powerful tool to understand complex dynamic systems. There are different levels of understanding on which complex systems can be studied: 1) the micro-constituents, 2) the mechanisms with which these constituents interact, 3) the algorithms that explain how these mechanisms are carried out, and finally, 4) the computational level (the goal of the system) (Marr and Poggio (1979); Willems et al. (2011)). Marr and Poggio have explored these levels in the context of computational neuroscience, making the argument that "these levels of description are only loosely related" (Marr and Poggio (1979)). Especially when studying systems that display collective behaviors, it is important to keep all these levels in mind and not deduct macro-level understanding from the system's constituent parts.

When studying the functional link between glycolysis and signaling in the segmentation clock, we operate at the "algorithmic level" of the system. Focusing only on the molecules that provide this link would be reductive, and it would not be possible to make a causal deduction regarding how the link works at a higher, functional level. In this chapter, I used the principle of entrainment to functionally investigate the interaction of glycolysis and signaling within the link.

To characterize the effect of FBP on other components of the segmentation clock, I perturbed Wnt oscillations with periodic pulses of 20 mM FBP at a period of 140 minutes (n*=4/4) (Figure 3.6). I also perturbed mouse tail explants with 140-minute pulses of 2 μM DAPT (n*=3/4) and 5μM Chiron (n*=11/14), a Notch and a Wnt perturbation, respectively (Figure 3.8, 3.9). Based on phase-locking and in-phase synchrony (small circSD, high KOP value), I considered the samples in the abovementioned conditions entrained. Signaling perturbations such as DAPT and Chiron have been shown to entrain PSM tissues in other ex-vivo assays, such as mouse PSM spreadouts (Sanchez et al. (2022)), but here I show that entrainment with these signaling molecules is possible also in intact mouse tail explants. Finally, I created an overview of the temporal evolutions of different perturbations until en-

trainment of the segmentation clock (Figures 3.7, 3.10). I scored the temporal evolution of the first Kuramoto order parameter and compared the time frames in which the KOP value reached a plateau in its evolution. FBP entrains Axin-2-Achilles oscillations three pulses before it entrains LuVeLu oscillations (n(FBP:Axin-2-Achilles)=2 pulses, n(FBP:LuVeLu)=5 pulses). Furthermore, both Chiron and FBP entrain LuVeLu oscillations simultaneously (n(Chiron and FBP)=5 pulses). This data indicated that FBP might have a more direct or immediate relationship with Wnt than Notch. Seeing that there might be direct and indirect dependencies between glycolysis and signaling pathways in the segmentation clock, I decided to use entrainment as a tool to disentangle the functional relationship between glycolysis and signaling towards the segmentation clock (Figure 3.11).

The rationale that I used was based on scoring changes in the phase of entrainment between single perturbations and combined perturbations of FBP and Chiron, as well as FBP and DAPT. If FBP can change the phase of the oscillations when combined with a signaling modulator, this indicates that FBP impacts the effect of signaling cues and might have a signaling role itself. Furthermore, how the oscillation phase responds to the combination pulse might provide insight into how glycolysis is functionally linked to signaling in the segmentation clock.

Single pulses of 20 mM FBP have locked LuVeLu oscillations at a phase of $\phi_{\text{ent}}=0$, corresponding to the oscillation peak. Chiron and DAPT pulses have locked LuVeLu oscillations at a phase of $\phi_{\text{ent}}=\pi$, which corresponds to the trough of the oscillation. I used this π-shifted relationship from these results to define a ground truth on which I based the control and the perturbation setup. In the controls, I alternatingly applied pulses of FBP and DAPT, or pulses of FBP and Chiron, at a π-shifted dynamic, which did not challenge the phase of entrainment defined by the single pulses. The perturbation pulse was a combination of FBP and Chiron or FBP and DAPT in the same pulse. This perturbation challenges the π-shifted relationship that the glycolytic and signaling perturbations create when applied separately. I hypothesized that if the phase of entrainment adjusted itself preferentially to either the phase of the glycolytic perturbation or the signaling perturbation, it might indicate that one of the perturbations is instructive to the other. I conducted all these experiments at Zeitgeber pulses of 140 minutes, which match the natural frequency of the oscillations.

When FBP and DAPT were combined into one single perturbation, entrainment was abolished, and only one sample got phase-locked (n*=1/10). On the other hand, 9 out of 11 samples got phase-locked by the combination pulse of FBP and Chiron. However, the phase of entrainment was not masked by the phase expected of either FBP (ϕ_{ent}=0) or Chiron (ϕ_{ent}=π), but rather got fixed somewhere in-between the two, at ϕ_{ent}=π/2. These results indicated that the functional dependencies between glycolysis and signaling in the segmentation clock are intricate. I would argue that the controls show that the proposed rationale stands and entrainment can be used to tackle complex biological questions, such as the one I pose here. However, since I did not get a phase-masking result from the combination pulses, I returned to the other dynamical systems theory predictions to understand the results.

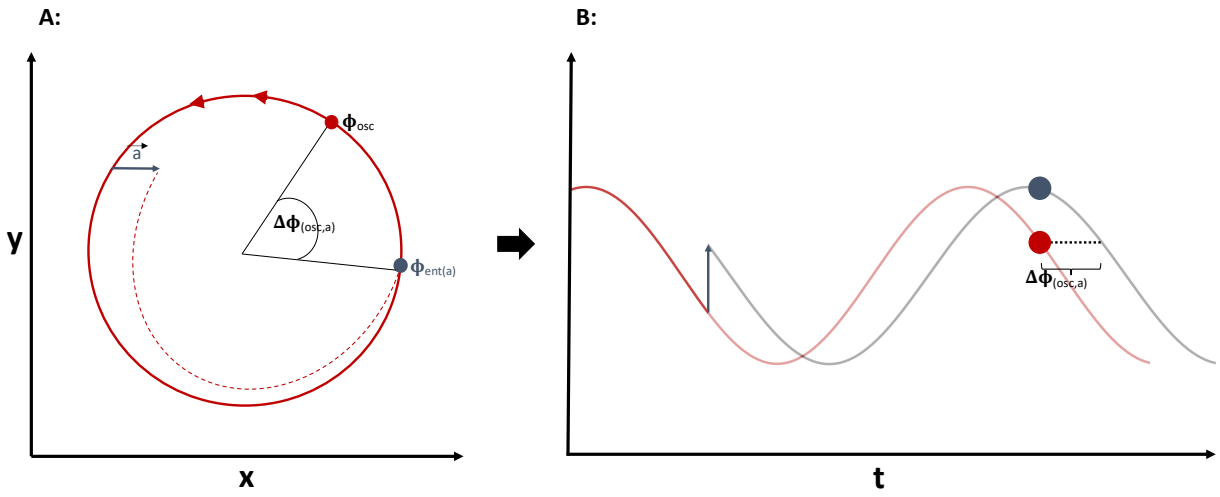

Figure 3.15: Entrained non-linear oscillators are attracted back to their limit cycle after an external perturbation.

The hypothetical limit cycle for a phase oscillator is shown in red. ϕ_{osc} depicts the phase of the endogenous oscillator.**(A:)** An external perturbation (vector **a**) shifts the phase of the oscillator by $\Delta\Phi$. **(B:)** The phase perturbation is reflected as a phase response on the entrained oscillator.

When entrainment occurs, the Zeitgeber pulse periodically perturbs the phase, which causes the oscillator to deviate from the limit cycle. A limit cycle is a closed trajectory on the

phase plane along which the oscillator cycles at an endogenous phase of ϕ_{osc}. Entrainment happens only if the oscillator is perturbed gently and can return back to its limit cycle. A perturbation changes the phase of the entrained oscillation by a step of $\Delta\Phi$ (Figure 3.15).

Dynamical systems theory assumes that if a phase oscillator oscillates along a symmetrical limit cycle and gets perturbed by two small opposing perturbations operating on the linear regime, the two opposing perturbations can cancel each other out on the oscillator's phase. This could explain the abolishing of entrainment that I see when I apply a combined pulse of DAPT and FBP, although the individual perturbations entrain the segmentation clock (Figure 3.16 (B)). This outcome indicates that the Zeitgeber strength of 20 mM FBP pulses and 2 μM DAPT pulses should be comparable because the two vectors must be similar in length. Functionally, it could be possible that one perturbation is acting as an activator of the oscillator while the other is a deactivator. In the case of FBP and Chiron, the vectorial addition leads to a new phase of entrainment, which according to the above assumptions, might well resemble an average phase value of the entrainment phases set by single perturbations (Figure 3.16, C). The synergistic effect that I see on the phase of entrainment from a combined FBP-Chiron pulse might indicate that both perturbations are operating within the same pathway.

Overall, the combinatorial entrainment approach provided further evidence of the signaling role of FBP. What I can say from the metabolic entrainment outcomes is that FBP not only entrains the segmentation clock by changing the entrainment phase based on detuning (Figure 3.14), but it also combines with signaling modulators and affects the entrainment phase according to predictions from the theory of dynamical systems. Combined, this data suggests that the role of FBP in the PSM goes beyond bioenergetic, and FBP perturbations are not generic but specific to signaling.

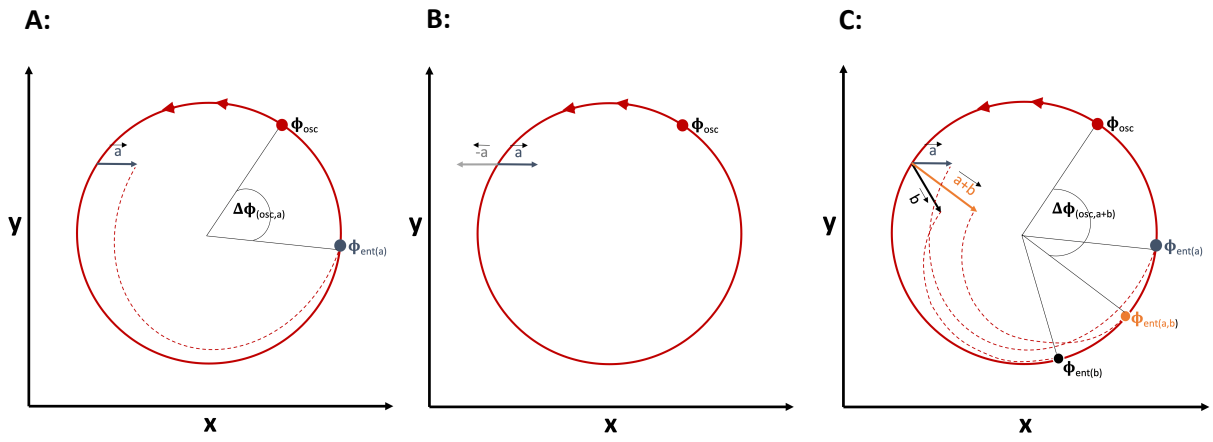

Figure 3.16: Schematic depiction of phase-prediction for a combined perturbation.

The hypothetical limit cycle for a phase oscillator is shown in red. ϕ_{osc} depicts the phase of the endogenous oscillator. External perturbations are shown as vectors. **(A:)** An external perturbation (vector **a**) shifts the phase of the oscillator by $\Delta\Phi$. **(B:)** Vectors **a** and **-a** cancel out upon addition, **(C:)** whereas vectorial addition of **a** and **b** would result in a perturbation that would entrain the oscillator to a new phase of entrainment, $\phi_{\text{ent(a+b)}}$.

3.4 Outlook

3.4.1 A molecular point of view on the link between glycolysis and signaling in the PSM.

I have used the novel approach of metabolic entrainment to disentangle the link between metabolism and signaling in the PSM. Metabolic entrainment shows that glycolysis has a signaling role on the segmentation clock, much like signaling perturbations, such as DAPT or Chiron. I have quantified how glucose, F6P, and FBP entrain the segmentation clock at different parameters. I did not see any evidence for pyruvate entraining the segmentation clock. However, I do not exclude that other metabolites between FBP and pyruvate could be linked to signaling. I could further explore the mechanistic role of glycolysis by testing entrainment efficiency with other metabolites. Since I have evidence that 20 mM FBP is changing the phase of entrainment of the clock with different detunings, I have reason to believe that FBP is perturbing the oscillator's phase. To further explore the mechanistic link between glycolysis and signaling, exploring interaction partners of FBP would be beneficial, especially in the setup where I have increased glycolytic flux. There is an ongoing effort by Hidenobu Miyazawa to identify protein partners of FBP by thermal proteome profiling

(TPP). We have also looked into glycolytic flux-induced transcriptional responses in the PSM (Miyazawa and Rada (2024)). A set of 90 genes that are regulated by the Wnt repressor Tcf7l2 have been identified. It is suspected that upon flux increase and FBP supplementation in the PSM, Tcf7l2 is activated, and this set of genes is downregulated (Miyazawa and Rada (2024)). Tcf7l2 offers a molecular lead whose interaction with FBP remains to be further investigated. When considering the functional link between signaling and glycolysis, it is particularly interesting to note that this Wnt repressor has been studied in the context of type 2 diabetes and insulin secretion in pancreatic β-cells (Del Bosque-Plata et al. (2021); Da Silva Xavier et al. (2009)).

3.4.2 The physiological relevance of the functional link between glycolysis and signaling.

Another important question is whether glycolysis affects developmental outcomes by controlling the dynamics of the segmentation clock. So far, in the lab we have evidence of elongation differences in Pfkfb3 tail explants compared to wild-type tails (Miyazawa and Aulehla (2018)). How tail growth rate, somite size, and number are affected by changes in glycolysis remains to be addressed. We observe that during entrainment with glucose, FBP, pyruvate and Chiron, tails undergo tissue shape changes at each external pulse (Miyazawa and Rada (2024)). I have attempted to quantify these morphological changes in the PSM. I think that this is not a result of osmolarity because I control for osmolarity changes in the medium. One possible direction will be to investigate if these are mechanical responses connected to changes in Ca^{2+} levels. So far, all I know is that this so-called twitching behavior of the tails corresponds to the external pulse, is consistently visible at the beginning of the pulse, and does not correlate with the efficiency of entrainment. However, in the future, I could investigate more systematically if embryo patterning is somehow being affected in the conditions where I notice this phenotype.

A hypothesis about the in-vivo relevance of the link between glycolysis and signaling is that a compensatory system of the segmentation clock, which responds to environmental nutrient fluctuations, is in place. Compensation, be it nutritional or by temperature, is a well-studied principle in circadian clocks (Kelliher et al. (2023); Izumo et al. (2003)). A nutritional compensation system of the segmentation clock could explain the small range of entrainment

that I achieve with glycolytic metabolites: the clock stays robust to nutrient changes in its environment. The clock's response becomes plastic once this compensation system is perturbed or the nutrient changes become drastic. This nutritional compensation system might physiologically explain a link between glycolysis and signaling in the segmentation clock. One could speculate that the activity of Pfk, the enzyme that produces FBP, is a bottleneck for the plasticity of the segmentation clock. Testing metabolic entrainment in the background of the Pfkfb3 mouse line would be a good setup to explore this plasticity. In this transgenic line, Pfkfb3 is overactivated and glycolytic flux is enhanced. Discovering a wider range of entrainment with FBP pulses in Pfkfb3b would be an incentive to explore the hypothesis that the nutritional compensation system is impaired upon Pfk overactivation and the segmentation clock is not as robust anymore.

3.4.3 The experimental approach of metabolic entrainment.

I used dynamical systems theory to explain the outcomes of the entrainment experiments with combined glycolytic and signaling perturbations. So far I see a synergistic effect on the clock's phase when I combine FBP and Chiron in a pulse, whereas combined FBP and DAPT pulses do not entrain the oscillations anymore. A future perspective is to expand this approach to understand the interaction between FBP, Wnt, and Notch. A possibility is to combine DAPT and Chiron and see how the perturbation affects the phase of the clock in order to compare it to the results I have so far with the other combination perturbations.

4.

Results: Part II

4.1 Ca^{2+} oscillations as a gateway to glycolytic oscillations in the PSM.

Metabolism is compartmentalized in time and space at tissue and subcellular level (Miyazawa and Aulehla (2018)). Often this spatio-temporal compartmentalization supports its modulatory or instructive role (Tu et al. (2005); Tu and McKnight (2006); Yang et al. (2011, 2012)). Rhythms in metabolic activity have been shown to be linked to gene expression and epigenetic modifications (Tu et al. (2005); Tu and McKnight (2006); Cai et al. (2011)). After exploring the link between glycolytic metabolites and signaling in the PSM (Aim 1) and uncovering a signaling role of glycolysis in the PSM (Aim2), I now wanted to explore the existence of such rhythmic glycolytic oscillations in the PSM (Aim 3).

Previous findings in the lab prompted the hypothesis about the presence of glycolytic oscillations in the PSM. There is evidence from previous data (Prior (2014)) that LuVeLu dynamics respond differently to F6P and FBP supplementation in the absence or presence of glucose (Figure 4.1). Mouse tail explants do not show LuVeLu oscillations in the absence of glucose. Addition of 20 mM F6P recovered LuVeLu oscillations, while the addition of 20 mM FBP (or any other glycolytic metabolite below FBP, except 1,3-bisphosphoglycerate (1,3bPG)) did not recover LuVeLu activity in these tails. This implied that F6P had to be present as a substrate for Pfk for the clock to oscillate in the absence of glucose. On the other hand, LuVeLu oscillations in mouse tail explants were maintained in the presence of 0.5 mM glucose. In the presence of glucose, the addition of 20 mM F6P did not affect LuVeLu oscillations; however, the addition of 20 mM FBP disrupted LuVeLu activity. This indicated that regulated production of FBP, which is also an allosteric regulator for Pfk, is important for signaling in mesodermal development.

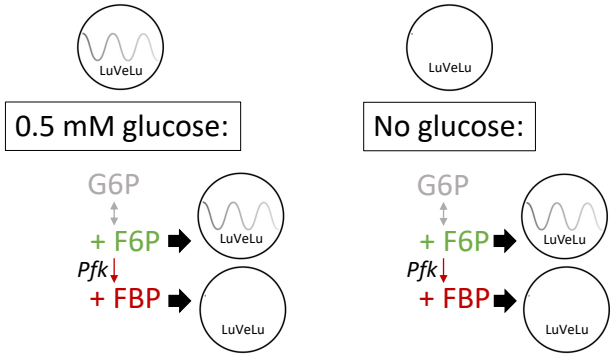

Figure 4.1: The effect of metabolite supplementation on LuVeLu oscillations in the absence or presence of glucose.

Summary of LuVeLu activity of mouse tail explants cultured in the presence or absence of glucose. In the presence of 0.5 mM glucose, LuVeLu activity oscillates normally before the addition of metabolites. In the absence of glucose, there is no LuVeLu activity before the addition of metabolites. Metabolites indicated in green either supported or induced LuVeLu oscillations after addition. Metabolites indicated in red either disrupted or did not induce LuVeLu oscillations after addition. Metabolites in grey were not tested. Data and figure adapted from Nicole Prior.

This data raised the question of whether the activity of the Pfk enzyme is a critical node linked to signaling in the PSM. As we know, Pfk activity is oscillatory in yeast cells, making the Pfk reaction one of the responsible components for glycolytic oscillations (Boiteux et al. (1975)). Its activity is tightly regulated by FBP and ATP; through allosteric activation by FBP, and through inhibition by ATP. These positive feedback loops by FBP, in interaction with negative feedback loops by ATP, result in oscillating Pfk activity and oscillating levels of glycolytic intermediates. I assumed that by providing exogenous FBP, Pfk and potential glycolytic oscillations are being bypassed. If there are glycolytic oscillations in the PSM that are functionally linked to the segmentation clock, this might explain why LuVeLu oscillations are getting disrupted by exogenous FBP. Glycolytic oscillations have not yet been uncovered in the PSM or any other embryonic context. Therefore, I decided to explore whether there are any glycolytic oscillations in the PSM.

To search for the presence of glycolytic oscillations in the PSM, I made use of the known link between Ca^{2+} oscillations and glycolytic oscillations in a different tissue, namely the pancreas (Bertram et al. (2007); Merrins et al. (2016)). It has been shown in pancreatic β-cells that oscillating Ca^{2+} levels have an anti-phase correlation to oscillating FBP levels

(Merrins et al. (2016)). Therefore, I first aimed to observe Ca^{2+} dynamics in the pancreas, where I hypothesize that any observation I make on Ca^{2+} oscillations, will be linked to glycolytic oscillations. Hence, I used Ca^{2+} oscillations of Min6 cells, a mouse insulinoma cell line, as a proxy for glycolytic oscillations. Min6 cells show prominent Ca^{2+} oscillations in response to glucose stimulation because Ca^{2+} oscillations play a crucial role in regulating insulin secretion in the pancreas (Bertram et al. (2014)). Since it is known that it is oscillatory Pfk activity that is responsible for generating glycolytic oscillations (Ghosh and Chance (1964)), in the next section, I tested how the substrate of Pfk (F6P) and its product (FBP) impact Ca^{2+} oscillations in Min6 cells.

4.1.1 F6P and FBP have different effects on Ca^{2+} oscillations in Min6 cells.

I wanted to see if bypassing Pfk has an effect on Ca^{2+} oscillations in Min6 cells. Therefore I supplemented Min6 cells with either 20 mM of F6P or 20 mM of FBP. At the beginning of the experiments, Min6 cells were showing dynamic Ca^{2+} activity. After the first 20 minutes of following endogenous Ca^{2+} oscillations, 20 mM of F6P or 20 mM FBP were pipetted into the well without disturbing the ongoing imaging process. From general qualitative observations, I noticed that F6P intensified Ca^{2+} oscillations in Min6 cells, whereas FBP disrupted them. I then selected cells that were still oscillating after F6P supplementation and followed their signal intensity throughout the measurement. As seen on the time series of the signal from representative traces, the application of F6P increased the frequency of Ca^{2+} oscillations or even initiated the oscillations in cells that had been inactive at the beginning of the measurement. Conversely, FBP application stopped observed Ca^{2+} oscillations in Min6 cells (Figure 4.2).

In summary, I qualitatively observed that supplementation of Min6 cells with 20 mM F6P supported and amplified Ca^{2+} oscillations, whereas supplementation with 20 mM FBP depleted Ca^{2+} oscillations. Since Ca^{2+} oscillations in Min6 cells are linked to glycolytic oscillations, if these patterns in Ca^{2+} dynamics result from bypassing Pfk activity, then the same pattern might be reflected on glycolytic oscillations too. Therefore, in the next section, I provided PSM cells with F6P and FBP and observed if I could reproduce this pattern of

Ca^{2+} oscillations in PSM cells as well. The replication of the same Ca^{2+} oscillations in PSM cells can thus hint at the presence of glycolytic oscillations.

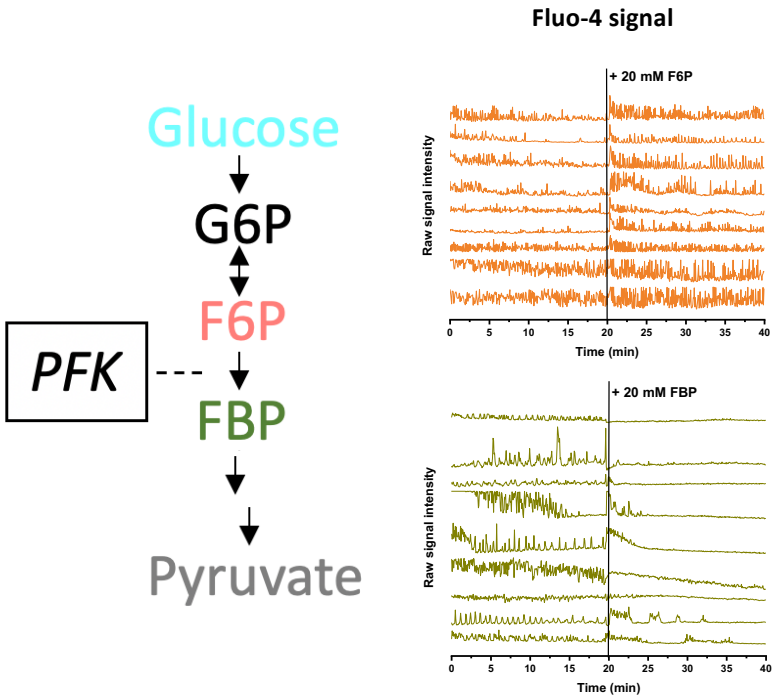

Figure 4.2: Representative intracellular [Ca^{2+}] traces in Min6 cells.

Representative intracellular [Ca^{2+}] traces in MIN6 cells depicted as raw intensity signal of Fluo-4 from single cells. The black line indicates the time of metabolite application. Cells were imaged in imaging buffer, containing 11 mM glucose. Frame interval: 4 seconds.

4.1.2 Comparing the effect of metabolite addition on Ca^{2+} oscillations in PSM RAFLs.

Having made the qualitative observation that F6P addition increases the frequency of Ca^{2+} oscillations in Min6 cells, whereas FBP addition depletes Ca^{2+} oscillations in these cells, I next tested the effect of F6P and FBP on Ca^{2+} oscillations in PSM cells. I used the RAFL method (randomization assay for low input) to prepare the PSM cells for imaging (Ho et al. (2024)). In RAFL assays, PSM cells are made to form a monolayer, which allows to track the oscillatory activity of single cells. In this setup, the cells show striking periodic Ca^{2+} activity, which we can monitor. This makes RAFL a convenient system for scoring Ca^{2+} oscillations in the PSM.

I imaged PSM RAFLs of mice expressing a genetically encoded Ca^{2+} indicator (GCaMP6s reporter line). After half the total time of imaging (6.25 minutes), I applied a glycolytic metabolite on the cells and, for the rest of the imaging time, monitored the presence or absence of Ca^{2+} oscillations. Then, I performed wavelet analysis on selected Ca^{2+} traces. Wavelet analysis is a time-frequency approach designed to identify the dominant oscillatory components in a signal. In this analysis, a wavelet function scans the signal of interest along the time axis for predefined periods ranging from 2 seconds to 75 seconds. The wavelet function can be imagined as a default wave-like signal of different, predefined periods, which is fitted to the detrended signal being analyzed. A high correlation of the signal with the wavelet gives a power value of above 3, which is considered high wavelet power, meaning that statistically significant oscillations are present. A low signal correlation with the wavelet results in a wavelet power below 3, which is considered a low wavelet power and represents white noise. Thus, a power spectrum is generated from which the period and other oscillatory components are extracted. In these experiments, I used the wavelet power output to quantify the presence or absence of Ca^{2+} oscillations in PSM RAFLs.

In PSM RAFLs cultured in a medium with a baseline of 2 mM glucose, I observed striking spontaneous bursts of Ca^{2+} with a sporadic pattern. These Ca^{2+} oscillations had periods ranging from 2 to 75 seconds. I tested whether the addition of 20 mM glucose, 20 mM F6P, 20 mM FBP, or 20 mM pyruvate would affect these Ca^{2+} oscillations (Figure 4.3). I selected cells that were still oscillating after glucose and F6P supplementation and followed their signal intensity changes compared to the beginning of the experiment. 4 out of 9 traces were oscillating at the beginning of the experiment, based on wavelet power analysis, and continued oscillating after glucose addition. The remaining 5 traces did not show any Ca^{2+} oscillations at the start of the experiment. Interestingly, I observed that glucose addition induced Ca^{2+} oscillations in the PSM in these 5 remaining traces. The average period of oscillations after the addition of glucose was 60.1 seconds. Similarly, F6P addition induced Ca^{2+} oscillations in the PSM in 5 out of 10 selected traces and did not disrupt oscillations on the other 5 traces, which were oscillating from the start of the experiment. After F6P supplementation, the average period droped from 56,6 seconds to 48,7 seconds, indicating that the oscillations became more frequent overall. FBP and pyruvate addition, on the other

hand, depleted Ca^{2+} oscillations. Based on wavelet power, all 9 of the selected traces were showing Ca^{2+} oscillations, and they were all depleted after supplementation with FBP and pyruvate. In summary, out of these four tested metabolites, supplementation with metabolites above Pfk induced or did not disrupt Ca^{2+}, whereas supplementation with metabolites below Pfk depleted Ca^{2+} in PSM cells.

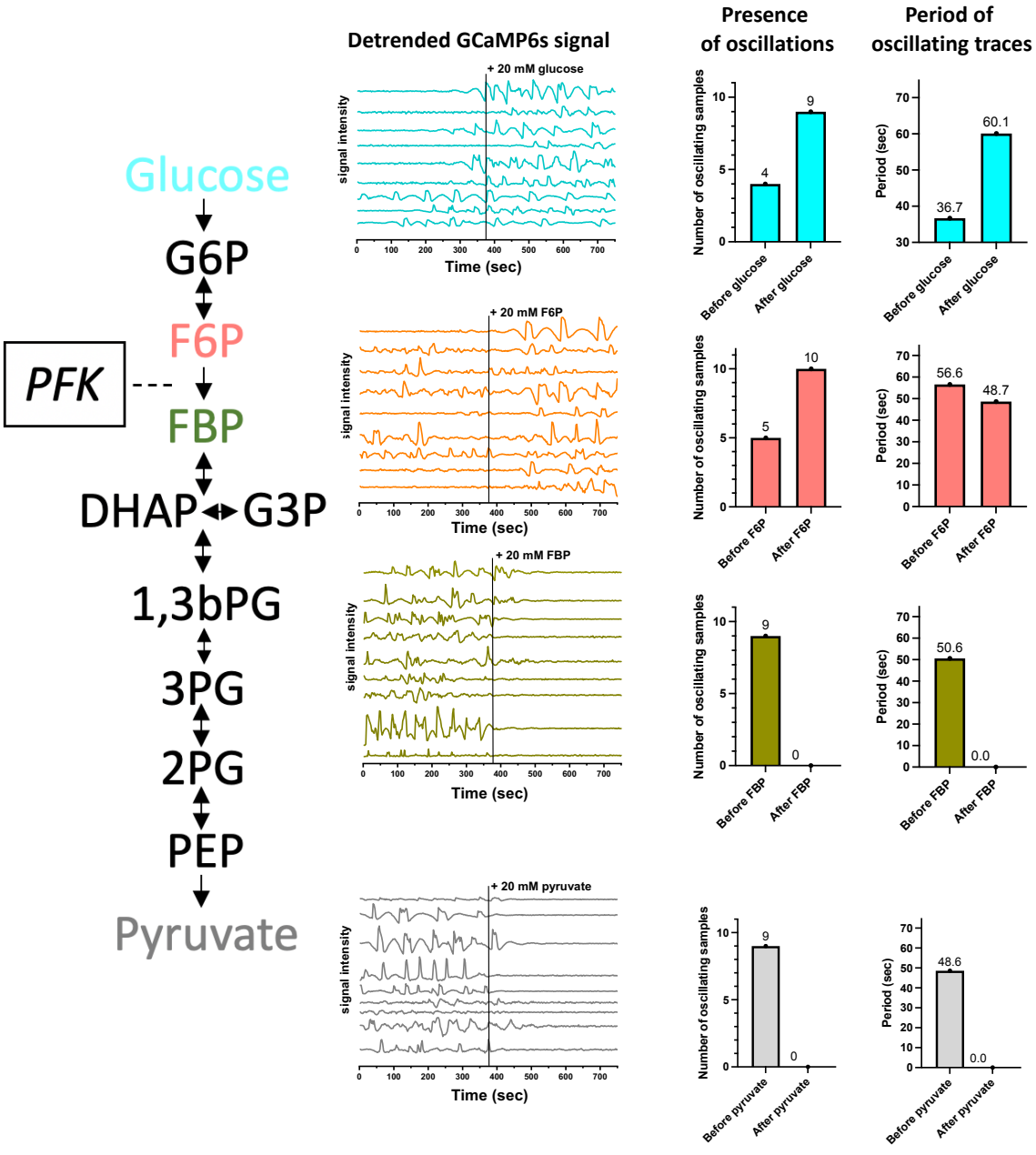

Figure 4.3: Representative traces of Ca^{2+} oscillations in PSM cells.

Representative intracellular [Ca^{2+}] traces in PSM RAFLs depicted as detrended GCaMP6s intensity signal from single cells. The detrending was done using a sinc-filter with a cut-off period of 75 seconds. The black line indicates the time of metabolite application. The graphs on the right show the number of representative traces that were oscillating, based on the average wavelet power of each depicted [Ca^{2+}]trace before and after metabolite application. Oscillations were considered present if the average wavelet power value was above 3.

4.2 Discussion

4.2.1 Are there glycolytic oscillations in the PSM?

In this chapter, I explored the presence of glycolytic oscillations in the PSM. I used Ca^{2+} signaling in the PSM as a proxy for glycolytic activity. I first characterized how Ca^{2+} oscillations respond to supplementation with metabolites in Min6 cells, a mouse pancreatic cell line. Glycolytic oscillations have been reported to exist and to be connected to Ca^{2+} oscillations (Merrins et al. (2013, 2016) in pancreatic β-cells. Since we know that it is oscillatory Pfk activity that is responsible for generating glycolytic oscillations (Ghosh and Chance (1964)), I tested how the substrate of Pfk (F6P) and its product (FBP) impact Ca^{2+} oscillations in Min6 cells. I observed that 20 mM F6P supplementation maintained Ca^{2+} oscillations and also increased their frequency (Figure 4.2), while supplementation with 20 mM FBP depleted Ca^{2+} oscillations. These differences in Ca^{2+} patterns were the motivation to test how Ca^{2+} signals in the PSM respond to metabolites above Pfk (i.e., glucose, F6P) and metabolites below Pfk (i.e., FBP, pyruvate).

First of all, it is noteworthy to mention that I observed oscillatory Ca^{2+} dynamics, which have not been mentioned before in the PSM cells. Based on the literature, fast intracellular calcium oscillations in the range of 10-60 seconds are common, while slower oscillations from minutes to hours can also occur due to additional feedback processes, allowing cells to encode stimulus strength over a wide range of frequencies (Politi et al. (2006); Dupont et al. (2011)). The Ca^{2+} oscillations I observed ranged from 2 seconds to 75 seconds, but the wavelet analysis could be expanded in the future to score Ca^{2+} dynamics of lower frequencies. The Ca^{2+} dynamics showed sporadic oscillations within single cells, and occasionally, the single-cell bursts would synchronize into localized wave patterns. The interest here was to see how the Ca^{2+} dynamics change after the addition of glycolytic metabolites.

The results from this chapter put the Pfk enzyme in the spotlight. Ca^{2+} oscillations in PSM were induced and maintained by glucose and F6P, whereas the addition of FBP and pyruvate depleted them (Figure 4.3). In yeast, it is known that addition of metabolites above Pfk induces glycolytic oscillations, whereas addition of metabolites below Pfk, does not (Boiteux and Hess (1974)). Considering that bypassing Pfk also disrupts Notch oscillations of the segmentation clock (Figure 4.1), it follows that regulation of Pfk activity might be important for segmentation clock dynamics.

Glycolytic oscillations span timescales of a couple of minutes, up until around 40 minutes at low levels of glucose (Olivos-Santes et al. (2019)), whereas the segmentation clock in mouse ticks in the range of hours. However, dynamic oscillations of different timescales have been shown to be linked. In the pancreas, Ca^{2+} oscillations in the range of seconds are physiologically linked to slow and fast insulin oscillations ranging from 5-15 minutes (Bertram et al. (2000); Christiansen et al. (2017)). In neural dynamics, specific patterns seem to occur as a result of neural cross-frequency coupling (Hyafil et al. (2015)). This is a possible mechanism for integrating information across temporal and spatial scales. If glycolytic oscillations are present in the PSM, one speculation is that these could be coupled to segmentation clock oscillations through oscillatory components other than frequency, such as phase or amplitude. Another possible connection between glycolytic oscillations and the segmentation clock could be through moonlighting functions of glycolytic enzymes, maybe Pfk itself. Maybe the temporal regulation of Pfk activity allows downstream glycolytic enzymes to exercise non-canonical functions when they are not fully occupied. Although this dynamic link between glycolysis and the segmentation clock remains to be revealed, it is an exciting viewpoint in exploring the functional link between glycolysis and signaling in the PSM.

4.3 Outlook

A direct way to visualize glycolytic activity is through imaging of metabolic sensors or fluorescence lifetime imaging microscopy (FLIM) of NADH autofluorescence. Hidenobu Miyazawa and I have been working on developing transgenic mouse lines that express fluorescent biosensors for FBP (Merrins et al. (2013); Koberstein et al. (2022). Hidenobu Miyazawa

is getting closer to establishing both mouse and medaka fish lines that express the HYLight FBP sensor (Koberstein et al. (2022)), which we can eventually use to detect glycolytic dynamics in tissue and single-cell levels. This sensor will make it possible to visualize both glycolytic and clock dynamics simultaneously and investigate how the link between glycolysis and signaling compares across species.

Two complex systems with entirely different constituent parts at the micro-level of understanding can still follow the same fundamental principles at the macro-level of understanding, thus allowing cross-investigation (Sanchez (2021)). Even though glycolytic oscillations and the segmentation clock consist of different molecular players, how these two oscillatory systems communicate with each other could still give an accurate, bigger-picture view of the link between glycolysis and signaling in the PSM. Especially if there is a dynamic aspect to glycolysis in the PSM, I think understanding the functional relationship between glycolysis and the segmentation clock through a wider understanding of the emergent properties and interactions of the system is very useful. In Sonnen et al., the combinatorial entrainment principle was used to decouple the phase relationship of Wnt and Notch oscillations (Sonnen et al. (2018)). If glycolytic oscillations in the PSM are confirmed, I can use entrainment to understand how they are coupled to the segmentation clock. An FBP sensor would make it possible to visualize the spatio-temporal organization of glycolysis in the PSM. Simultaneous imaging with Notch and Wnt reporters would allow to visualize both the dynamics of glycolysis and the segmentation clock. In this way, I could detangle the possible connections by quantifying the amplitudes and periodicities of glycolytic oscillations, their phase relationship to the segmentation clock, etc.

5.

Materials and Methods

5.1 Mouse lines

All mouse work was done under veterinarian supervision in the EMBL Laboratory Animal Resources (LAR) and was approved according to guidelines of European Commission, Directive 2010/63/EU and AVMA Guidelines 2007.

5.1.1 LuVeLu

The LuVeLu mouse reporter line was used for most of the experiments in the thesis. It expresses Venus, a YFP-variant that is driven by the Lfng promoter. A modified PEST domain was used to generate a highly destabilized version of the Venus protein. The generation of this reporter line has been described in more detail in Aulehla et al. (2008).

5.1.2 Axin2-Achilles

Axin2-GSAGS-Achilles is a mouse line that expresses Axin2 fused to Achilles, a YFP variant. This line was generated in the lab by Nobuko Tsuchida-Straeten.

5.1.3 GCaMP6s

GCaMP is a single fluorophore sensor that consists of a circularly permutated green fluorescent protein (cpGFP), the calcium-binding protein calmodulin (CaM), and a CaM-interacting M13 peptide. This sensor has slower kinetics, which makes it a more sensitive sensor. Its development and characterization have been described in Chen et al. (2013).

5.2 Microfluidic system

The microfluidic system was designed by Ina Sonnen and further optimized by Paul Gerard Layague Sanchez. Christoph Merten's lab protocols were used to design and prepare the microfluidic device. The polymer component of the microfluidic chips used in my work was prepared from a pre-existing microfluidic mold. Please refer to the above-mentioned protocols and their summary in Paul Gerard Layague Sanchez's dissertation thesis for more detailed information about the preparation of the mold. The rest of the steps that I used and optimized for the microfluidic system are summarized below.

5.2.1 Preparation of microfluidic chips

Polydimethylsiloxane (PDMS), the polymer component of the microfluidic device (referred to as the microfluidic chip), was prepared by mixing Sylgard 184 silicone elastomer (Dow) with curing agent (Dow) at a ratio of 1:1. The mix was degassed under vacuum in a desiccator for a few minutes and subsequently poured over the pre-existing microfluidic mold. The PDMS mold was degassed for up to fifteen minutes in the desiccator and finally incubated at 65 °C overnight, until it solidified. The solidified PDMS was cut out of the mold by using a surgical scalpel, and it was pressed open at the tubing inlets, sample inlets, and outlets of the chip with a biopsy punch (World Precision Instruments, 504646), creating clean, circular openings of a 1mm diameter. Next, a cover glass (70 mm x 70 mm, 1.5H, Marienfeld 0107999 098) and the PDMS (indented side facing upwards) were placed on an oven tray. The oven tray was inserted into a Diener Femto plasma oven for 1 minute, where the surfaces of the cover glass and the PDMS were modified with plasma at a radiation power of 2.5. After plasma exposure, the PDMS and the cover glass were taken out of the oven. The indented side of the PDMS was pressed on the surface of the cover glass and allowed to bond under manual pressure. The microfluidic device (Figure 5.1) was then kept at room temperature until use.

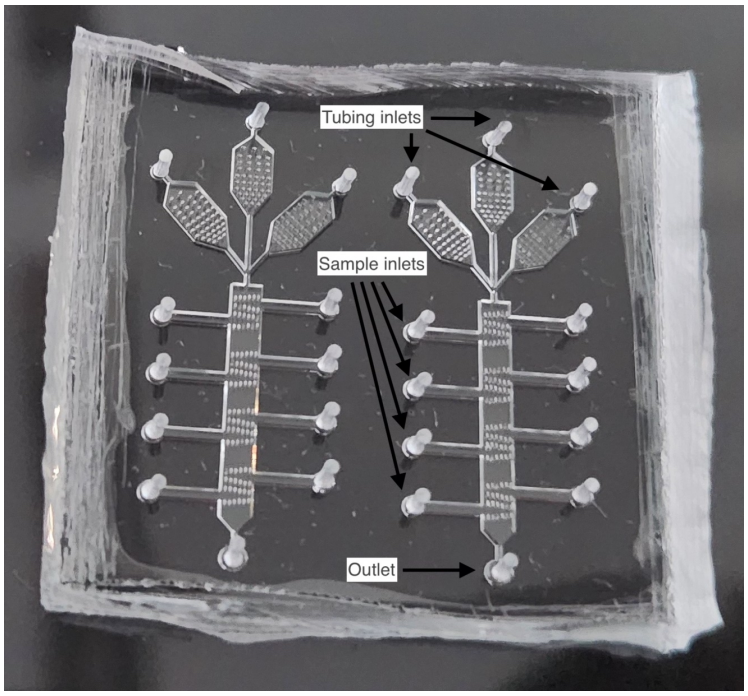

Figure 5.1: The microfluidic device: a microfluidic chip attached to a glass coverslip.

5.2.2 Medium preparation

Dissection medium and culture medium were prepared following the recipe below (Table 5.1).

Table 5.1: The components of dissection and culture medium.

Components (for 50 ml of medium)	Dissection medium	Culture medium
DMEM F-12 (Cell Culture technologies)	48.06 ml	48.06 ml
L-Glutamine (Gibco, 25030-081)	500 μl	500 μl
BSA (Equitech-Bio)	5% (0.5 g)	0.1% (0.02 g)
45% D-glucose solution (Sigma, G8769)	40 μl (2 mM)	40 μl (2 mM)
1 M HEPES (Gibco, 15630-106)	500 μl	-
Penicillin/Streptamycin (Gibco, 15140-122)	-	500 μl (1%)

A 0.22 μm PVD filter (Merck) was used to filter the culture medium before use. All compounds that were flushed into the microfluidic device during entrainment experiments were dissolved in culture medium (Table 5.1, Table 5.2, Table 5.1). The culture medium was equilibrated at 37°C under 5% CO2 until ready for use.

Table 5.2: Compounds that were used as periodic pulses and their respective concentrations during entrainment experiments.

Compound	Concentration(s)
45% D-glucose solution (Sigma, G8769)	0.5 mM
D-fructose-6-phosphate disodium salt (Sigma, F3627)	20 mM
D-fructose-1,6-bisphosphate-trisodium- -salt-octahydrate(ChemCruz, sc-221476A)	20 mM
Sodium pyruvate (Sigma, P4562)	20 mM
DAPT (Sigma-Aldrich, D5942)	2 μM
Chiron (SelleckChem, S1263)	5 μM
3-O-Methyl-D-glucopyranose (3-OMG) (Sigma, M4879)	20 mM and 1.5 mM

5.2.3 Preparation of microfluidic setup

The tubing of the microfluidic setup was prepared with PTFE tubing (APT AWG24T) with an inner diameter of 60 mm, outer diameter of 1,10 mm and a wall thickness of 0,25 mm. All tubing was wiped with ethanol before use. Two tubes (length: 1 m) were prepared for the outlets of the microfluidic device. Additional PTFE tubing of an arbitrary length was manually filled with PDMS by inserting one end of the tubing into a syringe needle (22G1 1/4 - Nr. 12) and then connecting a 10-mL syringe (BD Luer-Lok REF 300912) with a diameter of 14.5 mm to the needle. The contents of the syringe were manually pressed into the tubing and left to dry overnight. After the PDMS solidified, this tubing was cut into fragments of 1 cm in length, which are referred to as plugs. Around 22 plugs were prepared for each microfluidic device to close the openings on the microfluidic chip that were not connected to any tubing and would have otherwise remained open. The microfluidic device and the

plugs were immersed in a glass container filled with 500 ml PBS buffer, supplemented with 5% Pen/Strep. The tubes that were prepared for the outlets, were inserted in the outlet openings of the immersed microfluidic device and flushed with PBS + 5% Pen/Strep.

In the next step, 10 ml syringes were filled with 5 ml of medium. The number of syringes and the medium composition varied according to the experiment (Table 5.3). At least four tubes (length: 3 m) were prepared for the inlets of the microfluidic device. This number of tubes varied based on the number of syringes needed for the experiment.

The syringes and the microfluidic device (inside the glass container) were degassed in a desiccator under 70 millibar vacuum pressure (vwr vacuum pump). After two hours, the syringes and the glass container were taken out of the desiccator. The syringes were installed in the microfluidic pumps (World Precision Instruments, AL-400), and the glass container was set aside for later use. The syringes were connected to the tubes that were prepared for the inlets of the microfluidics device by inserting one end of the tube into a syringe needle (22G1 1/4 - Nr. 12) and then screwing the needle into the syringe. The tubes were flushed with medium for around one hour by setting the pumps to pump their medium content through the tubes at a rate of 900 μl/h .

Table 5.3: Preparation of syringe solutions for entrainment experiments with pulses of glucose.

Syringe	Volume (ml)	Components	Osmolarity control
1. medium	10 ml	2 mM glucose	-
2. medium	10 ml	2 mM glucose	-
3. pulse	10 ml	0.5 mM glucose	+1.5 mM 3-OMG
4. control	10 ml	2 mM glucose	-

Table 5.4: Preparation of syringe solutions with metabolites that were pulsed during entrainment experiments and description of solution compositions.

Syringe	Volume (ml)	Components	Osmolarity control
1. medium	10 ml	2 mM glucose	+ 20 mM 3-OMG
2. medium	10 ml	2 mM glucose	+ 20 mM 3-OMG
3. pulse	10 ml	2 mM glucose	
		+ 20 mM metabolite	-
4. control	10 ml	2 mM glucose	+ 20 mM 3-OMG

Table 5.5: Preparation of syringe solutions with signaling modulators that were pulsed during entrainment experiments and description of solution compositions.

Syringe	Volume (ml)	Components
1. medium	10 ml	2 mM glucose
2. medium	10 ml	2 mM glucose
3. pulse	10 ml	2 mM glucose + 2 μM DAPT
4. control	10 ml	2 mM glucose + 2 μM DMSO (Sigma, D8418)

5.2.4 Setting up microfluidic pumps

The microfluidic pumps that were used for entrainment experiments are programmable for different periods of external pulses. The settings of the pumps for a period of 140 minutes are shown in the tables below (Table 5.6, 5.7).

Table 5.6: Settings of microfluidic pump for pulses of metabolites during entrainment with a period of 140 min.

Phase	Setting	Rate (μl/h)	Volume (μl)	Function
01	LP:ST			Starts 1st pumping loop
02	LP:ST			Starts 2nd pumping loop
03	LP:ST			Starts 3rd pumping loop
04	PS:60			Pauses for 60 seconds
05	LP:55			Loops the "Pause" function 55 times
06	LP:2			Loops the "Pause" function 2 x 55 times
07	RATE	60	30	Pumps the metabolite for 30 mins
08	LP:30			Loops the whole program 30 times
09	STOP			Stops the program

Table 5.7: Settings of microfluidic pump for flushing medium during entrainment with a period of 140 min.

Phase	Setting	Rate (μl/h)	Volume (μl)	Function
01	LP:ST			Starts 1st pumping loop
02	RATE	60	110	Pumps the medium for 110 mins
03	LP:ST			Starts 2nd pumping loop
04	PS:60			Pauses for 60 seconds
05	LP:30			Loops the "Pause" function 30 times
06	LP:30			Loops the whole program 30 times
07	STOP			Stops the program

5.2.5 Mouse dissection and loading of PSM tissue in microfluidic device for live imaging

CD1 female mice were bred with males of the mouse line of interest. Pregnant CD1 female mice were sacrificed by cervical dislocation and dissected at embryonic day 10.5 (E10.5). The

embryos were recovered from the uterus and washed in a dissection medium. The tails of the embryos were cut using forceps and screened under a stereomicroscope (Leica M80) for the signal of reporter of interest. The reporter-positive tails were transferred into a fresh dissection medium and cleanly cut with a scalpel at the third somite anterior to the PSM. Using a P20 pipette, these tails were transferred into the chambers of the microfluidic device, which was kept immersed in PBS inside the glass container in the meantime. After loading the tails, all the sample inlets of the device were closed with plugs. The tubing connected to the syringes was inserted into the tubing inlets of the microfluidic device. This was done with the use of forceps while the microfluidic device was still immersed in the glass container so as not to introduce any bubbles in the device. After plugging all the inlets of the microfluidic device, the device was taken out of the glass container and placed inside the microfluidic chamber (Figure 5.2). The microfluidic chamber was designed by the EMBL Mechanical Workshop in such a way that it holds the microfluidic device and some of the tubing. The microfluidic chamber was closed with a lid, leaving open only the entry point for the inlet tubing and the exit point for the outlet tubing. A third opening of the microfluidic chamber was connected to an oxygen tank with 60% oxygen. The chamber was then placed on the stage of the microscope, inside an environment control box (EMBL Mechanical Workshop). The microfluidic device was fixed in place by a metallic attachment of the chamber and around two meters of the inlet tubing was adjusted inside the chamber. This was necessary in order for the medium to get calibrated at 5 % CO2 and warm up to 37 °C inside the environment control box before it encountered the samples.

All the pumps were initially set to pump on the samples at a rate of 20 μl/h for 15 minutes to start the calibration and warming of all media. Next, only the control and medium were set to pump on the samples at 60 μl/h for 45 minutes to allow the medium to fully calibrate and warm up before starting live imaging.

5.3 Confocal microscopy

Samples were imaged at an LSM 780 laser-scanning confocal microscope (Carl Zeiss Microscopy). The objective that was used was a plan-apochromat 20x air objective. The samples were imaged in z-stacks of three slices (8 μm spacing). A tile scan was done for

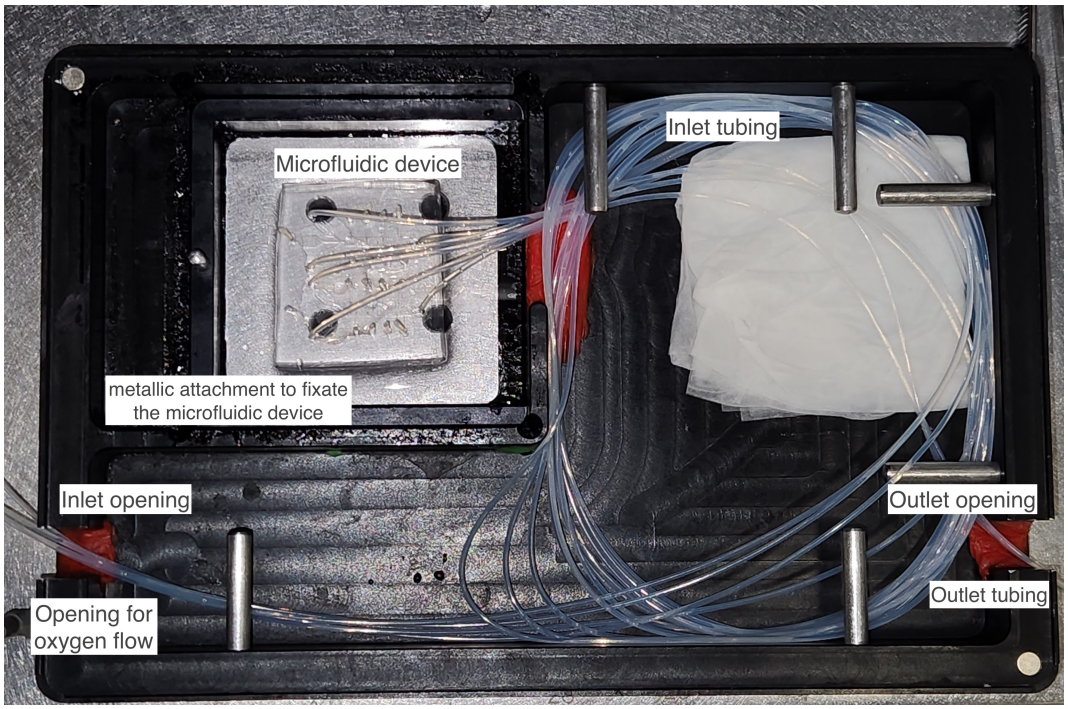

Figure 5.2: The microfluidic chamber containing the microfluidic device and inlet/outlet tubing.

each sample to capture a grid of two vertical tiles. A timelapse in the course of 24 hours was acquired, during which the images were taken every 10 minutes. A macro developed by Politi et al. (2018) controlled the motorized stage to move across samples within that time period of 10-min. The dimensions of each image were 512 by 512 pixels, and the bit depth was 16 bits.

5.4 Data analysis

The intensity analysis of posterior moving regions of interest (ROIs) was done in Fiji. Firstly, a maximum projection of z-stacks from time-lapse fluorescent imaging was made. The images underwent a Gaussian blur with a sigma value of 2. All samples were registered on the brightfield channel (using MultiStackReg on Fiji). The posterior ROIS were determined manually on select frames along the time-series and then looped over all frames using a Python script generated by Takehito Tomita. All ROIs were circular, with a defined diameter

of 30 pixels. The raw intensity time-series was then plotted as a z-axis profile. The raw time-series values were exported as a text file.

The quantification of oscillatory components was done using the wavelet analysis toolkit pyBOAT, developed by Gregor Mönke, available at https://github.com/tensionhead/pyBOAT (Mönke et al. (2020)). The wavelet analysis workflow detrends the raw oscillations using a sinc-filter. The frequency analysis is done by a wavelet transform, for which wavelet functions with defined frequencies are cross-correlated to the raw signal. This results in a power spectrum that is generated based on how high the cross-correlation is. Components of the oscillations, such as phase and period, are extracted from the high-power regions of the power spectrum.

The analysis of phase dynamics was done based on the protocol suggested by Paul François, whereas the workflow was developed in a Python script by Paul G. L. Sanchez, available at https://github.com/PGLSanchez/EMBL_OscillationsAnalysis/tree/master/EntrainmentAnalysis (Sanchez et al. (2022)). In summary, the phase difference is calculated by:

$$\Delta\phi = \phi(t+T) - \phi(t) \tag{5.1}$$

T represents the period of perturbation, ϕ(t+T) is the new phase, and ϕ(t) is the old phase. The pair of new phase vs. old phase was used for constructing stroboscopic maps. The first and last pairs of phases were left out because, in the regions at the beginning and end of the time series, the overlap with the wavelet function is partial. The centroid was determined from the average phases of the final pair of new phase vs old phase. The circular standard deviation is calculated by the following formula, in which R represents the first order Kuramoto parameter:

$$circSD = \sqrt{-2lnR} \tag{5.2}$$

5.5 Min6 cell culture and imaging

Min6 cells were cultured in a humidified environment at 37°C under 8% CO_2. The growth medium, DMEM (4.5 g/L glucose), was enriched with 15% FBS (Thermo Fisher Scientific, 16000-044) and 70 μM β-mercaptoethanol. Before culturing, the medium was filtered (Millex

GV, 0.22 μm) and was utilized within one week of preparation. Min6 cells were seeded onto 8-well LabTek microscope dishes (Thermo Scientific, 155411). The cells were stained with the calcium indicator dye Fluo-4 (Life Technologies, 5 μM in DMEM (1 g/L glucose)) for 30 minutes at 37°C and 5% CO $_2$ and then washed once with PBS before imaging. The medium was changed after 24 hours, and the cells were imaged after 48 hours. Imaging experiments were performed in DMEM (4.5 g/L glucose). Min6 cells were imaged for 40 minutes in total, at an interval of 4 seconds/frame. Min6 cells between passages 28 and 36 were used.

5.6 Randomization Assay for Low input (RAFL)

The procedure for RAFL assays, as outlined in Ho et al. (2024), begins with preparing an Ibidi microwell Fultrac plate by applying a coating of fibronectin (at a concentration of 50 μg/mL in PBS). The plate is incubated for at least 2 hours at -4 °C. In this work, individual mouse tail explants were dissected at the tailbud. After dissection, the PSM tissue is collected within the microwell insert in a volume of around 10 muL, followed by gentle pipetting to encourage the mechanical dissociation of cells within the inserts. The suspended cells are then plated onto the fibronectin-coated microwell. Once seeded, a brief centrifugation at 400 rcf for 30 seconds is performed to facilitate cell settling. Finally, the randomized PSM cells are cultured in the culture medium described above, at 37°C with 5% CO_2. The cells were imaged at an interval of 2.5 minutes/frame for a total of 300 frames. During the experiment, 150 μl of metabolite (dissolved in culture medium) was added on top of the microwells, filling the whole insert.

6.

Supplement

6.1 Phase readout of glucose entrainment.

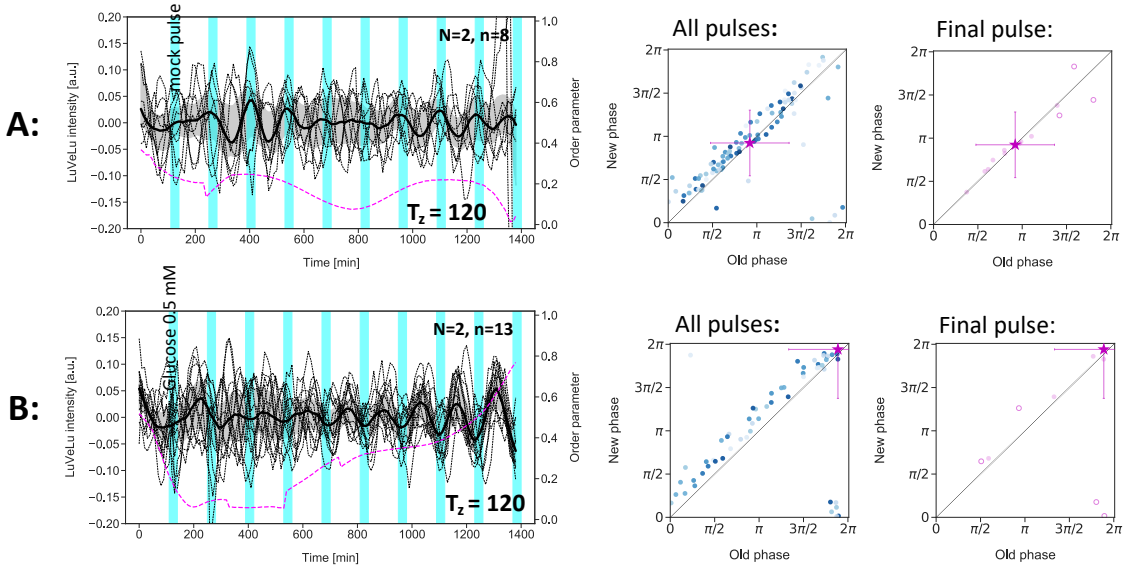

Figure 6.1: Stroboscopic maps depicting phase change during glucose entrainment.

(A,B:) Detrended time-series of LuVeLu oscillations in PSM explants. (See legend of 1.5) All samples were kept in a medium with a constant glucose concentration of 2.0 mM throughout the experiment. Periodic pulses of 0.5 mM glucose **(B)** were applied with a period of 120 minutes and a pulse length of 30-min (cyan). Non-metabolizable glucose (3-OMG) was added to the medium when glucose was absent to keep the molarity constant. In the control **(A)**, a mock pulse of medium (containing 2 mM glucose) was applied instead of the 0.5 mM glucose pulse. Corresponding stroboscopic maps that depict a step-wise progression of the phase of LuVeLu oscillations during the experiment are shown on the right side of each time-series graph. Each dot represents a snapshot of the phase of the oscillation at the beginning of the glucose pulse (old phase) plotted against the phase of the oscillations at the beginning of the *next* glucose pulse (new phase). The phase of entrainment can be read out from the region around the diagonal, to which the dots have converged (marked here with a magenta star). The spread of the dots represents in-phase synchrony and is quantified by circSD (magenta cross). The blue shading of the dots depicts the step-wise phase progression of every sample (n) in time. Darker

dots represent later time points. The magenta dots represent the phase dynamics of every sample (n) at the last external pulse. The filled magenta dots represent phase-locked LuVeLu oscillations (n*). The unfilled magenta circles represent non-phase-locked LuVeLu oscillations. n: total number of samples, N: number of experiments, n*: number of phase-locked samples within the total n. Data by Hidenobu Miyazawa.

6.2 Controls for entrainment experiments with pulses of 120 min.

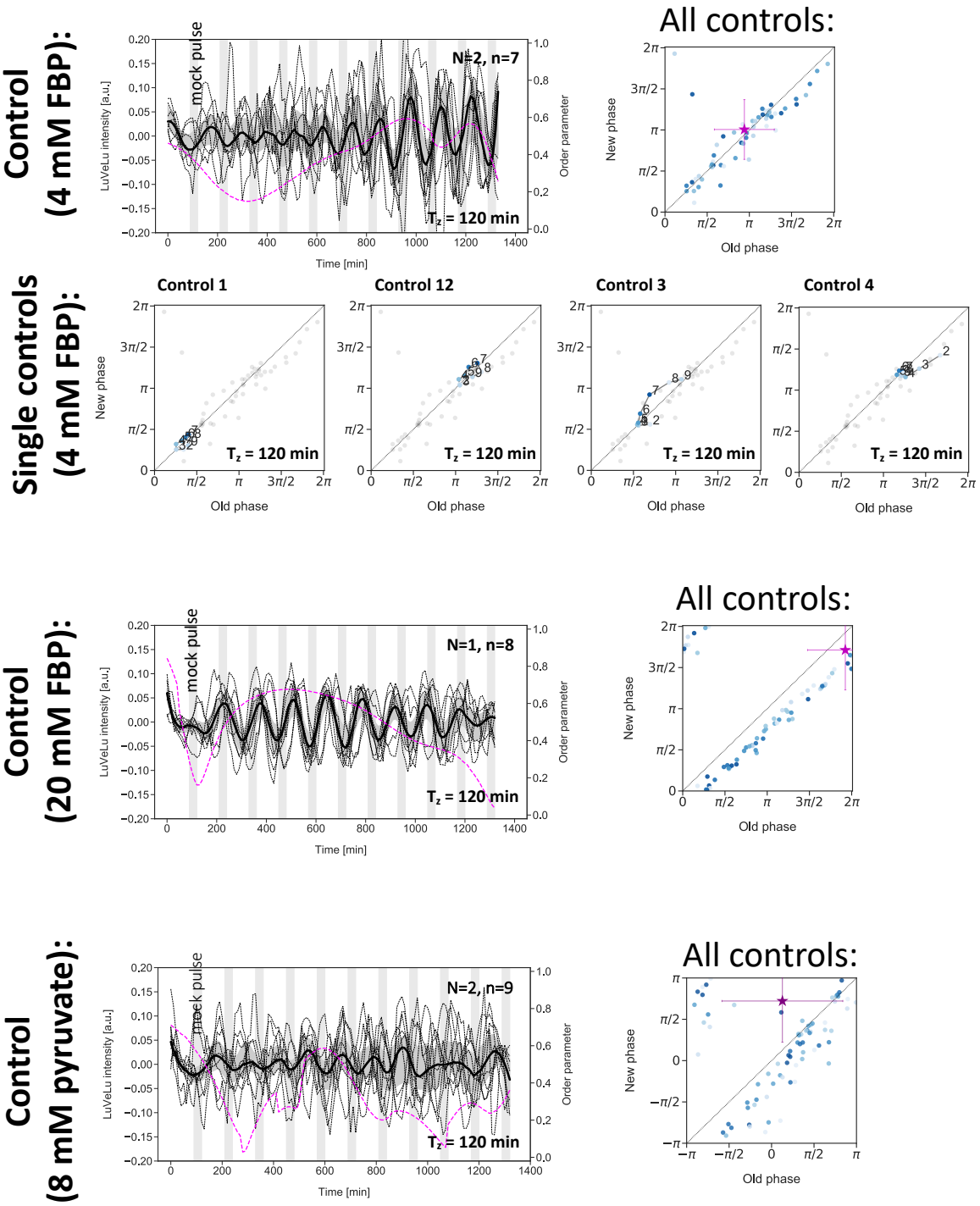

Figure 6.2: Controls for entrainment experiments with pulses of 120 min.

Detrended time-series of LuVeLu oscillations in PSM explants. The detrending was done using a sinc-filter with a cut-off period of 240 minutes. Dashed black lines show single-sample oscillations, the thick black line shows the median value of all oscillations, and the gray shading shows the first to third quartile range. The magenta line shows the Kuramoto order parameter. The y-axis on the right indicates the Kuramoto values, a value of one representing complete synchrony of oscillations. All samples were kept in a medium with a constant glucose concentration of 2.0 mM throughout the experiment. Mock pulses (containing medium with 2 mM glucose) were applied with a period of 120 minutes and a pulse length of 30-min (grey). Non-metabolizable glucose (3-OMG) was added to the medium to keep the molarity comparable to the perturbation condition. Corresponding stroboscopic maps that depict a step-wise progression of the phase of LuVeLu oscillations during the experiment are shown on the right side of each time-series graph. Each dot represents a snapshot of the phase of the oscillation at the beginning of the mock pulse (old phase) plotted against the phase of the oscillations at the beginning of the *next* glucose pulse (new phase). The phase of entrainment can be read out from the region around the diagonal, to which the dots have converged (marked here with a magenta star). The spread of the dots represents in-phase synchrony and is quantified by circSD (magenta cross). The blue shading of the dots depicts the step-wise phase progression of every sample (n) in time. n: total number of samples, N: number of experiments.

6.3 Controls for entrainment experiments with pulses of 140 min.

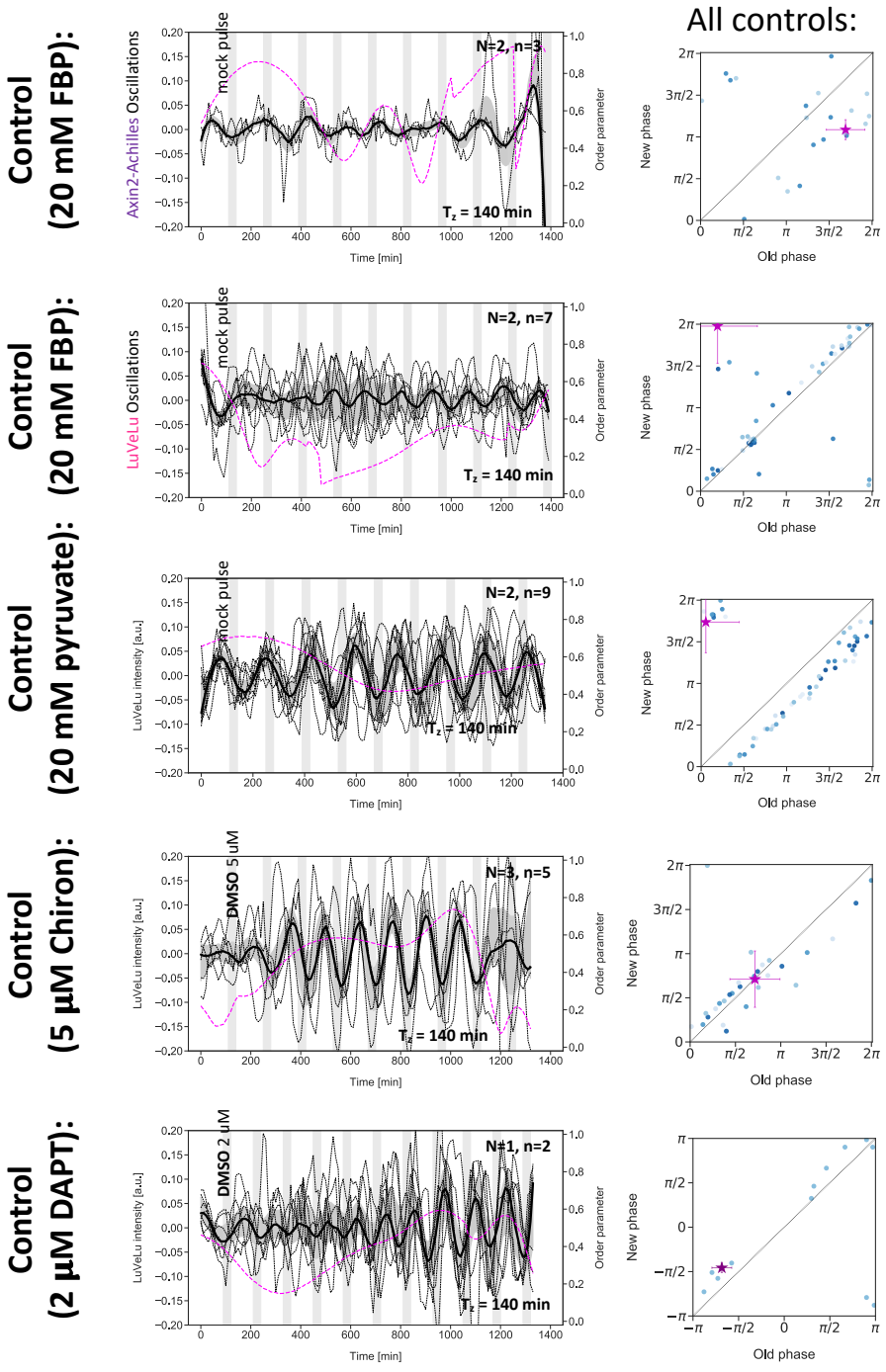

Figure 6.3: Controls for entrainment experiments with pulses of 140 min.

Detrended time-series of LuVeLu oscillations in PSM explants. The detrending was done using a sinc-filter with a cut-off period of 240 minutes. Dashed black lines show single-sample oscillations, the thick black line shows the median value of all oscillations, and the gray shading shows the first to third quartile range. The magenta line shows the Kuramoto order parameter. The y-axis on the right indicates the Kuramoto values, a value of one representing complete synchrony of oscillations. All samples were kept in a medium with a constant glucose concentration of 2.0 mM throughout the experiment. Mock pulses (containing medium with 2 mM glucose) were applied with a period of 140 minutes and a pulse length of 30-min (grey). Non-metabolizable glucose (3-OMG) was added to the medium to keep the molarity comparable to the perturbation condition. Corresponding stroboscopic maps that depict a step-wise progression of the phase of LuVeLu oscillations during the experiment are shown on the right side of each time-series graph. Each dot represents a snapshot of the phase of the oscillation at the beginning of the mock pulse (old phase) plotted against the phase of the oscillations at the beginning of the *next* glucose pulse (new phase). The phase of entrainment can be read out from the region around the diagonal, to which the dots have converged (marked here with a magenta star). The spread of the dots represents in-phase synchrony and is quantified by circSD (magenta cross). The blue shading of the dots depicts the step-wise phase progression of every sample (n) in time. n: total number of samples, N: number of experiments.

7.

Abbreviations

Table 7.1: Abbreviations.

Abbreviations	
Pfk	phosphofructokinase
F6P	fructose-6-phosphate
FBP	fructose-1,6-bisphosphate
PSM	presomitic mesoderm
E10.5	embryonic day 10.5
RAFL	Randomization Assay for Low Input
DAPT	N-[N-(3,5-Difluorophenacetyl-L-alanyl)]-(S)-phenylglycine t-butyl ester
3-OMG	3-O-methyl-glucose
circSD	circular standard deviation
KOP	first Kuramoto order parameter
ϕ_{ent}	entrainment phase
T_z	Zeitgeber period
Wnt	wingless/integrated
FGF	fibroblast growth factor
GSK-3β	glycogen synthase kinase-3 β
Lfng	lunatic fringe
PTFE	polytetrafluoroethylene
NADH	nicotinamide adenine dinucleotide hydrogen

References

A. Aulehla, W. Wiegraebe, V. Baubet, M. B. Wahl, C. Deng, M. Taketo, M. Lewandoski, and O. Pourquié. A β-catenin gradient links the clock and wavefront systems in mouse embryo segmentation. *Nature Cell Biology*, 10(2):186–193, 2008. doi: 10.1038/ncb1679.

A. Balanov, N. Janson, D. Postnov, and O. Sosnovtseva. *Synchronization: From Simple to Complex*. Springer, 2008. ISBN 978-3-540-72127-7.

R. Bertram, J. Previte, A. Sherman, T. A. Kinard, and L. S. Satin. The phantom burster model for pancreatic β-cells. *Biophysical Journal*, 79(6):2880–2892, 2000. doi: 10.1016/S0006-3495(00)76525-8.

R. Bertram, A. Sherman, and L. S. Satin. Metabolic and electrical oscillations: Partners in controlling pulsatile insulin secretion. *American Journal of Physiology - Endocrinology and Metabolism*, 293(4):890–900, 2007. doi: 10.1152/ajpendo.00359.2007.

R. Bertram, A. Sherman, and L. S. Satin. Electrical, Calcium, and Metabolic Oscillations in Pancreatic Islets. *Islets of Langerhans*, (2):1–20, 2014. doi: 10.1007/978-94-007-6884-$0_1 0 - 3$.

A. Boiteux and B. Hess. Oscillations in glycolysis, cellular respiration and communication. *Faraday Symposia of the Chemical Society*, 9(0):202–214, 1974. ISSN 03015696. doi: 10.1039/FS9740900202.

A. Boiteux, A. Goldbeter, and B. Hess. Control of oscillating glycolysis of yeast by stochastic, periodic, and steady source of substrate: a model and experimental study. *Proceedings of the National Academy of Sciences of the United States of America*, 72(10):3829–3833, 1975. doi: 10.1073/pnas.72.10.3829.

M. R. Bond and J. A. Hanover. A little sugar goes a long way: The cell biology of O-GlcNAc. *Journal of Cell Biology*, 208(7):869–880, 2015. doi: 10.1083/jcb.201501101.

V. Bulusu, N. Prior, M. T. Snaebjornsson, A. Kuehne, K. F. Sonnen, J. Kress, F. Stein, C. Schultz, U. Sauer, and A. Aulehla. Spatiotemporal Analysis of a Glycolytic Activity Gradient Linked to Mouse Embryo Mesoderm Development. *Developmental Cell*, 40(4): 331–341, 2017. doi: 10.1016/j.devcel.2017.01.015.

L. Cai, B. M. Sutter, B. Li, and B. P. Tu. Acetyl-CoA Induces Cell Growth and Proliferation by Promoting the Acetylation of Histones at Growth Genes. *Molecular Cell*, 42(4):426–437, 2011. doi: 10.1016/j.molcel.2011.05.004.

C. H. Chang, J. D. Curtis, L. B. Maggi, B. Faubert, A. V. Villarino, D. O'Sullivan, S. C. C. Huang, G. J. Van Der Windt, J. Blagih, J. Qiu, J. D. Weber, E. J. Pearce, R. G. Jones, and E. L. Pearce. Posttranscriptional control of T cell effector function by aerobic glycolysis. *Cell*, 153(6):1239, 2013. doi: 10.1016/j.cell.2013.05.016.

T. W. Chen, T. J. Wardill, Y. Sun, S. R. Pulver, S. L. Renninger, A. Baohan, E. R. Schreiter, R. A. Kerr, M. B. Orger, V. Jayaraman, L. L. Looger, K. Svoboda, and D. S. Kim. Ultrasensitive fluorescent proteins for imaging neuronal activity. *Nature*, 499(7458):295–300, 2013. doi: 10.1038/nature12354.

C. M. Child. Differential Dye Reduction and Reoxidation in Triturus Development. *Physiological Zoology*, 16(1):61–76, 1943. doi: 10.1086/physzool.16.1.30151669.

C. M. Child. *Patterns and problems of development*. The University of Chicago Press, Chicago, Ill, 2011. doi: 10.5962/bhl.title.6415.

S. C. Christiansen, A. L. Fougner, Ø. Stavdahl, K. Kölle, R. Ellingsen, and S. M. Carlsen. A Review of the Current Challenges Associated with the Development of an Artificial Pancreas by a Double Subcutaneous Approach. *Diabetes Therapy*, 8(3):489–506, 2017. doi: 10.1007/s13300-017-0263-6.

G. Da Silva Xavier, M. K. Loder, A. McDonald, A. I. Tarasov, R. Carzaniga, K. Kronenberger, S. Barg, and G. A. Rutter. TCF7L2 regulates late events in insulin secretion from pancreatic islet β-cells. *Diabetes*, 58(4):894–905, 2009. doi: 10.2337/db08-1187.

L. Del Bosque-Plata, E. Martínez-Martínez, M. Á. Espinoza-Camacho, and C. Gragnoli. The Role of TCF7L2 in Type 2 Diabetes. *Diabetes*, 70(6):1220–1228, 2021. doi: 10.2337/DB20-0573.

G. Dupont, L. Combettes, G. S. Bird, and J. W. Putney. Calcium oscillations. *Cold Spring Harbor Perspectives in Biology*, 3(3):1–18, 2011. doi: 10.1101/cshperspect.a004226.

K. L. Eckel-Mahan, V. R. Patel, R. P. Mohney, K. S. Vignola, P. Baldi, and P. Sassone-Corsi. Coordination of the transcriptome and metabolome by the circadian clock. *Proceedings of the National Academy of Sciences of the United States of America*, 109(14):5541–5546, 2012. doi: 10.1073/pnas.1118726109.

D. J. Emlen and H. F. Nijhout. Hormonal control of male horn length dimorphism in the dung beetle Onthophagus taurus (Coleoptera: Scarabaeidae). *Journal of Insect Physiology*, 45(1):45–53, 1999. doi: 10.1016/S0022-1910(98)00096-1.

Y. Feng, G. De Franceschi, A. Kahraman, M. Soste, A. Melnik, P. J. Boersema, P. P. De Laureto, Y. Nikolaev, A. P. Oliveira, and P. Picotti. Global analysis of protein structural changes in complex proteomes. *Nature Biotechnology*, 32(10):1036–1044, 2014. doi: 10.1038/nbt.2999.

A. Ghosh and B. Chance. Oscillations of glycolytic intermediates in yeast cells. *Biochemical and Biophysical Research Communications*, 16(2):174–181, 1964. doi: 10.1016/0006-291X(64)90357-2.

S. Gibb, A. Zagorska, K. Melton, G. Tenin, I. Vacca, P. Trainor, M. Maroto, and J. K. Dale. Interfering with Wnt signalling alters the periodicity of the segmentation clock. *Developmental Biology*, 330(1):21–31, 2009. doi: 10.1016/j.ydbio.2009.02.035.

S. Gibb, M. Maroto, and J. K. Dale. The segmentation clock mechanism moves up a notch. *Trends in Cell Biology*, 20(10):593–600, 2010. doi: 10.1016/j.tcb.2010.07.001.

S. F. Gilbert. Ecological developmental biology: Developmental biology meets the real world. *Developmental Biology*, 233(1):1–12, 2001. doi: 10.1006/dbio.2001.0210.

S. F. Gilbert. Developmental plasticity and developmental symbiosis: The return of eco-devo. *Current Topics in Developmental Biology*, 116:415–433, 2016. doi: 10.1016/bs.ctdb.2015.12.006.

S. F. Gilbert. *Ecological Developmental Biology*, volume 1–8. John Wiley Sons, Ltd, 2017. ISBN 9780470015902. doi: 10.1002/9780470015902.a0020479.pub2.

S. Hardivillé and G. W. Hart. Nutrient regulation of signaling, transcription, and cell physiology by O- GlcNAcylation. *Cell Metabolism*, 20(2):208–213, 2014. doi: 10.1016/j.cmet.2014.07.014.

S. Heidenreich, P. Weber, H. Stephanowitz, K. M. Petricek, T. Schütte, M. Oster, A. M. Salo, M. Knauer, I. Goehring, N. Yang, N. Witte, A. Schumann, M. Sommerfeld, M. Muenzner, J. Myllyharju, E. Krause, and M. Schupp. The glucose-sensing transcription factor ChREBP is targeted by proline hydroxylation. *Journal of Biological Chemistry*, 295(50): 17158–17168, 2020. doi: 10.1074/jbc.RA120.014402.

O. Hertwig. *The Biological Problem of To-day: Preformation or Epigenesis?*, volume A10. 1896. doi: 10.1525/aa.1897.10.4.02a00020.

A. Hirao, Y. Tahara, I. Kimura, and S. Shibata. A balanced diet is necessary for proper entrainment signals of the mouse liver clock. *PLoS ONE*, 4(9):6909, 2009. doi: 10.1371/journal.pone.0006909.

C. Ho, L. Jutras-Dubé, M. Zhao, G. Mönke, I. Z. Kiss, P. François, and A. Aulehla. Nonreciprocal synchronization in embryonic oscillator ensembles. *bioRxiv*, 2024. doi: 10.1101/2024.01.29.577856.

A. Hubaud and O. Pourquié. Signalling dynamics in vertebrate segmentation. *Nature Reviews Molecular Cell Biology*, 15(11):709–721, 2014. doi: 10.1038/nrm3891.

A. Hyafil, A. L. Giraud, L. Fontolan, and B. Gutkin. Neural Cross-Frequency Coupling: Connecting Architectures, Mechanisms, and Functions. *Trends in Neurosciences*, 38(11): 725–740, 2015. doi: 10.1016/j.tins.2015.09.001.

M. Izumo, C. H. Johnson, and S. Yamazaki. Circadian gene expression in mammalian fibroblasts revealed by real-time luminescence reporting: Temperature compensation and damping. *Proceedings of the National Academy of Sciences of the United States of America*, 100(26):16089–16094, 2003. doi: 10.1073/pnas.2536313100.

W. Johannsen. Elemente der Exakten Erblichkeitslehre. Deutsch wesentlich erweiterte Ausgabe in fünfundzwanzig Vorlesungen. *Science*, 30(780):851–853, 1909. doi: 10.1126/science.30.780.851.

M. Kamakura. Royalactin induces queen differentiation in honeybees. *Nature*, 473(7348): 478–483, 2011. doi: 10.1038/nature10093.

J. S. Kari and R. B. Huey. Size and seasonal temperature in free-ranging Drosophila subobscura. *Journal of Thermal Biology*, 25(4):267–272, 2000. doi: 10.1016/S0306-4565(99)00096-0.

C. M. Kelliher, E. L. Stevenson, J. J. Loros, and J. C. Dunlap. Nutritional compensation of the circadian clock is a conserved process influenced by gene expression regulation and mRNA stability. *PLoS Biology*, 21(1), 2023. doi: 10.1371/journal.pbio.3001961.

M. Kirschner, J. C. Gerhart, K. Hara, and G. A. Ubbels. Initiation of the Cell Cycle and Establishment of Bilateral Symmetry in Xenopus Eggs. *The Cell Surface: Mediator of Developmental Processes*, pages 187–215, 1980. doi: 10.1016/b978-0-12-612984-7.50019-0.

J. N. Koberstein, M. L. Stewart, C. B. Smith, A. I. Tarasov, F. M. Ashcroft, P. J. Stork, and R. H. Goodman. Monitoring glycolytic dynamics in single cells using a fluorescent biosensor for fructose 1,6-bisphosphate. *Proceedings of the National Academy of Sciences of the United States of America*, 119(31), 2022. doi: 10.1073/pnas.2204407119.

D. C. Lee, H. A. Sohn, Z. Y. Park, S. Oh, Y. K. Kang, K. M. Lee, M. Kang, Y. J. Jang, S. J. Yang, Y. K. Hong, H. Noh, J. A. Kim, D. M. J. Kim, K. H. Bae, D. M. J. Kim, S. J.

Chung, H. S. Yoo, D. Y. Yu, K. C. Park, and Y. I. Yeom. A lactate-induced response to hypoxia. *Cell*, 161(3):595–609, 2015. doi: 10.1016/j.cell.2015.03.011.

M. F. Madsen, S. Danø, and P. G. Sørensen. On the mechanisms of glycolytic oscillations in yeast. *The FEBS Journal*, 272(11):2648–2660, 2005. doi: https://doi.org/10.1111/j.1742-4658.2005.04639.x. URL https://febs.onlinelibrary.wiley.com/doi/abs/10.1111/j.1742-4658.2005.04639.x.

D. Marr and T. Poggio. From understanding computation to understanding neural circuitry. *Neuroscience Research Program Bulletin*, 15(2):470–488, 1979.

M. J. Merrins, A. R. Van Dyke, A. K. Mapp, M. A. Rizzo, and L. S. Satin. Direct measurements of oscillatory glycolysis in pancreatic islet β-cells using novel fluorescence resonance energy transfer (FRET) biosensors for pyruvate kinase M2 activity. *Journal of Biological Chemistry*, 288(46):33312–33322, 2013. doi: 10.1074/jbc.M113.508127.

M. J. Merrins, C. Poudel, J. P. McKenna, J. Ha, A. Sherman, R. Bertram, and L. S. Satin. Phase Analysis of Metabolic Oscillations and Membrane Potential in Pancreatic Islet β-Cells. *Biophysical Journal*, 110(3):691–699, 2016. doi: 10.1016/j.bpj.2015.12.029.

H. Miyazawa and A. Aulehla. Revisiting the role of metabolism during development. *Development (Cambridge)*, 145(19), 2018. doi: 10.1242/dev.131110.

H. Miyazawa and J. Rada. Glycolysis–Wnt signaling axis tunes developmental timing of embryo segmentation. *bioRxiv*, 2024. doi: 10.1101/2024.01.22.576629.

H. Miyazawa, M. T. Snaebjornsson, N. Prior, E. Kafkia, H. M. Hammarén, N. Tsuchida-Straeten, K. R. Patil, M. Beck, and A. Aulehla. Glycolytic flux-signaling controls mouse embryo mesoderm development. *eLife*, 11, 2022. doi: 10.7554/ELIFE.83299.

A. P. Moczek. Integrating micro- and macroevolution of development through the study of horned beetles. *Heredity*, 97(3):168–178, 2006. doi: 10.1038/sj.hdy.6800871.

A. P. Moczek and D. J. Emlen. Male horn dimorphism in the scarab beetle, Onthophagus taurus: Do alternative reproductive tactics favour alternative phenotypes? *Animal Behaviour*, 59(2):459–466, 2000. doi: 10.1006/anbe.1999.1342.

G. Mönke, F. A. Sorgenfrei, C. Schmal, and A. E. Granada. Optimal time frequency analysis for biological data - pyboat. *bioRxiv*, 2020. doi: 10.1101/2020.04.29.067744.

H. F. Nijhout. Development and evolution of adaptive polyphenisms. *Evolution and Development*, 5(1):9–18, 2003. doi: 10.1046/j.1525-142X.2003.03003.x.

H. F. Nijhout, A. M. Kudla, and C. C. Hazelwood. Genetic assimilation and accommodation: Models and mechanisms. *Current Topics in Developmental Biology*, 141:337–369, 2021. doi: 10.1016/bs.ctdb.2020.11.006.

M. Oginuma, P. Moncuquet, F. Xiong, E. Karoly, J. Chal, K. Guevorkian, and O. Pourquié. A Gradient of Glycolytic Activity Coordinates FGF and Wnt Signaling during Elongation of the Body Axis in Amniote Embryos. *Developmental Cell*, 40(4):342–353.e10, 2017. doi: 10.1016/j.devcel.2017.02.001.

E. Olivos-Santes, H. E. Romero-Campos, G. Dupont, and V. González-Vélez. A modelling study of glycolytic oscillations and electrical activity in pancreatic alpha cells. *Revista Mexicana de Ingenieria Biomedica*, 40(2), 2019. doi: 10.17488/RMIB.40.2.4.

J. O. Park, L. B. Tanner, M. H. Wei, D. B. Khana, T. B. Jacobson, Z. Zhang, S. A. Rubin, S. H. J. Li, M. B. Higgins, D. M. Stevenson, D. Amador-Noguez, and J. D. Rabinowitz. Near-equilibrium glycolysis supports metabolic homeostasis and energy yield. *Nature Chemical Biology*, 15(10):1001–1008, 2019. doi: 10.1038/s41589-019-0364-9.

K. Peeters, F. Van Leemputte, B. Fischer, B. M. Bonini, H. Quezada, M. Tsytlonok, D. Haesen, W. Vanthienen, N. Bernardes, C. B. Gonzalez-Blas, V. Janssens, P. Tompa, W. Versées, and J. M. Thevelein. Fructose-1,6-bisphosphate couples glycolytic flux to activation of Ras. *Nature Communications*, 8(1), 2017. doi: 10.1038/s41467-017-01019-z.

A. Pikovsky, M. Rosenblum, J. Kurths, and R. C. Hilborn. *Synchronization: A Universal Concept in Nonlinear Science* , volume 70. American Association of Physics Teachers (AAPT), 2002. doi: 10.1119/1.1475332.

A. Politi, L. D. Gaspers, A. P. Thomas, and T. Höfer. Models of IP3 and Ca2+ oscillations: Frequency encoding and identification of underlying feedbacks. *Biophysical Journal*, 90 (9):3120–3133, 2006. doi: 10.1529/biophysj.105.072249.

A. Z. Politi, Y. Cai, N. Walther, M. J. Hossain, B. Koch, M. Wachsmuth, and J. Ellenberg. Quantitative mapping of fluorescently tagged cellular proteins using FCS-calibrated four-dimensional imaging. *Nature Protocols*, 13(6):1445–1464, 2018. doi: 10.1038/nprot.2018.040.

N. Prior. *The Role of Central Carbon Metabolism in the Post-Implantation Mouse Embryo*. PhD thesis, 2014.

J. Qian and F. A. Scheer. Circadian System and Glucose Metabolism: Implications for Physiology and Disease. *Trends in Endocrinology and Metabolism*, 27(5):282–293, 2016. doi: 10.1016/j.tem.2016.03.005.

A. Rachinsky and K. Hartfelder. Corpora allata activity, a prime regulating element for caste-specific juvenile hormone titre in honey bee larvae (Apis mellifera carnica). *Journal of Insect Physiology*, 36(3):189–194, 1990. doi: 10.1016/0022-1910(90)90121-U.

R. A. Relyea. Predators come and predators go: The reversibility of predator-induced traits. *Ecology*, 84(7):1840–1848, 2003. doi: 10.1890/0012-9658(2003)084[1840:PCAPGT]2.0.CO;2.

R. A. Relyea. Fine-tuned phenotypes: Tadpole plasticity under 16 combinations of predators and competitors. *Ecology*, 85(1):172–179, 2004. doi: 10.1890/03-0169.

P. Richard. The rhythm of yeast. *FEMS Microbiology Reviews*, 27(4):547–557, 2003. doi: 10.1016/S0168-6445(03)00065-2.

N. Roll-Hansen. Sources of Wilhelm Johannsen's Genotype Theory. *Journal of the History of Biology*, 42(3):457–493, 2009. doi: 10.1007/S10739-008-9166-8.

N. Roll-Hansen. The holist tradition in twentieth century genetics. Wilhelm Johannsen's genotype concept. *Journal of Physiology*, 592(11):2431–2438, 2014. doi: 10.1113/jphysiol.2014.272120.

M. Sanaki-Matsumiya, M. Matsuda, N. Gritti, F. Nakaki, J. Sharpe, V. Trivedi, and M. Ebisuya. Periodic formation of epithelial somites from human pluripotent stem cells. *Nature Communications*, 13(1):1–14, 2022. doi: 10.1038/s41467-022-29967-1.

P. G. L. Sanchez. *Entrainment of coupled, phase-shifted signaling oscillations in the presomitic mesoderm*. PhD thesis, 2021.

P. G. L. Sanchez, V. Mochulska, C. M. Denis, G. Mönke, T. Tomita, N. Tsuchida-Straeten, Y. Petersen, K. Sonnen, P. François, and A. Aulehla. Arnold tongue entrainment reveals dynamical principles of the embryonic segmentation clock. *eLife*, 11, 2022. doi: 10.7554/ELIFE.79575.

M. T. Snaebjornsson. *A potential regulatory role of glycolysis during mouse embryonic development*. PhD thesis, 2014.

K. F. Sonnen, V. M. Lauschke, J. Uraji, H. J. Falk, Y. Petersen, M. C. Funk, M. Beaupeux, P. François, C. A. Merten, and A. Aulehla. Modulation of Phase Shift between Wnt and Notch Signaling Oscillations Controls Mesoderm Segmentation. *Cell*, 172(5):1079–1090.e12, 2018. doi: 10.1016/j.cell.2018.01.026.

K. Tornheim, V. Andrés, and V. Schultz. Modulation by citrate of glycolytic oscillations in skeletal muscle extracts. *Journal of Biological Chemistry*, 266(24):15675–15678, 1991. doi: 10.1016/s0021-9258(18)98460-7.

B. P. Tu and S. L. McKnight. Metabolic cycles as an underlying basis of biological oscillations. 7(9):696–701, 2006. doi: 10.1038/nrm1980.

B. P. Tu, A. Kudlicki, M. Rowicka, and S. L. McKnight. Cell biology: Logic of the yeast metabolic cycle: Temporal compartmentalization of cellular processes. *Science*, 310(5751):1152–1158, 2005. doi: 10.1126/science.1120499.

R. A. Waterland and R. L. Jirtle. Transposable Elements: Targets for Early Nutritional Effects on Epigenetic Gene Regulation. *Molecular and Cellular Biology*, 23(15):5293–5300, 2003. doi: 10.1128/mcb.23.15.5293-5300.2003.

A. Weismann. *The germ-plasm; a theory of heredity*. Scribner's, New York, 1893.

R. M. Willems, T. Kleinsorge, and S.-L. Yeh. Re-appreciating the why of cognition: 35 years after Marr and Poggio. 2011. doi: 10.3389/fpsyg.2011.00244.

K. Xu, N. Yin, M. Peng, E. G. Stamatiades, S. Chhangawala, A. Shyu, P. Li, X. Zhang, M. H. Do, K. J. Capistrano, C. Chou, C. S. Leslie, and M. O. Li. Glycolytic ATP fuels phosphoinositide 3-kinase signaling to support effector T helper 17 cell responses. *Immunity*, 54(5):976–987.e7, 2021. doi: 10.1016/j.immuni.2021.04.008.

W. Yang, Y. Xia, H. Ji, Y. Zheng, J. Liang, W. Huang, X. Gao, K. Aldape, and Z. Lu. Nuclear PKM2 regulates β-catenin transactivation upon EGFR activation. *Nature*, 480 (7375):118–122, 2011. doi: 10.1038/nature10598.

W. Yang, Y. Zheng, Y. Xia, H. Ji, X. Chen, F. Guo, C. A. Lyssiotis, K. Aldape, L. C. Cantley, and Z. Lu. ERK1/2-dependent phosphorylation and nuclear translocation of PKM2 promotes the Warburg effect. *Nature Cell Biology*, 14(12):1295–1304, 2012. doi: 10.1038/ncb2629.

C. S. Zhang, S. A. Hawley, Y. Zong, M. Li, Z. Wang, A. Gray, T. Ma, J. Cui, J. W. Feng, M. Zhu, Y. Q. Wu, T. Y. Li, Z. Ye, S. Y. Lin, H. Yin, H. L. Piao, D. G. Hardie, and S. C. Lin. Fructose-1,6-bisphosphate and aldolase mediate glucose sensing by AMPK. *Nature*, 548(7665):112–116, 2017. doi: 10.1038/nature23275.

L. Zhang, Y. Li, Y. Dai, D. Wang, X. Wang, Y. Cao, W. Liu, and Z. Tao. Glycolysis-related gene expression profiling serves as a novel prognosis risk predictor for human hepatocellular carcinoma. *Scientific Reports*, 11(1):18875, 2021. doi: 10.1038/s41598-021-98381-2.

L. Zheng, R. G. Roeder, and Y. Luo. S phase activation of the histone H2B promoter by OCA-S, a coactivator complex that contains GAPDH as a key component. *Cell*, 114(2): 255–266, 2003. doi: 10.1016/S0092-8674(03)00552-X.